ADVANCED ENERGY MATERIALS
www.advenergymat.de

Heteroatom-Doped and Oxygen-Functionalized Nanocarbons for High-Performance Supercapacitors

Subrata Ghosh, Suelen Barg,* Sang Mun Jeong,* and Kostya (Ken) Ostrikov**

Electrochemical capacitors (best known as supercapacitors) are high-performance energy storage devices featuring higher capacity than conventional capacitors and higher power densities than batteries, and are among the key enabling technologies of the clean energy future. This review focuses on performance enhancement of carbon-based supercapacitors by doping other elements (heteroatoms) into the nanostructured carbon electrodes. The nanocarbon materials currently exist in all dimensionalities (from 0D quantum dots to 3D bulk materials) and show good stability and other properties in diverse electrode architectures. However, relatively low energy density and high manufacturing cost impede widespread commercial applications of nanocarbon-based supercapacitors. Heteroatom doping into the carbon matrix is one of the most promising and versatile ways to enhance the device performance, yet the mechanisms of the doping effects still remain poorly understood. Here the effects of heteroatom doping by boron, nitrogen, sulfur, phosphorus, fluorine, chlorine, silicon, and functionalizing with oxygen on the elemental composition, structure, property, and performance relationships of nanocarbon electrodes are critically examined. The limitations of doping approaches are further discussed and guidelines for reporting the performance of heteroatom doped nanocarbon electrode-based electrochemical capacitors are proposed. The current challenges and promising future directions for clean energy applications are discussed as well.

1. Introduction

In the current age of global connectivity and electrification, the demand for long-lasting and fast-responding energy storage devices is rapidly gaining scale and momentum. The current technology platform based on lithium-ion batteries does not meet the requirements of high-power applications. There is a strong current demand in energy storage technologies suited for both high energy density and high power density applications. Electrochemical capacitors, commonly referred to as supercapacitors, offer higher energy densities than conventional capacitors, ultrafast charge/discharge rates, remarkable power density, prolonged cycle life, and low maintenance cost.[1,2] These beneficial features make supercapacitors a prime candidate for high-power applications in high-speed transportation and technologies that require fast on–off response such as uninterruptable power supply, hybrid electric vehicles, grid stabilization systems, forklifts, load cranes, military weapons, aerospace equipment, etc.[1,3] However, the energy density of the supercapacitors has not yet reached the theoretically predicted high values. This is one of the reasons for the limited technology and investment readiness of supercapacitors in large-scale commercial applications. Therefore, the demand for the high charge-storage capacity and hence higher energy densities of supercapacitors without sacrificing their power density and cycle life necessitates further research and development.

There are two conventional routes to achieve the above-mentioned goal: i) increasing the capacitance and ii) widening the potential window since the energy density (E) is proportional to the specific capacitance (C) and the square of potential window (V) via the relation $E = 1/2CV^2$. An enhancement in the specific capacitance can be achieved by proper architecturing the geometry and porosity, tuning the wettability, forming heterostructures, and properties of the electrode materials while the operational voltage window of the device is defined by the choice of electrolyte (aqueous, organic, ionic, or redox additive electrolytes) as well as the electrode configuration (symmetric or asymmetric).[4–11] Since the selection of electrode materials and their geometry plays a pivotal role in the supercapacitor performance, search for novel high-performance and cost-effective electrode materials is crucial. The diversity of viable electrode materials is huge, including nanocarbons, various 2D materials, conducting polymers, as well as metal oxides,

Dr. S. Ghosh, Dr. S. Barg
Department of Materials
School of Natural Sciences
The University of Manchester
Oxford Road, Manchester M13 9PL, UK
E-mail: subrata.ghosh@manchester.ac.uk, subrataghosh.phys@gmail.com; suelen.barg@manchester.ac.uk

Dr. S. Ghosh, Prof. S. M. Jeong
Department of Chemical Engineering
Chungbuk National University
Cheongju, Chungbuk 28644, Republic of Korea
E-mail: smjeong@chungbuk.ac.kr

Prof. K. (Ken) Ostrikov
School of Chemistry and Physics and Centre for Materials Science
Queensland University of Technology
Brisbane, QLD 4000, Australia
E-mail: kostya.ostrikov@qut.edu.au

The ORCID identification number(s) for the author(s) of this article can be found under https://doi.org/10.1002/aenm.202001239.

DOI: 10.1002/aenm.202001239

hydroxides, nitrides, and sulfides.[12–24] From morphological perspective, vertically oriented nanostructures with multiple large surfaces support efficient ion transport, enable gainful use of the entire (active) surface thus leading to much improved charge accumulation, storage, and release.[25–30]

These materials are classified based on the way they store electric charge, following either the electrostatic double-layer (EDL) capacitance or the pseudocapacitance mechanisms. The pseudocapacitive charge storage mechanism is due to the adsorbed monolayer formation of metal ions or protons on the electrode surface, rapid surface/near-surface redox reactions, and fast ionic intercalation into the near-surface atomic layers. While the pseudocapacitors already present ten-to-hundred times higher charge storage capacity than the carbon materials, they show low electrical conductivity, insufficient power density, poor mechanical/electrochemical stability, narrow windows of operation voltage, and some other problems, that limit their prospects for technological R&D.[8,13,24,31] In this regard, carbon-based materials represent the obvious choice for supercapacitor technology owing to their unique combination of features such as versatile dimensionality (0D–3D), abundance on Earth, large surface areas, tunable porous architectures, excellent electrical conductivity, easy functionalization, leading to the high EDL capacitance and remarkable electrochemical stability.[12,32–35] Carbon-based materials can also be operated over a wide temperature range of –100 to 60 °C, with extremely low failure rates.[36] Since energy storage and release occur by nanoscale charge separation or EDL formation across the electrode–electrolyte interface, carbon-based supercapacitors offer very fast charge–discharge cycles suitable for prolonged operation.

Substitutional doping with, nitrogen (N), boron (B), sulfur (S), phosphorus (P), fluorine (F), silicon (Si), chlorine (Cl), functionalizing with oxygen (O), and their mixtures into the carbon surface is an effective way to simultaneously tailor the fundamental properties and improve the electrochemical properties and is rapidly gaining momentum in the advanced energy materials field and catalysis.[37–40] The changes in electrode materials and performance (in the appropriate electrolyte) rely on several factors such as the type of dopant (e.g., electron donor or acceptor), dopant concentration, and specific doping configurations. For example, B-doped and N-doped carbon nanostructures exhibit p-type and n-type semiconducting features, respectively. N-doped carbon shows more pronounced hydrophilic characteristics compared to B-doped and pristine carbon nanostructures due to the difference in the degree of polarity of functional groups, whereas B-doped carbon structures exhibit less intrinsic resistance than the N-doped ones.[41] **Figure 1** shows the current status of doped nanocarbons as supercapacitor electrodes in terms of gravimetric capacitance compared to other existing electrode materials. The doping or codoping do not necessarily result in the high-performance supercapacitor electrode (**Figure 2**a,b).[42] Figure 2b reveals that the B/N and P/N-doped nanocarbons can discharge at a higher frequency than pristine and other doped nanocarbons. Choosing appropriate dopant(s) with the optimized amount and specific configuration is crucial to eliminate the negative effects such as decomposition of organic electrolyte leading to reduced electrical conductivity, electrochemical stability, and charge storage capacity. In addition to the above factors, the choice of electrolyte is critical since the nature of the on-surface functional groups and their electrochemical properties strongly rely on the type of electrolyte used. Hence, proper combination of dopants, nanocarbons, and electrolytes is essential to materialize the full application potential of supercapacitors.

2. Scope of the Review

While research in the area of doped nanocarbon based supercapacitors has been very intense in the last few decades, only a limited number of reviews with specific focal points are available.[43–46] There are several aspects that require more exhaustive coverage and in-depth discussion, especially of the underlying mechanisms. One such area is the structure–property–performance relation versus the suitable electrolytes. Here we focus on doped nanocarbon electrode materials for supercapacitors, and provide the insights and updates related to the following knowledge gaps which have not received the coverage they merit in the currently available reviews:

- Charge storage performance of pristine nanocarbons and discussion on their limitations in applications as compared with pseudocapacitive materials.
- Effect of doping on the nanocarbons leading to distinctive effects compared to the existing pseudocapacitive nanomaterials.
- Influence of single- and multi- element dopants and the specific bonding configurations on the physicochemical properties of the electrode materials and its correlation with the overall supercapacitor performance.
- Mechanisms of the interaction of electrolytes with the surface functional groups on nanocarbons of different structure, topology and dopant content.
- Relationships between the electrode–electrolyte interactions and the operating voltage window (and hence the energy density) along with the device performance characterized by the stability, rate performance, self-discharge rates, etc.

A unique feature of this review are tabulated summaries of the energy storage properties of doped nanocarbons. Table 1 presents the changes in the fundamental physicochemical properties of nanocarbons caused by heteroatom doping, whereas Table 2 summarizes the parameters of supercapacitor electrodes made of doped nanocarbons under various operation conditions such as electrolytes and mass loading. Furthermore, the challenges and future directions for the doped nanocarbons as viable supercapacitor electrode materials are highlighted. Importantly, this review aims to fill the gap in standardization of evaluation of performance of supercapacitors utilizing nanocarbon-based electrodes by providing the guiding principles which we believe should be followed to consistently report research on supercapacitor performance based on heteroatom-doped electrodes. This effort may potentially lead to standardization of nanocarbon doping well beyond the existing energy storage applications. Finally, we hope that the present review will serve as a one-stop reference on heteroatom doping of carbon nanomaterials for next-generation clean energy applications and will be of interest to the broad advanced energy materials research community.

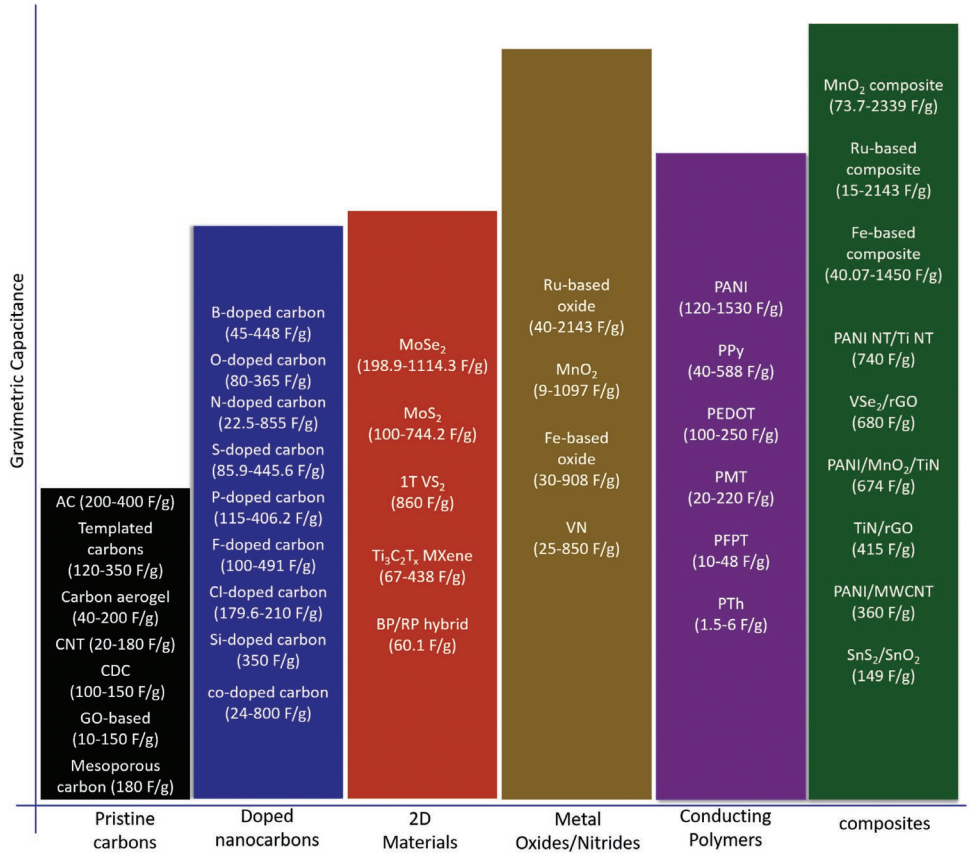

Figure 1. Comparison of the gravimetric capacitance of supercapacitor electrode materials. The data for gravimetric capacitance of supercapacitor materials with some selected nanostructures are taken from the corresponding articles: pristine carbon,[13] MnO_2-based materials,[22] Fe-based materials,[18,23] RuO_2-based structure,[15] VN structure,[24] 2D materials,[16,21] and conducting polymers.[13] Specific capacitance of doped nanocarbon is taken from the references cited in this article and also presented are the electrode performances in details in Table 1 (AC: activated carbon; MWCNT: multi-walled carbon nanotube; CDC: carbide derived carbons; rGO: reduced graphene oxide; HPC: hierarchical porous carbon; BP: black phosphorene; RP: red phosphorene; PANI: polyaniline; PPy: polypyrrole; PTh: polythiophene; PMT: poly(3-methylthiophene); PEDOT: poly(3,4-ethylenedioxythiophene); PEPT: poly(4-flourophenyl-3-thiophene)), VN: vanadium nitride.

3. Features of Doped Nanocarbons

Generally, the specific capacitance of carbon nanostructure is limited within the volumetric capacitance of 400 F cm^{-3}[47] and gravimetric capacitance of 10–200 F g^{-1} (up to 400 F g^{-1} in few cases) as shown in Figure 1.[13] Though there are predictions on achieving an EDL capacitance of graphene of 550 F g^{-1} by utilizing its full surface area (the theoretical surface area is 2630 m^2 g^{-1}), it is challenging in practice to prepare a monolayer graphene by chemical or thermal reduction from

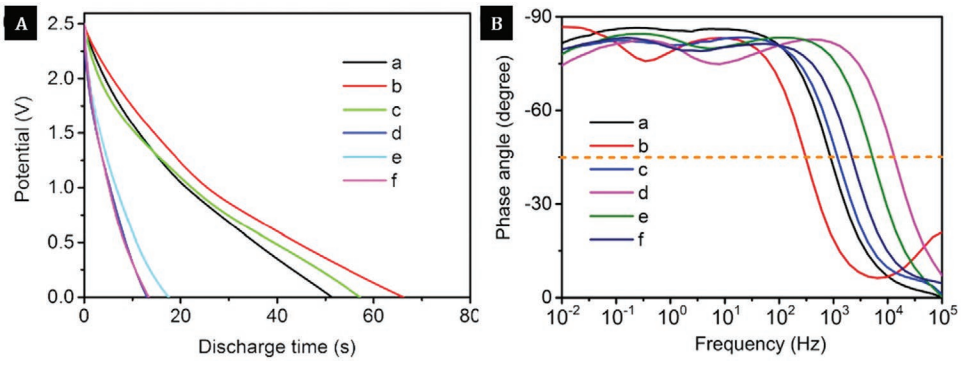

Figure 2. Effects of heteroatom doping on supercapacitor charge–discharge profile and frequency response. A) Galvanostatic discharge curve and B) phase angle plot of a) pristine; b) N-doped; c) B-doped; d) P/N-doped; e) B/N-doped; and f) Si-doped carbon nanostructures. Reproduced with permission.[42] Copyright 2017, Elsevier.

graphene oxide (GO).[48,49] The major reasons behind the limited energy density of carbon-based supercapacitors are

1. Purely physical charge-storage mechanisms dominate without any Faradaic processes involved. Only around 0.17–0.2 delocalized electrons from conduction band per atom are stored in EDLC in an aqueous electrolyte whereas this number is 2.5 per atom for electroactive surfaces of pseudocapacitive materials depending on the oxidation states; ≈1–3 localized electrons per atom can be stored by redox reactions in bulk-phase electrode materials used in conventional batteries.[50,51]
2. Although EDL capacitance is proportional to the electrode surface area ($C_{dl} = \varepsilon A/d$), the excessive increase of surface area (A) has been observed to result in reduced mesoporosity, lowered carrier density, higher pore volume and hence decreased charge storage capacity. The micropores are generally not fully wetted in aqueous electrolytes. In addition, the specific capacitance becomes saturated according to the surface area above 1200 $m^2\ g^{-1}$ calculated using density-functional theory (DFT) (corresponding Brunauer–Emmett–Teller (BET) surface area is estimated to be 1500 $m^2\ g^{-1}$).[52] Introducing porosity beyond certain level results in a lower specific capacitance of nanocarbons. Moreover, the higher surface area is not favorable for high-power operation since it reduces the volumetric capacitance of supercapacitor electrodes.[53]
3. The limited density of states at the Fermi level (DOS(E_F)) and lack of space to accommodate the charge inside the pores in spite of having a higher surface area of carbon nanostructures. The former is related to quantum capacitance ($C_Q = e^2$ DOS(E_F), where e is the electric charge and E_F is the Fermi energy), whereas the spatial confinement limits the space-charge capacitance ($C_{SC} = \sqrt{2\varepsilon n e^2/E_F}$, where ε is the dielectric permittivity). The space-charge capacitance arises due to the screening of electrolyte charge in the inner layers by outer layers since carrier density (n per volume) of each layer follows an exponential dependence on the screening length (λ) $\approx \exp(-x/\lambda)$. As a result, nanocarbons exhibit lower total capacitance because $1/C_{total} = 1/C_Q + 1/C_{SC} + 1/C_{dl}$.[52,54–57]
4. The series capacitance is introduced by the dielectric dead layer which is a layer of a very low dielectric constant between the electrode surface charge and the electrolyte solution. The existence of the dielectric dead layer is caused by the adsorption of a thin layer of hydrocarbon impurities (5–8.5 Å) on the carbon surface.[58,59]
5. Low packing density of carbon nanostructures resulting in low volumetric energy density and chemical inertness and hydrophobicity of nanocarbons in aqueous electrolytes resulting in poor interaction with the electrolyte.

An effective strategy adopted to overcome the above-mentioned problem is synthesizing the hybrid carbon-pseudocapacitive composite material, where the advantageous features of both carbon and pseudocapacitive materials are combined.[60–64] Specifically, the heteroatom-doped carbon nanostructures are cost-effective and can outperform the pseudocapacitive materials and/or their composites with carbon.[65–67] For example, N-rich carbon nanorods prepared by pyrolysis of polyaniline (PANI) nanorod arrays and ammonium sulfate have exhibited specific capacitance of 776 F g^{-1} at 1 A g^{-1} with 94.4% retention at 40 A g^{-1} after 5000 charge–discharge cycles versus reference electrode whereas PANI nanorod arrays showed the capacitance of 408.36 F g^{-1} at 1 A g^{-1} with 49.19% retention after 500 cycles.[68] In addition, heteroatom doped nanocarbons have several key features over pseudocapacitive materials while they are utilized as a supercapacitor electrode as follows:

1. Incorporating heteroatom dopants into the carbon surface has been shown to significantly improve/enhance several properties of nanocarbons such as the chemically active sites, wettability, porosity, charge distribution, charge density, spin density, interlayer spacing, electrical conductivity, and contributions of the quantum, space-charge, and pseudocapacitance leading to significant enhancement of the supercapacitive properties of the carbon structures.[41,69,70] Noteworthy, surface areas of nanocarbons that are higher than the theoretical surface area of graphene can be obtained after appropriate doping.[71–73]
2. On the other hand, integration of carbon nanostructures with pseudocapacitive materials improves the electrical conductivity, surface area, mechanical/electrochemical stability, and other physicochemical properties of the pseudocapacitive materials.[74,75]
3. Heteroatoms do not add any significant mass to the carbon structures, whereas pseudocapacitive materials introduce additional mass into the composite leading to lower specific capacitance in comparison to the pristine pseudocapacitive materials.[76]
4. The possibility of the widened potential window up to 1.7 V in aqueous electrolyte,[77] 2.4 V in the "water-in-salt" (superconcentrated lithium bis(trifluoromethane sulfonyl)imide (LiTFSI) aqueous solution) electrolyte,[78] and designing a 2.6 V aqueous symmetric supercapacitor[79] with doped nanocarbons has been reported. Achieving up to 2.6 V potential window is even rare for the aqueous supercapacitors based on pseudocapacitive materials in the symmetric configuration. Increasing the potential window is essential to increase capacitance and hence achieve higher energy densities.[80,81]
5. Doped nanocarbons showed an ultrafast frequency response with the smallest relaxation time constant.[42] The pseudocapacitive electrodes show a higher radius of semicircle in the Nyquist plot indicating higher charge transfer resistance compared to the doped nanocarbons.
6. Heteroatom dopants on the carbon surface serve as an effective bridging element for hetero-nanostructures growth and help achieve higher electrolyte ion adsorption than in the pure carbon,[82–86] as an enhancer to improve supercapacitor performance of active electrode[87] or current collector.[88] Eventually, heteroatom doped carbon structures can be used as a current-collector free electrode whereas a metal current collector is essential for metal oxide or conducting polymers electrode, which increases the total mass of electrode.[88]
7. Doped-carbon nanostructures represent usually a less expensive option than the pseudocapacitive materials.

With these key features in mind, the heteroatom dopants that improve the physicochemical properties of carbon-based materials intrinsically and hence the overall supercapacitor performance are summarized in **Figure 3**.

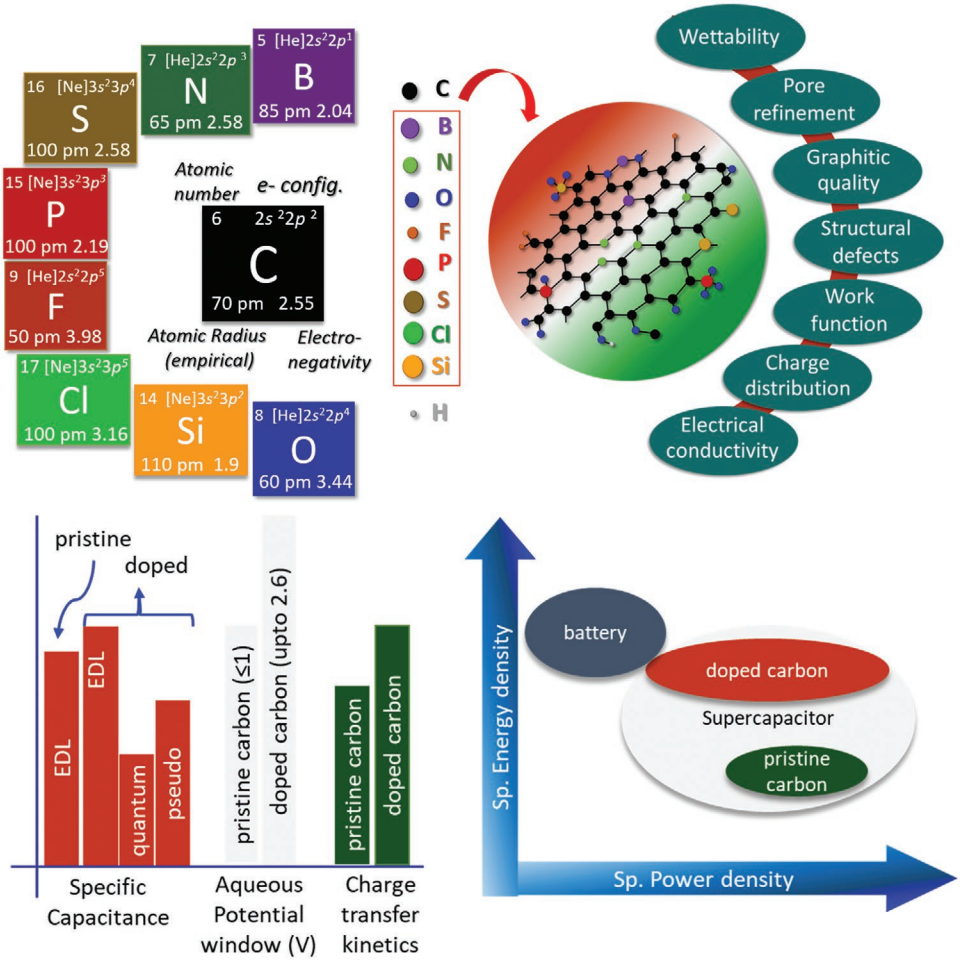

Figure 3. Focus and scope of the review. Schematic of carbon doping and its influences on the physicochemical properties for energy storage applications.

4. Single-Element Doping

In this section, the influence of single element doping on the supercapacitive properties of nanocarbons is examined. We will start from a few key considerations summarized below.

- The presence of oxygen functional groups on carbon surfaces is inevitable due to moisture absorption or synthesis procedure which is not considered as oxygen-functionalization. Here, the effect of single element doping on pristine or doped nanocarbons is discussed where the pristine or doped nanocarbons are considered as a single entity and only one foreign functional element is controlled by tuning the process parameters. Reduced graphene oxide (rGO) is an example of an energy material where nitrogen doping has been carried out in a controlled manner and their supercapacitive properties are discussed although rGO itself intrinsically contains oxygen.[89] For the codoping, more than two foreign atoms are controlled simultaneously during the synthesis as discussed in Section 5.
- Importantly, we mentioned the technique to evaluate the supercapacitor performance of electrode for each study as 3E in case of 3-electrode with respect to the associated reference electrode and 2E in case of 2-electrode system, since the 3-electrode set up is commonly used to evaluate the performance of active materials where the results from 2E test reflects its practicality in real-world applications.[90] We have nonetheless included parameters from 3E-tests because they are reported in the cited references, in part to show the changes in the electrochemical performance of nanocarbons after doping.
- The quantification of parameters such as rate performance and cycle-life is performed using published data in the relevant figures of the cited references if not presented explicitly in the respective references.
- Since the graphene and GO or rGO are different in definition and physical properties,[91] wherever applicable we use the term "rGO" even if the cited references name it graphene.
- Decorating nanocarbons by metal particles like Ag, Cu, etc., although is sometimes termed as "doping" in literature,[92] are not considered as doping since the definition of doping in the matrix is conventionally used for the case where a heteroatom replaces an atom in the matrix, or addition of a heteroatom takes place in the lattice with charge contribution. Although these metal nanoparticles could be considered as "heteroatoms" for

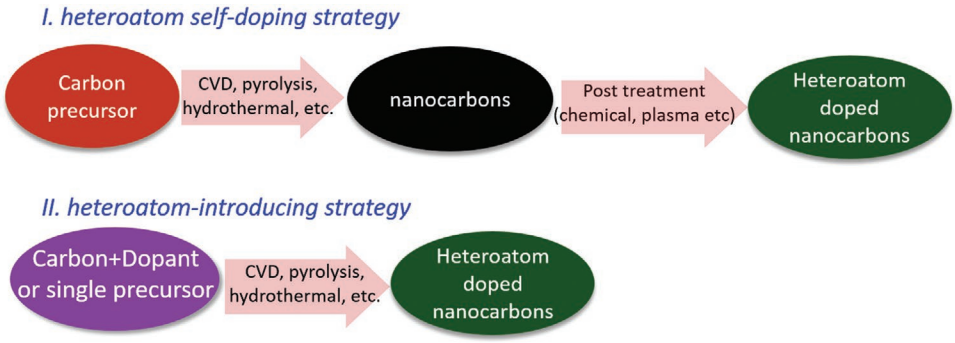

Figure 4. Common approaches for synthesizing heteroatom doped nanocarbons.

the carbon matrix, we believe the most appropriate term in this case is "decoration with metal nanoparticles."[93–96]

The doped and functionalized carbon nanostructures are extensively synthesized by various techniques which is outside the scope of the present review. The adsorption energy of boron (–1.268 eV), Si (–1.244 eV), and nitrogen (–2.372 eV) on the pristine graphene ensures the stable adsorption of adatoms on graphene.[97] It is noteworthy that there are different preferable sites for the adsorption on the graphene matrix depending on the dopant type. For example, bridge sites are most favorable for N-adsorption whereas top sites are better for other adatoms.[97] The dopant concentration, doping configuration, geometry of the grown structure, and their physical properties can be controlled by the process parameters to tune their supercapacitor performances. A broader account of the synthesis of doped nanocarbons can be found elsewhere.[45,73,98–101] In general, the heteroatom functionalization and doping are carried out using the following two strategies (**Figure 4**).

a) *Heteroatom-introducing strategy* where heteroatoms are introduced into carbon matrix by post-treatment of the already formed carbon structures, including chemical activation, heat treatment under relevant atmosphere, microwave irradiation, plasma functionalization, etc.
b) *Heteroatom self-doping strategy* where both carbon and heteroatom precursors or the precursors containing both carbon and heteroatom elements are subjected to the synthesis process.

Importantly, the use of natural precursors to synthesize doped nanocarbons finds significant attention since they may contain multidopants while the process are inexpensive, environment-friendly, and industrially feasible.[102–106]

4.1. Boron Doping

Boron has been explored as a promising substituent foreign atom, which can introduce a hole in the carbon framework and act as an electron acceptor. The three valence electrons of Boron cause the Fermi level shift toward the valence band and result in higher charge carrier concentration and density of states at the Fermi level, collectively enhancing the supercapacitive properties.[107]

4.1.1. Role of B-Configurations and B-Content

The B-doping is relatively simple and easy since the electronegativity of boron is 2.04 which is lower than that of carbon (2.55) and hence the binding energy of B—C bonds is lower compared to C—C bonds. While boron is doped into the carbon matrix, the π electrons are redistributed which softens the C—C bonds and strengthens the C—O bonds upon oxygen adsorption.[107] The possible bonding configurations of boron with carbon are BC_3, BC_2O, and BCO_2. The corresponding schematic and relevant X-ray photoelectron (XP) spectra of B-doped rGO are presented in **Figure 5**A–C.[108] The role of each configuration in the physicochemical properties and hence the electrochemical capacitor properties are discussed here. BC_3 and BC_2O enhance electrical conductivity of the electrode and redox properties, while interfacial redox reactions on carbon surface are induced by BC_2O and B_2O_3.[109,110] The reactive B–O groups make the surface hydrophilic and lead to the higher electrochemically active surface area, although the measured BET surface area is found to be lower in B-doped carbon structures than in its pristine counterpart.[111] Although B-doped mesoporous rGO (B-rGO) exhibits higher gravimetric capacitance of 336.4 F g^{-1} at 0.1 A g^{-1} in 6 M KOH versus a saturated calomel electrode (SCE), the rate performance is poor with respect to the rGO and calcined B-rGO under the same test conditions (**Table 1**). We can thus argues that the observed higher rate performance of calcined B-rGO than of the rGO and B-rGO can be attributed to the higher surface area and lower pseudocapacitive contribution, which is consistent with literature.[110]

The rich physical properties of B-doped nanocarbons help improve their supercapacitive properties. For instance, threefold enhancement in the gravimetric capacitance (448 F g^{-1} at 100 mV s^{-1} in 6 M KOH, 3E) and 108% retention after 3000 scans at 50 mV s^{-1} of thermally annealed GO after 6.04 ± 1.44 at% boron incorporation is related to the enhanced electrical conductivity and defect-like pore formation in the carbon framework.[114] Whereas, an almost equal amount of gravimetric capacitance (446.24 F g^{-1} at 0.5 A g^{-1} in 6 M KOH, 3E) with 53% rate capability at 20 A g^{-1} and 87% retention after 1000 charge–discharge cycles for B-doped rGO is obtained with only 1.4 at% B-content.[115] Interestingly, the mixture of GO and boric acid was treated by dielectric barrier discharge plasma, which results in boron atoms incorporation in sp^3-C defect sites and subsequent restoration of sp^2-C hybridized

Table 1. Physicochemical properties of heteroatom doped nanocarbons compared to pristine counterparts (supercapacitor parameters are from 3E test device configuration with respect to the associated reference electrode unless mentioned otherwise).

Ref.	Nanocarbons	BET surface area [$m^2 g^{-1}$], pore volume [$cm^3 g^{-1}$], avg. pore diameter [nm]	Contact angle [°]	Intensity ratio of Raman bands D–G (I_D/I_G)	Atomic percentage of from XPS	Interlayer spacing from XRD [nm]	Electrical conductivity or sheet resistance	Gravimetric/volumetric/areal capacitance, rate performance and cycle stability, charge-transfer resistance, electrolyte
[110]	Mesoporous rGO (MrGO)	864, 0.932	–	1.06	–	0.35	–	148.9 F g^{-1} at 0.1 A g^{-1}, 53.1% at 5 A g^{-1}, 0.17 Ω, 6 M KOH
	B-MrGO	997, 1.158	–	1.14	C/O/B: 70.6/16.4/12.9	0.361	–	336.4 F g^{-1} at 0.1 A g^{-1}, 31.5% at 5 A g^{-1} 93% after 5k cycles in, 0.11 Ω, 6 M KOH
	Calcined B-MrGO	1102, 1.175	–	1.27	C/O/B: 73.3/15.1/11.5	0.362	–	169.3 F g^{-1} at 0.1 A g^{-1}, 64.5% at 5 A g^{-1}, 98% after 5k cycles, 0.08 Ω, 6 M KOH
[163]	Pristine-MWCNT	–	113.84 Water	1.22	–	–	–	61.46 F g^{-1} at 100 mV s^{-1}, 4.99 Ω, 1 M Na_2SO_4
	Microwave treated MWCNT	–	36.48 Water	1.26	–	–	–	214.45 F g^{-1} at 100 mV s^{-1}, 4.87 Ω, 1 M Na_2SO_4
	O_2-Plasma treated MWCNT	–	19.87 Water	1.42	–	–	–	238.23 F g^{-1} at 100 mV s^{-1}, 4.18 Ω, 99.13% after 50 cycles, 1 M Na_2SO_4
[164]	Biochar	440, 0.455, 4.8	–	0.95	C/O: 77.61/9.86	–	–	60.4 F g^{-1} at 20 mV s^{-1}, 8.2 Ω, 6 M KOH
	O_2-plasma activated Biochar	654, 0.936, 4.9	–	>1.8	C/O: 79.25/15.69	–	–	171.4 F g^{-1} at 20 mV s^{-1}, 3.3 Ω, 6 M KOH
	NaOH- activated biochar	1144, 0.550, 2.3	–	0.82	C/O: 84.85/12.86	–	–	99.5 F g^{-1} at 20 mV s^{-1}, 14.5 Ω, 6 M KOH
[165]	rGO-RT	213.7	–	1.07	O1s/C1s ratio: 24.34	0.363	3.6 S cm^{-2}	187.9[a] F g^{-1} (0.88 mF cm^{-2})[a] at 50 mV s^{-1}, 1 M H_2SO_4
	rGO-200 °C	264.4	–	1.095	O1s/C1s ratio: 19.07	0.361	6.32 S cm^{-2}	225 F g^{-1} (1.19 mF cm^{-2}) at 50 mV s^{-1}, 1 M H_2SO_4
	rGO-1000 °C	432.8	–	1.2	O1s/C1s ratio: 4.34	0.338	20.93 S cm^{-2}	81.8[a] F g^{-1} (0.4 mF cm^{-2})[a] at 50 mV s^{-1}, 1 M H_2SO_4
[166]	rGO-800 °C	335	≈50 Water	1.66	C/O/P: 95.69/4.31/0	0.3351	–	57 F g^{-1} at 1 A g^{-1}, 75.5% at 30 A g^{-1}, 42.5% after 20k cycles, 6 M KOH (2E)
	P-doped rGO-800 °C	327	14.3 Water	1.68	C/O/P: 93.16/4.9/1.93	0.359	–	72 F g^{-1} at 1 A g^{-1}, 80.4% at 30 A g^{-1}, 62.2% after 20k cycles, 6 M KOH (2E)
	passivated P-doped RGO-800 °C	420	–	1.52	C/O/P: 90.2/6.95/2.85	0.3738	–	108 F g^{-1} at 1 A g^{-1}, 89.2% at 30 A g^{-1}, 70.4% after 20k cycles, 6 M KOH (2E)
[167]	CNF	404.12, 0.18	–	–	–	–	0.24 S cm^{-1}	56.96 F g^{-1} at 1 mA cm^{-2}, 48%[a] at 20 mA cm^{-2}, 2.9 Ω, 6 M KOH
	Si-CNF	420.33, 0.28	–	–	–	–	0.35 S cm^{-1}	88.99 F g^{-1} at 1 mA cm^{-2}, 77%[a] at 20 mA cm^{-2}, 81% at 1 mA cm^{-2} after 100 cycles, 1.56 Ω, 6 M KOH
	Si-CNF/ graphene	437.64, 0.26	–	–	C/Si/O: 88.97/4.97/6.96	–	0.40 S cm^{-1}	144.79 F g^{-1} at 1 mA cm^{-2}, 78.6%[a] at 20 mA cm^{-2}, 46% at 1 mA cm^{-2} after 100 cycles, 0.61 Ω, 6 M KOH
[71]	Nanoporous carbon (NC)	455	88.9 in $TEABF_4$	–	C/O/F 82.9/17.1/0	–	–	–
	F-rich NC1	1400	–	–	C/O/F: 84.7/7.5/7.8	–	–	56 F g^{-1} at 0.5 A g^{-1}, 58%[a] at 10 A g^{-1}, 66.7%[a] after 10k cycles, ≈6.81 Ω[a], $TEABF_4$/PC (2E)
	F-rich NC4	3231	55.1 in $TEABF_4$	–	C/O/F: 73.3/8.7/17.5	–	–	168 F g^{-1} at 0.5 A g^{-1}, 91% at 10 A g^{-1}, 91.5%[a] after 10k cycles, ≈2.59 Ω[a], $TEABF_4$/PC (2E)
[168]	OMC with few-layered graphene (OMG)	1991, 1.27, 3.59	124 (water); 131 (1 M H_2SO_4); 103 (6 M KOH)	1.4	C/O/Cl: 88.45/9.85/0.7	–	7.9	179 F g^{-1} at 0.5 A g^{-1}, 81.2%[a] at 10 A g^{-1} (3E), 108% after 10k cycles, 0.88 Ω (2E), 1 M H_2SO_4

Table 1. Continued.

Ref.	Nanocarbons	BET surface area [$m^2 g^{-1}$], pore volume [$cm^3 g^{-1}$], avg. pore diameter [nm]	Contact angle [°]	Intensity ratio of Raman bands D–G (I_D/I_G)	Atomic percentage of from XPS	Interlayer spacing from XRD [nm]	Electrical conductivity or sheet resistance	Gravimetric/volumetric/areal capacitance, rate performance and cycle stability, charge-transfer resistance, electrolyte
								183[a] F g^{-1} at 0.5 A g^{-1}, 107%[a] at 10 A g^{-1} (3E), 103% after 10k cycles (2E), 6 M KOH
	Cl-doped OMG	1882, 1.24, 3.62	123 (water); 133 (1 M H_2SO_4); 129 (6 M KOH)	1.17	C/O/Cl: 88.6/9.4/1.91	–	7.7	250 F g^{-1} at 0.5 A g^{-1}, 99.6%[a] at 10 A g^{-1} (3E), 109% after 10k cycles, 0.44 Ω (2E), 1 M H_2SO_4
								220 F g^{-1} at 0.5 A g^{-1}, 101.8% at 10 A g^{-1} (3E), 116% after 10k cycles (2E), 6 M KOH
[116]	3D-CNF	338, 1.432, 20.8	–	–	–	–	–	88 F g^{-1} (26 μF cm^{-2}) at 0.5 A g^{-1}, 48.86% at 5 A g^{-1}, 91.5% after 10k cycles, 0.91 Ω, 2 M KOH
	3D-N-CNF	79.6, 0.349, 18.5	26.9 in water	1.08	C/O/N/B: 84.04/6.14/9.82/0	–	–	126 F g^{-1} (83.9 μF cm^{-2}) at 0.5 A g^{-1}, 37.9% at 5 A g^{-1}, 91.1% after 10k cycles, 0.9 Ω, 2 M KOH
	3D-BN-CNF	351.5, 1.789, 20.3	0 in water	0.95	C/O/N/B: 80.6/6.86/11.24/1.3	–	–	295 F g^{-1} (158.2 μF cm^{-2}) at 0.5 F g^{-1}, 49.8% at 5 A g^{-1}, 94.5% after 10k cycles, 0.39 Ω, 2 M KOH
[73]	Precarbonized carbon	<10, 0.012	–	–	C/O/N/S: 76.88/9.37/13.30/0.45	–	–	60 F g^{-1} (196 mAh g^{-1}, 70 F cm^{-3}, 1 mF cm^{-2}) at 0.5 A g^{-1}, 5.4%[a] at 100 A g^{-1}, 3.2 Ω, 2 M KOH
	N,O-AC-500 °C	505, 0.37	–	2.41	C/O/N: 79.51/ 14.23/6.26	0.349	–	743 F g^{-1} (144 mAh g^{-1}, 639 F cm^{-3}, 147.1 μF cm^{-2}) at 0.5 A g^{-1}, 5.2% at 50 A g^{-1}, 1.75 Ω, 2 M KOH
	N,O-AC-600 °C	3289, 1.565	–	3.68	C/O/N: 89.11/ 3.54/7.35	0.351	–	524 F g^{-1} (84 mAh g^{-1}, 351 F cm^{-3}, 15.9 μF cm^{-2}) at 0.5 A g^{-1}, 55%[a] at 100 A g^{-1}, 1.23 Ω, 2 M KOH
	N,O-AC-800 °C	2866, 1.257	–	4.62	C/O/N: 93.35/ 6.00/0.65	0.358	–	304 F g^{-1} (17 mAh g^{-1}, 222 F cm^{-3}, 10.6 μF cm^{-2}) at 0.5 A g^{-1}, 64%[a] at 100 A g^{-1}, 0.72 Ω, 2 M KOH
[169]	Si/P codoped carbon-1 (SiPDC-1)	530.36, 0.27, 3.021	–	1.5	C/O/Si/P: 76.5/17.72/3.64/2.14	–	–	201 F g^{-1} (0.38 F m^{-2}) at 5 mV s^{-1}, 60%[a] at 100 mV s^{-1}, 1 M H_2SO_4
								198 F g^{-1} (0.37 F m^{-2}) at 5 mV s^{-1}, 66% at 100 mV s^{-1}, 6 M KOH
	SiPDC-2	641.51, 0.33, 4.188	–	1.28	C/O/Si/P: 58.84/28.14/8.8/4.2	–	–	276 F g^{-1} (0.43 F m^{-2}) at 5 mV s^{-1}, 79%[a] at 100 mV s^{-1}, 91% after 2k cycles, 1 M H_2SO_4
								244 (0.38 F m^{-2}) at 5 mV s^{-1}, 81% at 100 mV s^{-1}, 94% after 2k cycles, 6 M KOH
	SiPDC-3	478.52, 0.24, 3.055	–	1.57	C/O/Si/P: 64.3/25.37/8.01/2.24	–	–	147 F g^{-1} (0.31 F m^{-2}) at 5 mV s^{-1}, 62%[a] at 100 mV s^{-1}, 1 M H_2SO_4
								146 (0.31 F m^{-2}) at 5 mV s^{-1}, 42% at 100 mV s^{-1}, 6 M KOH
[72]	ONS-C-600 °C	1395, 0.75	34	0.97	O/N/S:15.93/ 5.12/5.44	–	–	259 F g^{-1}[a] at 1 A g^{-1}, 60.6%[a] at 20 A g^{-1} in KOH
	ONS-C-700 °C	2917, 2.40	48	0.92	O/N/S: 9.94/ 1.60/3.31	–	–	409 F g^{-1} at 1 A g^{-1}, 66.5%[a] at 20 A g^{-1}, 90.4% after 20k cycles in KOH
	ONS-C-800 °C	2377, 1.65	53	0.89	O/N/S: 9.21/ 0.64/1.04	–	–	362 F g^{-1}[a] at 1 A g^{-1}, 62.6% at 20 A g^{-1}
	ONS-C-900 °C	2042, 1.49	56	0.85	O/N/S: 6.53/ 0.61/2.71	–	–	315 F g^{-1}[a] at 1 A g^{-1}, 60.6%[a] at 20 A g^{-1}

Table 1. Continued.

Ref.	Nanocarbons	BET surface area [$m^2 g^{-1}$], pore volume [$cm^3 g^{-1}$], avg. pore diameter [nm]	Contact angle [°]	Intensity ratio of Raman bands D–G (I_D/I_G)	Atomic percentage of from XPS	Interlayer spacing from XRD [nm]	Electrical conductivity or sheet resistance	Gravimetric/volumetric/areal capacitance, rate performance and cycle stability, charge-transfer resistance, electrolyte
[80]	GO nanoribbons (GNR)	110, 0.32, 5.6	–	0.9	C/O: 72.8/27.2	–	–	91 F g^{-1} at 0.5 A g^{-1}, 3.2 Ω, 1 M Na_2SO_4
	N-doped GNR	245, 0.91, 8.5	–	1.0	C/O/N/S: 87/6.1/6.9/0	–	–	289 F g^{-1} (214 F cm^{-3}) at 0.5 A g^{-1}, 37% at 20 A g^{-1}, 2.1 Ω, 1 M Na_2SO_4
	S-doped GNR	197, 0.85, 7.3	–	1.05	C/O/N/S: 92.5/6.0/0/1.5	–	–	227 F g^{-1} (161 F cm^{-3}) at 0.5 A g^{-1}, 23% at 20 A g^{-1}, 1.8 Ω, 1 M Na_2SO_4
	NS-doped GNR	312, 1.07, 8.9	–	1.1	C/O/N/S: 83.3/5.7/7.2/3.8	–	–	442 F g^{-1} (283 F cm^{-3}) at 0.5 A g^{-1}, 57.5% at 20 A g^{-1}, 98.6% after 10k cycles, 0.9 Ω, 1 M Na_2SO_4
[102]	P/N-doped carbon-1	362.82, 0.2, 3.605	–	1.44	C/O/N/P: 87.46/9.31/1.16/2.06	–	–	117 F g^{-1} (0.32 F m^{-2}) at 5 mV s^{-1}, 24% at 100 mV s^{-1}, 1 M H_2SO_4
								270 F g^{-1} (0.42 F m^{-2}) at 5 mV s^{-1}, 38% at 100 mV s^{-1}, 6 M KOH
	P/N-doped carbon-2	648.54, 0.4, 3.464	–	1.39	C/O/N/P: 86.09/10.74/1.13/2.04	–	–	184 F g^{-1} (0.25 F m^{-2}) at 5 mV s^{-1}, 58% at 100 mV s^{-1}, 98% after 2k cycles, 1 M H_2SO_4
								209 F g^{-1} (0.32 F m^{-2}) at 5 mV s^{-1}, 55% at 100 mV s^{-1}, 98% after 2k cycles, 6 M KOH
	P/N-doped carbon-3	999.67, 0.57, 3.161	–	1.55	C/O/N/P: 85.51/10.82/1.47/2.20	–	–	286 F g^{-1} (0.29 F m^{-2}) at 5 mV s^{-1}, 21% at 100 mV s^{-1}, 1 M H_2SO_4
								118 F g^{-1} (0.12 F m^{-2}) at 5 mV s^{-1}, 47% at 100 mV s^{-1}, 6 M KOH
[170]	N/P-CNF	7.78	–		C/N/O/P: 77.94/7.55/10.94/3.58	0.349	–	212 F g^{-1} at 0.5 A g^{-1}, 73%[a] at 30 A g^{-1}, 1 M H_2SO_4
	N/P/Si-CNF-5	10.94	–		C/N/O/Si/P: 77.21/7.93/11.05/0.6/3.21	0.356	–	243.7 F g^{-1} (253.4 F cm^{-3}) at 0.5 A g^{-1}, 83% at 30 A g^{-1}, 110% after 8k cycles, 1 M H_2SO_4
	N/P/Si-CNF-15	8.49	–		C/N/O/Si/P: 72.95/6.85/15.77/1.99/2.44	0.363	–	224.9 F g^{-1} at 0.5 A g^{-1}, 76%[a] at 30 A g^{-1}, 1 M H_2SO_4
[171]	Carbon cloth	–	129	0.742	–	–	0.813 Ω $sq.^{-1}$	–
	N-doped porous carbon	–	55	0.952	C/O/N: 93.18/4.48/2.34/	–	0.58 Ω $sq.^{-1}$	258.4 F g^{-1} at 1 A g^{-1}, 79.6% at 20 A g^{-1}, 1 M H_2SO_4
								263.4 F g^{-1} at 1 A g^{-1}, 74.8%[a] at 20 A g^{-1}, 6 M KOH
	N,S-doped porous carbon	–	111	0.969	C/O/N/F/S: 91.51/6.34/1.32/0/0.82	–	0.534 Ω $sq.^{-1}$	246.5 F g^{-1} at 1 A g^{-1}, 82.8% at 20 A g^{-1}, 1 M H_2SO_4
								213.3 F g^{-1} at 1 A g^{-1}, 84.5%[a] at 20 A g^{-1}, 6 M KOH
	N,F-doped porous carbon	–	72	1.032	C/O/N/S/B: 92.93/4.72/0.26/1.42/0.68	–	0.447 Ω $sq.^{-1}$	311.5 F g^{-1} at 1 A g^{-1}, 87.8% at 20 A g^{-1}, 1 M H_2SO_4
								309.3 F g^{-1} at 1 A g^{-1}, 81.3%[a] at 20 A g^{-1}, 6 M KOH
	N,S,B-doped porous carbon	–	42	0.961	C/O/N/F: 90.1/6.72/2.83/0.35	–	1.275 Ω $sq.^{-1}$	281.6 F g^{-1} at 1 A g^{-1}, 82.1% at 20 A g^{-1}, 1 M H_2SO_4
								273.7 F g^{-1} at 1 A g^{-1}, 73.5%[a] at 20 A g^{-1}, 6 M KOH
	N,F,B-doped porous carbon	–	24	0.945	C/O/N/F/B: 88.67/6.50/4.00/0.30/0.53	–	0.783 Ω $sq.^{-1}$	350.3 F g^{-1} at 1 A g^{-1}, 83.2% at 20 A g^{-1} in 1 M H_2SO_4, 100% after 10k cycles
								356.3 F g^{-1} at 1 A g^{-1}, 81.2%[a] at 20 A g^{-1}, in 6 M KOH

Table 1. Continued.

Ref.	Nanocarbons	BET surface area [$m^2 g^{-1}$], pore volume [$cm^3 g^{-1}$], avg. pore diameter [nm]	Contact angle [°]	Intensity ratio of Raman bands D–G (I_D/I_G)	Atomic percentage of from XPS	Interlayer spacing from XRD [nm]	Electrical conductivity or sheet resistance	Gravimetric/volumetric/areal capacitance, rate performance and cycle stability, charge-transfer resistance, electrolyte
[172]	N,P,Si doped carbon-1	471.04, 0.25, 2.792	–	–	C/O/N/P/Si: 56.78/28.73/2.15/2.34/10.00	–	0.027 S cm^{-1} with binder	144 F g^{-1} (0.31 F m^{-2}) at 5 mV s^{-1}, 75% at 100 mV s^{-1} in 1 M H_2SO_4
								318 F g^{-1} (0.67 F m^{-2}) at 5 mV s^{-1}, 68% at 100 mV s^{-1} in 6 M KOH
	N,P,Si doped carbon-2	228.4, 0.15, 3.424	–	1.21	C/O/N/P/Si: 30.54/46.55/1.92/3.65/17.34	–	0.003 S cm^{-1} with binder	169 F g^{-1} (0.74 F m^{-2}) at 5 mV s^{-1}, 63% at 100 mV s^{-1}, 1 M H_2SO_4
								213 F g^{-1} (0.93 F m^{-2}) at 5 mV s^{-1}, 70% at 100 mV s^{-1}, 6 M KOH
	N,P,Si doped carbon-3	231.28, 0.17, 3.875	–	–	C/O/N/P/Si: 27.14/54.17/0.56/0.88/17.25	–	0.000 S cm^{-1} with binder	66 F g^{-1} (0.28 F m^{-2}) at 5 mV s^{-1}, 88% at 100 mV s^{-1}, 1 M H_2SO_4
								24 F g^{-1} (0.10 F m^{-2}) at 5 mV s^{-1}, 56% at 100 mV s^{-1}, 6 M KOH

[a]Extracted and/or calculated data from the corresponding figure of cited reference.

network.[115] The latter process is called "self-healing" phenomenon which improves the structural properties of doped nanocarbons and hence the electrochemical features. The utilization of B-doped rGO in micro-supercapacitor applications and its corresponding electrochemical behavior is presented in Figure 5D–F. It can be seen that the areal capacitance of B-doped rGO microsupercapacitors starts to decrease after a certain level of B-precursor loading during the growth process.[113]

4.1.2. Inevitable O-Functionalities

Along with the structure and morphology of B-doped nanocarbons,[114,115] Oxygen content or C/O ratio is also different which may also affect the capacitive properties. Moreover, the O-content is often observed to increase in the final carbon structure upon an increase in B-concentration,[107,109,110,116] whereas it is also found to decrease with B-content in some reports.[113,114] However, the improved interfacial capacitance, including the

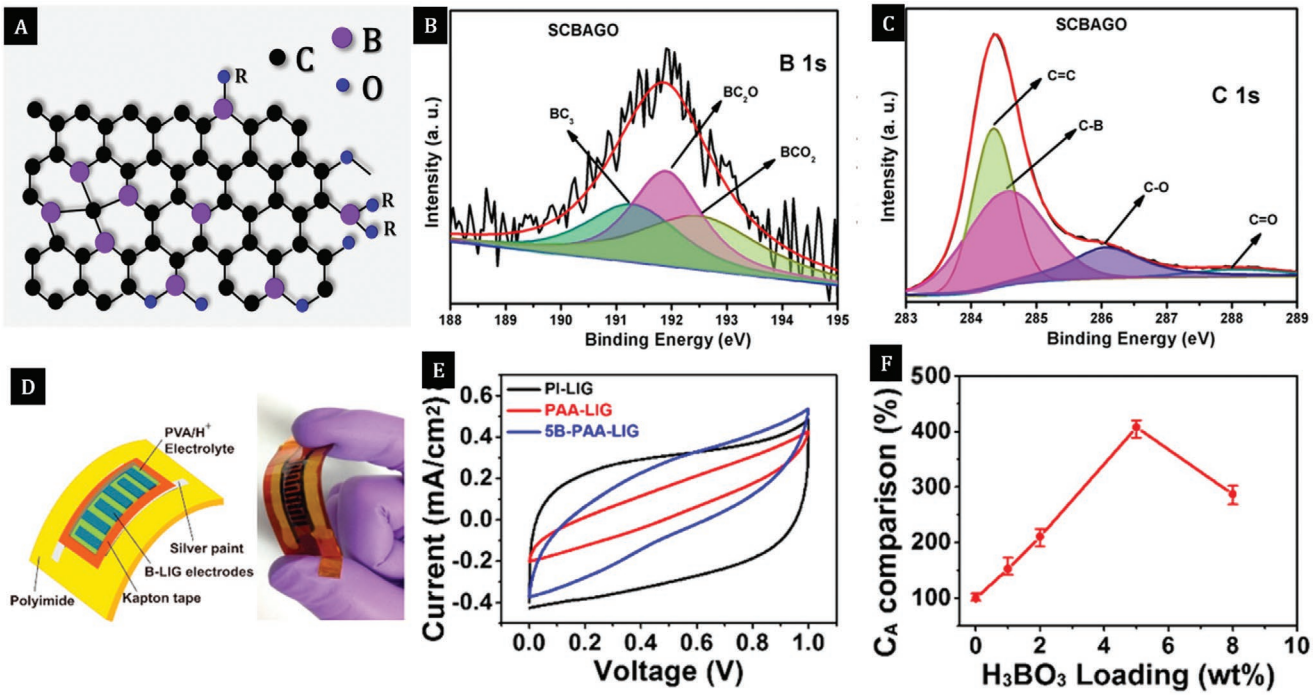

Figure 5. Structural modifications and supercapacitor performance induced by B doping. A) Schematic of possible B configuration in graphene matrix; B) B1s and C) C1s spectra of B-doped rGO. Reproduced with permission.[112] Copyright 2019, Elsevier. Supercapacitor performance of D–F) B-doped laser-induced rGO micro-supercapacitors with the schematic of the device. Reproduced with permission.[113] Copyright 2015, American Chemical Society.

pseudocapacitance and EDL capacitance, of B-doped ordered mesoporous carbon in both acidic and alkaline electrolyte is achieved by the O-functionalities induced pseudocapacitance and the improved EDL capacitance due to the B-substitution.[107] These data suggest that the improved capacitive performance of B-doped nanocarbons is due to the combination of B-doping related physicochemical features and unavoidable O-functionality related changes in the structure.

4.1.3. Wettability and Effect of Electrolyte

The wettability depends on the nature of electrolyte used and functional groups attached on the surface of the electrode, which can be used to improve the electrode–electrolyte interaction and ionic accessibility to the electrode. It has been reported that the wetting angle in 2 M KOH electrolyte drops from 26.9 to zero after B-doping onto N-doped porous carbon nanofiber network.[116] Surface-bonded B-atoms are favorable to attract the anions in electrolyte due to the electron deficiency.[117] Hence, B-doped mesoporous carbon is reported to have a higher gravimetric and interfacial capacitance in 6 M KOH in 3E configurations.[107] On the contrary, N-doping in the B/N codoped porous carbon nanowire arrays only results in the pseudocapacitive contribution in 6 M KOH electrolyte.[118] Apart from KOH and H_2SO_4, B-doped rGO and porous B-doped diamond based symmetric supercapacitor device demonstrated its ability to work with the voltage of 2.4 V in 1 M $NaClO_4$ aqueous electrolyte[112] and 2.6 V in Na_2SO_4,[79] respectively. However, impact of B-doping on capacitive properties is prominent in H_2SO_4 compared to neutral Na_2SO_4.[119] Since the potential window of sp^2-bonded carbons is limited to only 1.2 V in aqueous electrolyte,[120] the focus is shifted to the conductive B-doped diamond owing to their ability to operate in a broader potential window along with notable electrochemical properties.[79,121]

The results examined in this section suggest that in spite of remarkable changes in the properties of B-doped nanocarbons, the specific capacitance mostly remains within a similar range compared to pristine nanocarbons. Therefore, introduction of alternative dopants or codoping may be a likely promising solution, as discussed in the following sections.

4.2. Nitrogen Doping

Nitrogen-doping has been received significant attention to enhance the charge-storage performance of nanocarbons. The functional groups formed by nitrogen with carbon are electrochemically more stable than a carbon-oxygen functional group, can serve as electron donors and are alkaline in nature. The N-doping can improve the wettability, structural quality, electrical conductivity, electrochemically active sites and also provides pseudocapacitance (**Figure 6**).[122–125] In addition,

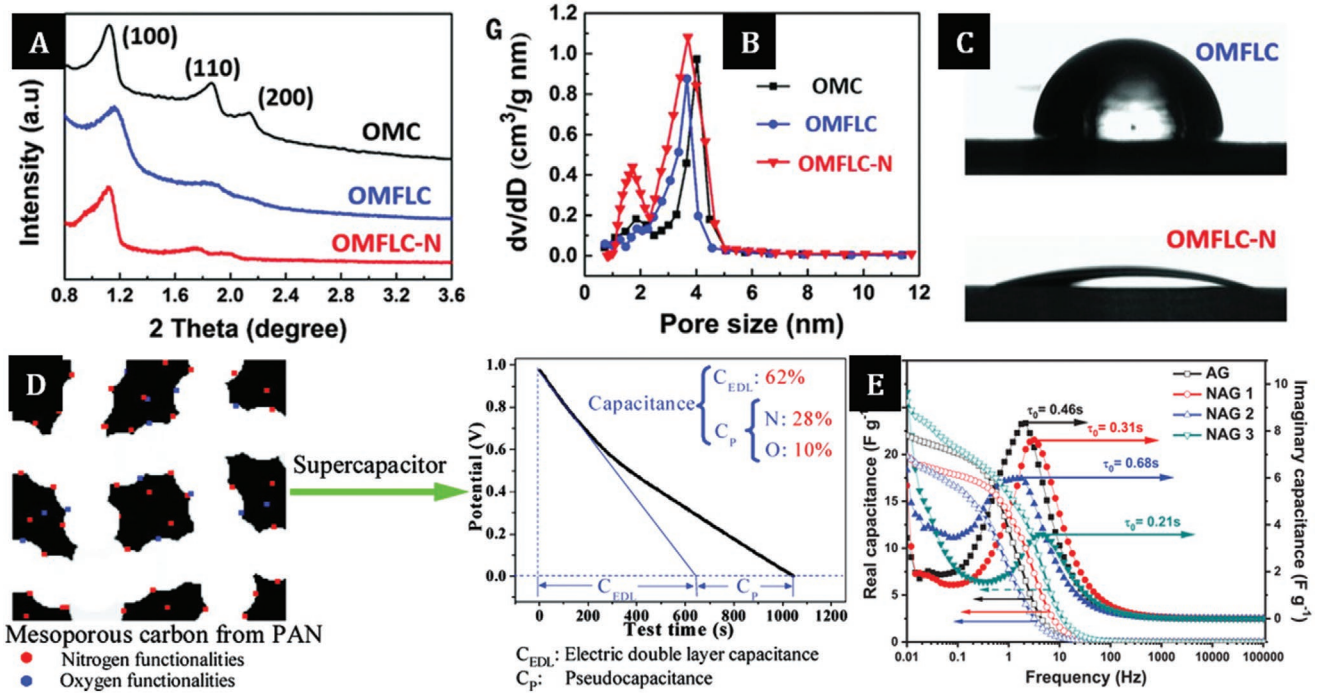

Figure 6. Structural and capacitive features of N-doped nanocarbons. A) Low-angle X-ray diffraction patterns and B) pore size distributions of ordered mesoporous few-layer carbon (OMFLC), OMC, and OMFLC-N; C) wetting angles of 0.5 M H_2SO_4 droplet on OMFLC (85°) and OMFLC-N (S1) (21°) substrates. Reproduced with permission.[66] Copyright 2015, American Association for the Advancement of Science. D) capacitive contribution from nitrogen-enriched nanocarbons with a 3D continuous mesopore structure. Reproduced with permission.[122] Copyright 2010, American Chemical Society. E) Real and imaginary capacitance versus frequency plot with time constant of arc-discharge plasma-fabricated graphene (AG) and N-doped AG. Reproduced with permission.[54] Copyright 2019, Wiley-VCH.

synthesizing N-doped nanocarbons is relatively simple and nitrogen is abundant in nature. The higher electronegativity of N (3.04) compared to carbon (2.55) assists in better electrolyte ion adsorption. Moreover, N-doping in the lattice inhibits the formation of hydrocarbons which are known to form a dielectric dead layer which negatively affects the supercapacitor performance.[58] Furthermore, faster ionic and electronic transport has been observed for N-doped arc-discharge plasma-produced graphene compared to the pristine counterpart.[54] Specifically, the relaxation time constant of the N-doped plasma-produced graphene is found to be only a half of the pristine graphene.[54]

4.2.1. Effect of Nitrogen Content and Atomic Configurations

An enhancement in the specific capacitance of the electrode is found to have a linear relationship with N-content up to 7 wt% in 1 M aqueous H_2SO_4 electrolyte and diluted tetraethylammonium tetrafluoroborate ($TEABF_4$) in propylenecarbonate (PC).[126] Significant efforts have been undertaken to increase the N-content by 29.82 at% in graphitic materials by fluorination (with XeF_2 in Teflon container at 200 °C for 30 h in Ar) followed by the annealing treatment,[37] 45% N/C doped carbons derived from melamine,[127] 21.86 at% in nitrogen-rich carbon nanorod arrays by low-temperature pyrolysis using PANI nanorod arrays and ammonium sulfate,[68] and some other methods. It is important to note that the specific capacitance of N-doped nanocarbons is limited to 128.2 F g^{-1} with 45% N/C,[127] 390 F g^{-1} at 5 A g^{-1} with 29.82 at% N_2,[37] and 203.8 F g^{-1} at 0.1 A g^{-1} with 9.7 at% N_2.[128] In fact, the gravimetric capacitance and surface area has been found to decrease drastically and creates undesirable pore distributions with increasing N-content beyond a limit.[127,129] Importantly, N-doped mesoporous carbon with 8.2 at% N-content shows the highest gravimetric capacitance of 840 F g^{-1} at 1 A g^{-1} (2E).[66] Hence, optimizing N-content in the carbon matrix is highly recommended to obtain the best performance from an electrode. The electron-donor properties of N-doped carbon surface rely on the position of nitrogen atoms in the carbon matrix and the bonding environment. The possible C—N bonds are amides, aromatic amines, protonated amides, pyridine (N-6), pyrrolic-N/pyridone-N (N-5), quaternary/graphitic nitrogen (N-Q), oxidized pyridine-N (N-X), and nitrogen oxide (N-O_x) (**Figure 7**A,B). The presence of N-configurations in the carbon matrix is dependent on the energy supplied during the synthesis. Usually, peripheral bonding like amides, aromatic amines, and protonated amides occurs at low process temperatures with localized charge and they are generally unstable. Whereas, pyridine, pyrrole, aromatic amines, quaternary nitrogen, and protonated pyridine are formed at a relatively higher processing temperature with a delocalized charge and play a crucial role in electrochemical

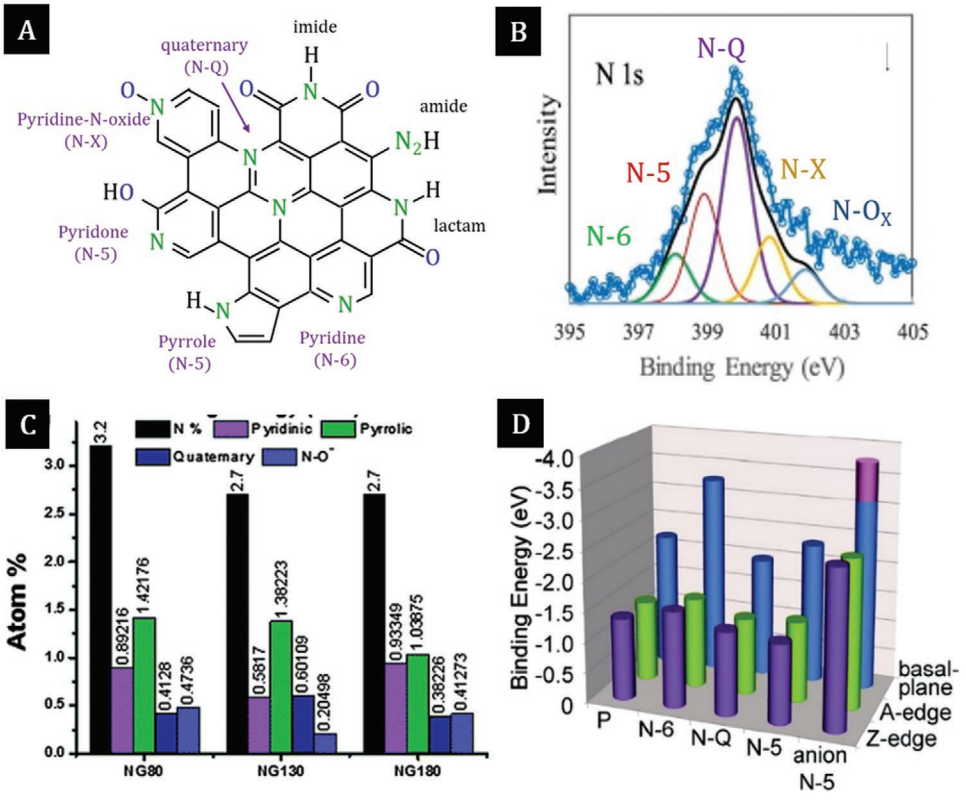

Figure 7. Possible N-bondings with carbon. A) N-configuration in graphene matrix. B) N1s spectra. Reproduced with permission.[131] Copyright 2019, Elsevier. C) Atomic percentage of various N-configurations in N-doped graphene samples. Reproduced with permission.[132] Copyright 2013, The Royal Society of Chemistry. D) Binding energies between K^+-ions and N-configurations. Reproduced with permission.[133] Copyright 2011, American Chemical Society.

performances.[69,130,131] The formation of quaternary nitrogen (N-Q) generally requires high temperatures (above 750 °C) and N-Q is more stable at high carbonization temperatures than the N-group based configurations at the periphery of graphitic structure.[89,122]

Each configuration has a specific role in enhancing the physicochemical properties of the electrode material. The negatively charged pyridinic-N (N-6) has a relatively larger dipole moment that improves the wettability of the electrode and charge transfer kinetics.[87] The pyrrolic-N (N-5), which is also negatively charged, plays a similar role in improving the wettability and pseudocapacitance.[134] The high content of N-6 and N-5 groups of N-rGO (basic in nature) lead to an enhanced charge density and favorable proton adsorption whereas rGO is acidic in nature mostly due to the higher population of the carboxylic groups.[89] Thus, the presence of N-6 and N-5 configurations is attributed for the excellent capacitive properties of N-rich carbon nanorods with the gravimetric capacitance of 707.58 F g^{-1} at 2 A g^{-1} in 1 M H_2SO_4 and 553.12 F g^{-1} KOH at 2 A g^{-1} than in 1 M Na_2SO_4 (3E).[68] The redox reactions of N-6 and N-5 groups are suppressed in the alkaline medium due to the lack of protons in an electrolyte and their basic nature.[89] Since the charge-distribution is different for each N-configuration, they have a difference in reduction/oxidation since, for example, N-X is an oxidizing agent (–0.264*e*) whereas N-6 is a reducing agent (+0.23*e*).[135] Moreover, protonated N-6 (+0.139*e*) can be transformed into N-Q (+0.173*e* to –0.059*e*) during the electrochemical charge storage process.[135] The redox reactions for the N-configurations in the acidic electrolyte are given as follows (Equations (1)–(3))[89,126,135,136]

Pyridinic-N (N-6)

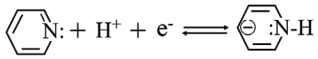

(1)

Pyrrolic-N (N-5)

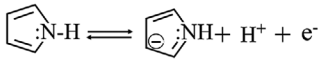

(2)

Pyridone-N (N-X)

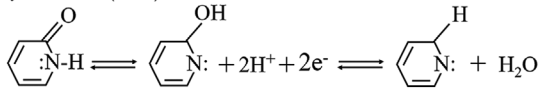

(3)

Unlike in the previous report,[68,89] the gravimetric capacitance of N-doped carbon nanotube (CNT) is found higher in 6 M KOH (160 F g^{-1}) than in 1 M H_2SO_4 (67 F g^{-1}).[137] This observation is attributed to the i) higher pseudocapacitive contribution from the N-6 in basic medium, ii) better interaction with the anions of electrolyte, and iii) EDL formation by structural disorder and the presence of N-Q groups in the carbon structure since N-Q group is positively charged and attracts the electrolyte anions.[137] Interestingly, the K^+ ion adsorption energy is found to follow the following order: N-6 (–2.06 eV) < N-6 with H-terminated dangling bonds (–1.92 eV) < N-O (–1.34 eV) < N-5 (–1.05 eV) < N-Q (–0.8 eV). With the lowest intrinsic resistance, the highest charge carrier concentration and lower K^+ ion adsorption energy, N-5 rich rGO electrode shows better performance in an alkaline electrolyte.[132] Along with these primary N-configurations, it has been shown that the amine group also plays a significant role in enhancing the pseudocapacitance via the redox reaction (Equation (6)).[138] The redox reactions involving the N-configurations in an alkaline medium are as follows[135,138]

Pyrrolic-N (N-5)

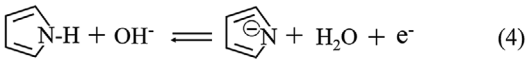

(4)

Pyridinic-N (N-6)

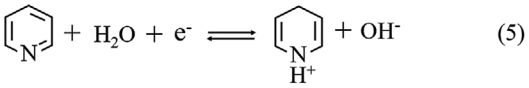

(5)

Amine

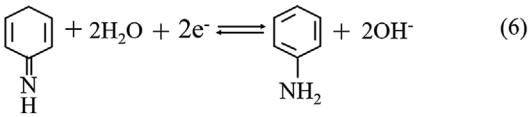

(6)

The positively charged quaternary-N (N-Q) and pyridinic N–O contribute a pair of electrons to the conductive π-system, which results in the improved electron transfer across the electrode–electrolyte interface and enhances the electronic conductivity.[134] The quaternary-N contributes the pseudocapacitance based on the N-Q contribution as estimated from the comparison of XPS results between two N-doped graphene samples.[54] Hence, further investigations are required to clarify the role of N-Q as a pseudocapacitive contributor. Importantly, one can control the presence of specific N-configurations in carbon matrix by tuning the growth parameters. A careful examination of the XPS results reveals a simultaneous increase in the amount of oxygen concentration from 2.69 at% to 4.13 at% along with the N-content (2.25–3.43 at%) in the structure.[54] Therefore, the increased O-content and its corresponding changes in the current scenario could contribute to the improved supercapacitive performance.

Pseudocapacitive features also depend on the specific plane of N-configuration: basal and edge planes (Figure 7D). It has been reported that the Faradaic reactions take place for N-6, N-5, and pyrone oxygen present at the edges.[130] On the other hand, the pyridine-N at basal planes are found to introduce structural defects and hence increase the localized electronic sites in the carbon matrix which results in the higher inner-resistance and lower power capability.[139] It has also been reported that the formation of strong ionic bonding between N-5 and basal plane defects during reversible charge–discharge can reduce the Coulombic efficiency of the system.[133] Contrary to those reports, N-6 and N-5 at the basal plane show the largest binding energy difference which influence the ability to accommodate higher amounts of electrolyte ions at the electrode surface and hence to improve the capacitance. In addition to N-content and specific type of N-bond, the relative ratio between the abundance of N-bonding types is also crucial to obtain the best supercapacitative performance from N-doped nanocarbons.[140] The pseudocapacitive contribution due to N-configurations can be quantified from the relation between the charge density and scan rate as shown in **Figure 8**A,B.[89] A good correlation between the areal concentration of N-6 and N-5 configurations and the interfacial capacitance in 1 M H_2SO_4 is established whereas no correlation is found for N-Q configurations (Figure 8C–F).[141] Moreover, the pseudocapacitive behavior of high N-content carbon

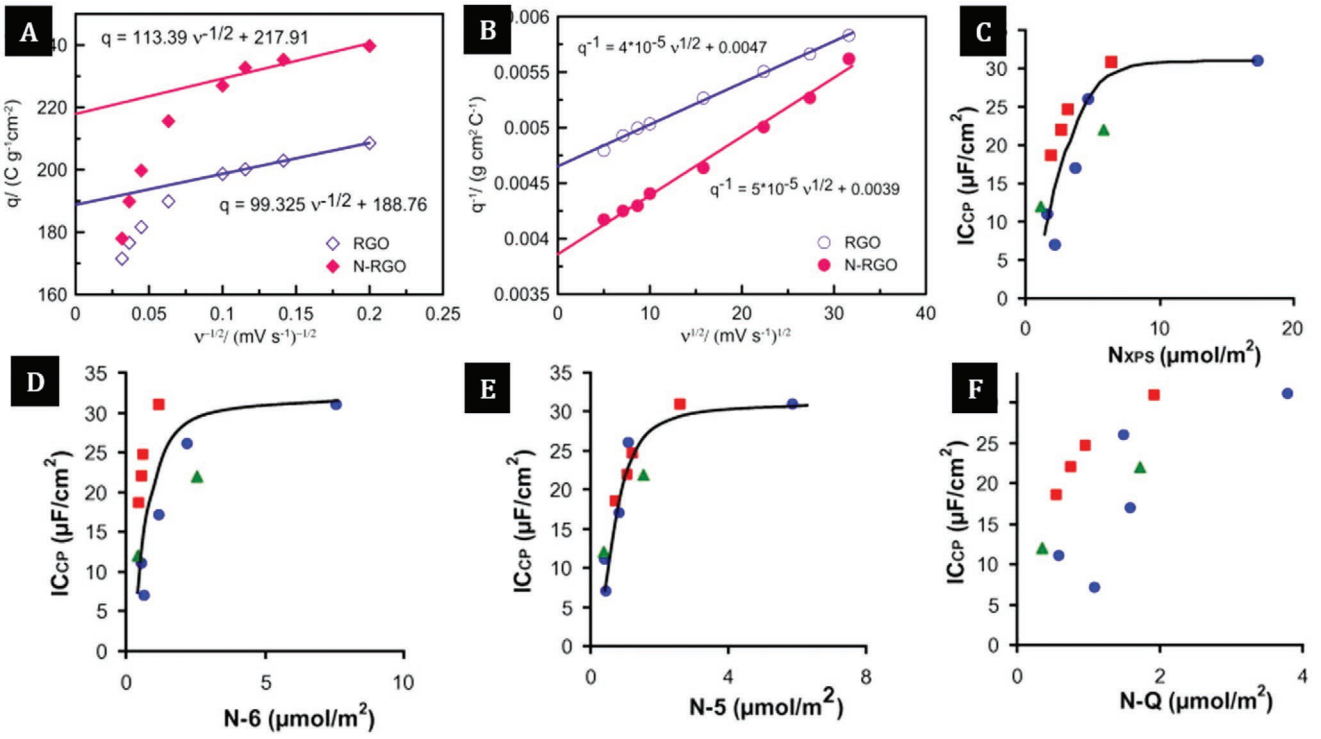

Figure 8. Capacitative performance of N-doped nanocarbons. Dependence of A) q on $\nu^{-1/2}$ and B) $1/q$ on $\nu^{1/2}$ for rGO and N-rGO in 1 M H_2SO_4 (q is the total charge and ν is the scan rate). Reproduced with permission.[89] Copyright, 2012, Elsevier. Interfacial capacitance (IC_{CP}) of N-doped carbon structure at 100 mA g^{-1} in 1 M H_2SO_4 versus areal concentrations of C) nitrogen, D) N-6, E) N-5, and F) N-Q (blue circles are the data from this reference and data represented by other symbol are from the other references). Reproduced with permission.[141] Copyright, 2011, Elsevier.

microspheres appears to be different while they are tested as a positive or a negative electrode in H_2SO_4 electrolyte versus Ag/AgCl. Specifically, when used as a negative electrode, the microspheres display a lower potential range and hence higher capacitance than when used as a positive electrode.[142] This fact can be attributed to the fast and efficient Faradaic reactions between pyridinic-N, pyrrolic/pyridine-N, and H^+ at the negative electrode–electrolyte interface. This information suggests that N-doped nanocarbon can be a choice as a negative electrode needed for the design of next-generation asymmetric supercapacitors.

4.2.2. Quantum Capacitance

The first-principles study shows that the quantum capacitance of N-doped graphene is increased from 94.689 to 279.385 μF cm^{-2} when N/C ratio is decreased from 0.2 to 0.02 in the graphene matrix.[97] Therefore, one needs to pay attention to designing doped nanocarbons with the optimized dopant content such that the quantum capacitance, EDL capacitance and pseudocapacitance are balanced since the total capacitance is a series combination of all of them. Along with structural defects, pyrrolic-N generates a higher DOS(E_F) which boosts the quantum capacitance of the structure.[143,144] Theoretical predictions on the charge-storage performance place the pyridinic-rich carbon structure above the pyrrolic-rich one since the quantum capacitance of pyrrolic-N (N-5) is low irrespective of N-concentration which limits the total capacitance (**Figure 9**A–B).[57] In addition, graphitic-N, and pyridine-N have been found to enhance the quantum capacitance proportionally to the N-concentration.[57] Therefore, the role of N-5 in quantum capacitance and hence total capacitance is a subject of further research.

4.2.3. Influence of Pores

Another significant influencer on the supercapacitive property of N-doped nanocarbons are the pores and porosity associated with any specific N-configuration. For instance, pyridine-N, pyrrolic-N, and quinone-O species with micropores (>1 nm) have a positive influence toward the pseudocapacitance.[134,136] Waste bone derived activated carbon with the higher density of micropores, optimized pore size distribution and pseudocapacitance due to the N-configurations exhibit excellent supercapacitive features.[145] N-doped hollow carbon spheres with open pore structure showed good performance as a supercapacitor electrode due to the high surface area, larger mesoporous channels, suitable pore size distribution, and thin outer shell that ensures the accessibility and pathways for electrolyte ions, as compared to N-doped hollow carbon spheres with the closed and semiclosed pore structure.[146] Hence, tuning the porosity of doped nanocarbons along with controlled N-content and its configuration is an effective means to yield high-performance supercapacitor electrode materials.

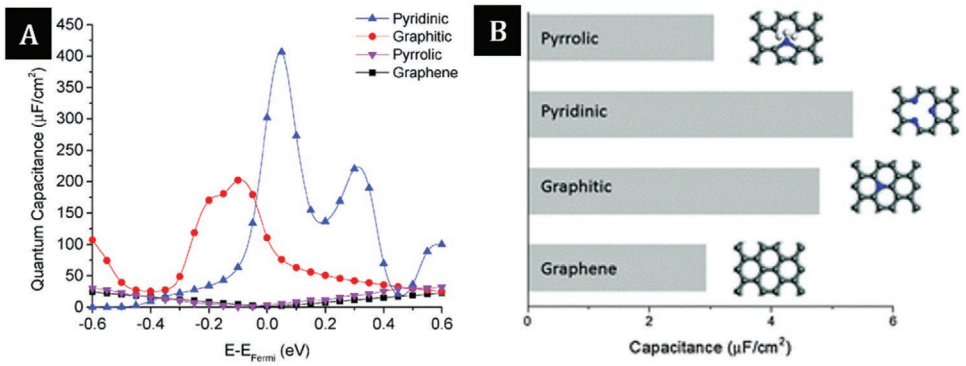

Figure 9. Quantum capacitance. A) Quantum capacitances of N-configurations and B) plot of capacitive contribution from each N-configuration. Reproduced with permission.[57] Copyright 2016, PCCP Owner Societies.

4.2.4. Graphitic Carbon Nitride

With these significant signs of progress and advantageous features in N-doped carbon, graphitic carbon nitride (g-C_3N_4) may be a promising candidate as a supercapacitor electrode.[147] For example, hierarchical N-doped porous carbon covered g-C_3N_4 nanosheets exhibit a gravimetric capacitance of 740 F g^{-1} at 2 A g^{-1} in 1 M H_2SO_4 (3E).[148] Unfortunately, pristine g-C_3N_4 has several flaws like low surface area, poor conductivity, restacking, etc., that limit the power density and energy density of the system.[147]

4.3. Sulfur

Sulfur (S) is also regarded as a promising doping element in a carbon matrix to enhance the physicochemical properties like electrical conductivity and specific capacitance. The increased conductivity after S-doping is due to the overlap of p-orbital between S atom and sp^2-hybridized carbon atoms which form an extended p-system with a filled valence band. Due to the electron-richness of S, the dipole moment is increased upon the application of electric field leading to the enhanced polarization which results in the higher capacitance in the carbon structures according to the following relation[149]

$$\frac{C}{A} = \varepsilon_r \varepsilon_0 / d \quad \text{and} \quad P \propto \varepsilon_r - 1/\varepsilon_r + 2 \tag{7}$$

where ε_r and ε_0 are the electrolyte dielectric constants and dielectric constant of free space, A is the electroactive surface area of electrode, and d is the mean distance of ions to the electrode surface.

4.3.1. Effect of Sulfur Content and Atomic Configurations

The physicochemical properties of nanocarbons also change with doping which is discussed throughout this review and summarized in Table 1. For example, rich S-doped porous carbons with 8.245 wt% (8.102 at%) S-content show the gravimetric capacitance of 350 F g^{-1} at 1 A g^{-1} in 3-E[152] whereas gravimetric capacitance of 445.6 F g^{-1} at 5 mV s^{-1} is reported from the S-incorporated rGO aerogel[153] with just 1.9 at % S-content. Importantly, the former doped nanocarbon also contains 0.554 at% N whereas the latter S-incorporated rGO aerogel contains 5.9 at% oxygen and shows porous structure. Therefore, tuning the structure and balancing the S-content for the specific atomic configurations are crucial to enhance the charge-storage properties of the electrode. However, the amount of S-content in the carbon-matrix is not generally seen as the N-content and/or O-content. For example, thiourea based N/S codoped nanocarbon contains 17.62 wt% of nitrogen but the S-content is only 1.69 wt% at the carbonization temperature of 600 °C and both contents decrease at higher carbonization temperature.[154] Recently, doped mesoporous activated carbon with 9.86 wt% (4.07 at%) S-content has been achieved using the simple hydrothermal method at 600 °C.[155]

Like other dopants, sulfur also bonds with carbon in different configurations, namely thiophene-S (C–S–C), sulfoxide (C–SO_x–C, x = 2–4), sulfone/sulfate group (SO_x) and sulfonic acid, each playing a specific and distinct role in the physicochemical changes in the structure (**Figure 10**A,B). Among these, aromatic sulfides are found to be stable under pyrolysis at 1000 °C whereas SO_2 evolution is observed from sulfone and sulfoxide groups.[149] The sulfoxide group provides pseudocapacitance and improves the hydrophilic nature.[149] The sulfone/sulfate group is related to the pseudocapacitive contribution and hence an improvement in specific capacitance of S-containing porous CNT has been noticed.[156] A 38% enhancement in the specific capacitance (20% in gravimetric capacitance) of S-doped mesoporous carbons is achieved, presumably due to the presence of aromatic sulfide.[149] Furthermore, the 34% enhancement in specific capacitance (72% in gravimetric capacitance) is achieved after introducing sulfoxide and sulfone group into the mesoporous carbons in 6 M KOH electrolyte.[149] On the contrary, a reduction of the sulfate/sulfone group in the matrix is reported to be beneficial because more reversible pseudosites of the doped nanocarbons become available for Faradaic redox reactions in 0.5 M H_2SO_4 electrolyte.[157] Furthermore, S-doped nanocarbons outperform in H_2SO_4 electrolyte in terms of pronounced specific capacitance, long-term stability and rate

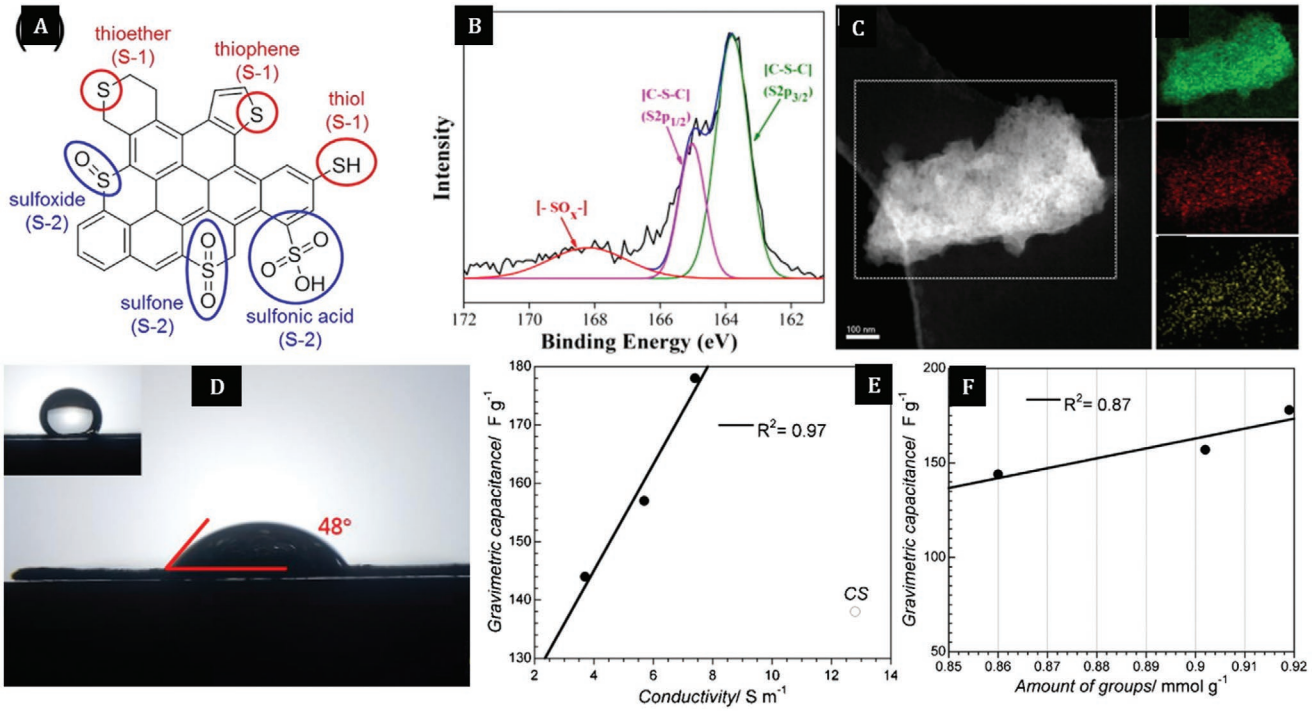

Figure 10. Possible S-bondings with carbons and associated physicochemical changes by S-doping. A) Schematic of possible S-configuration in carbon matrix. Reproduced with permission.[69] Copyright 2015, American Chemical Society. B) S2p spectra of N/S codoped graphene nanoribbons. Reproduced with permission.[80] Copyright 2016, Elsevier. C) HAADF-STEM of oxidative derivatives of 4,4′-thioldiphenol derived mesoporous carbons with C, O, S mapping images. Reproduced with permission.[149] Copyright 2012, Elsevier. D) Water contact angle of S-doped carbon nano-onions ink. Reproduced with permission.[150] Copyright 2019, American Chemical Society. Dependency of specific capacitance of sulfur-doped nanoporous carbons modified by graphene on E) DC conductivity and F) amount of groups (oxygen or sulfur). Reproduced with permission.[151] Copyright 2014, Wiley-VCH.

capabilities.[149,153,158] The proposed redox reactions in H_2SO_4 are as follows[159]

Sulphone group to sulfoxide group

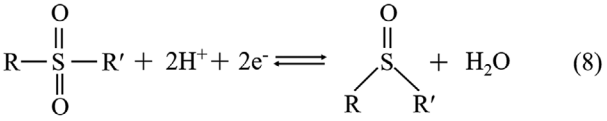

$$R-\overset{\overset{O}{\|}}{\underset{\underset{O}{\|}}{S}}-R' + 2H^+ + 2e^- \rightleftharpoons \overset{\overset{O}{\|}}{S}(R)(R') + H_2O \quad (8)$$

Sulfoxide group to sulfenic acid

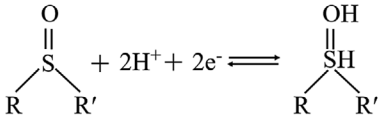

$$\overset{\overset{O}{\|}}{S}(R)(R') + 2H^+ + 2e^- \rightleftharpoons \overset{OH}{\overset{\|}{S}}H(R)(R') \quad (9)$$

Adsorption of proton by sulfenic group

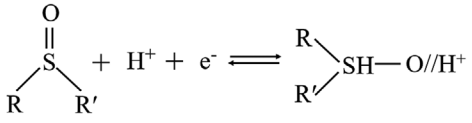

$$\overset{\overset{O}{\|}}{S}(R)(R') + H^+ + e^- \rightleftharpoons R'(R)S{-}O//H^+ \quad (10)$$

The question which still remains unanswered is whether there is any correlation between the specific S-configuration and the nature or pH of the aqueous electrolyte? Likewise, the sulfone group appears to be unstable at higher current densities in 6 M KOH electrolyte.[156] Beside these S-configurations, thiophene-S also improves the surface properties and ion transportations.[149,160] Moreover, the oxidized thiophene-S species, a product of high-temperature oxidation of thiophene-S, is found to be effective in terms of better electrical conductivity, higher rate capability, better structural stability and higher pseudocapacitive contribution.[160] In addition, the positive charge introduced by the thiophene-S group to the neighboring carbon atoms attracts the electrolyte ions and hence an improvement in charge-storage capacity is observed.[150,151]

4.3.2. Influence of Pores

The addition of sulfur prevents pore shrinkage and undesired pore formation.[161] The presence of mesopores along with the high S-content ensures excellent supercapacitor performance by the 1.4 V symmetric device with gravimetric capacitance 137.7 F g^{-1} at 1 A g^{-1} in H_2SO_4 electrolyte and energy density of 9.345 Wh kg^{-1} at 687 W kg^{-1}.[155] Moreover, the presence of sulfur in small pores of nanocarbons brings positive charges which attract anions and facilitate electrode–electrolyte interactions.[151] Thus, S-doped activated carbon structures performs better in terms of gravimetric capacitance and hence energy density in 6 M KOH than in 1 M H_2SO_4 electrolyte.[158] The possible redox reactions in KOH medium are as follows[149]

$$>S-OH + OH^- \leftrightarrow >S=O + 2e^- + H_2O \quad (11)$$

$$>S=O + 2OH^- \leftrightarrow >SOO + 2e^- + H_2O \quad (12)$$

4.3.3. Wettability

The hydrophilic characteristic of S-doped carbon nano-onions ink are shown in Figure 10D. A fully wetted surface in the organic electrolyte has been observed when S-content is high in the S-rich cryogel.[162] S-doped carbon nano-onions with 3.57 at% S-content and 2.86 at% O-content show the water wetting angle of 48°.[150] Generally, a higher amount of sulfur compared to oxygen is evidenced from the XPS results of the S-doped nanocarbons.[153,156,158,160,161] On contrary, the increase in O-content from 5.8 to 12.4 wt% along with sulfoxide and sulfone group introduction is hard to avoid under realistic experimental conditions.[149] Although sulfoxide groups were predicted to impart hydrophilic surface properties,[149] the surface hydrophobicity actually increased after S-incorporation into the carbon matrix.[151] The O-functionalities with 11.5 at% content can be attributed to the hydrophilic nature of S-doped nanoporous carbons rather than the S-content (1.9 at%) and sulfoxide groups.[151] Therefore, the hydrophilic features of S-doped nanocarbons may be partially due to the presence of O-functionalities, yet this point requires further clarification. Hence, the effect of O-functionalities on the capacitance enhancement in mesoporous carbon monolith cannot be ignored. An improvement in the gravimetric capacitance of doped nanocarbons can be achieved by tuning the content of functional groups (oxygen or sulfur), as shown in Figure 10F, although doped nanocarbons possess lower surface area and low pore volume than their pristine counterpart.[151,162] Therefore, it might not be accurate to conclude that the enhanced supercapacitive performance of doped nanocarbons solely owes to the introduction of S-dopant.

Although S-doping is promising, the use of S-based precursor in high-temperature synthesis has safety issues due to volatility of sulfur and toxic nature of byproducts. In addition, the rate capability of S-doped carbon is another issue. This is because the atomic radius of S (100 pm) is larger than that of carbon (70 pm) and hence a significant amount of strain and defect sites are introduced in the carbon matrix.[104] Leakage current is another recurring problem with the S-doped carbon, exacerbated by device degradation due to the presence of sulfone and sulfoxide groups.[154] The leakage current is higher in H_2SO_4 than in neutral electrolyte.[159] Hence, using appropriate electrolyte for S-doped carbon or codoping with other heteroatoms to maximize the benefits of S-doping remains a persistent research question, which we continue to discuss below.

4.4. Phosphorous

From the same group in the periodic table, phosphorous has a larger atomic radius and higher electron-donating ability than Nitrogen. Thus the bond length increases to 1.765 Å and the P atoms protrude out from the graphene plane by 1.19 Å. P-doping into nanocarbons introduces new states around the Fermi level without any shift and enhances the integrated quantum capacitance of P-doped CNTs.[173]

4.4.1. Surface Features and Porosity

The H_3PO_4 activation is a relatively simple approach to synthesize P-doped nanocarbons. In addition to the introduction of P-group in the carbon matrix, the activation process also helps optimize the pores in the structure.[174,175] Along with the doping, internal structures with balanced pore sizes and distribution are essential for rapid and efficient ion transport and better rate performance. Unlike other dopants, the BET surface area, micropore volume and total pore volume of the P-doped nanocarbons are higher compared to the pristine counterpart.[175] Noting the enhanced gravimetric capacitance of 315.2 F g^{-1} at 0.42 A g^{-1} in 6 M KOH (3E), it is important to summarize that P-doping in graphene structures leads to i) distortion of graphene wrinkles due to longer P—C bond than C—C bond which results in the higher surface area, increased inter-layer spacing of GO (≈3.63 Å compared to pristine GO of 3.55 Å), ii) improved electrical conductivity, and iii) induced topological defects.[176] All these changes can be regarded as intentional atomic-scale modifications, and explored to further improve the energy storage performance. Experimental data supporting the positive influence of P-doping on the charge-storage performance of nanocarbon are also reported.[177] Remarkably, the highest gravimetric capacitance of 348.8 F g^{-1} at 5 mV s^{-1} is exhibited by P-doped hierarchical carbon aerogels in 6 M KOH (3E) even at higher mass loading of 60 mg cm^{-2} whereas the gravimetric capacitance is 406.2 F g^{-1} at mass loading of 2 mg cm^{-2}.[178] Supercapacitor performances of doped nanocarbons with higher mass loading (at least 10 mg cm^{-2}) are more appropriate for real-world application.[179,180] To a large extent, the impressive supercapacitive performance of P-doped hierarchical carbon aerogels can be attributed to the higher surface area, abundant pores for easy accessibility of electrolyte ions and active sites provided by the P-dopant. The activated and passivated P-doped carbon structure is found to be electrochemically stable in a wider potential window in aqueous electrolyte even after several charge–discharge cycles.[166,175] In fact, P-doped GO/carbon fiber is operated in a potential range of –1.2 to 0 V in 6 M KOH versus Hg/HgO.[176] The stable voltage for the symmetric device of rGO, P-doped rGO, and passivated P-doped rGO in 6 M KOH are 1, 1.3, and 1.4 V, respectively.[166] This observation is also important for rational design of doped nanocarbons to obtain the best charge storage performance.

Interestingly, P-doped microporous carbon, prepared by H_3PO_4 activation, shows a higher gravimetric capacitance of 220 F g^{-1} in 1 M H_2SO_4 at 1 A g^{-1} and widened voltage of 1.5 V which is higher compared to activated charcoal trademarked Norit (140 F g^{-1} at 1 A g^{-1} and 1.2 V). It is important to note that Norit possesses higher BET surface area of 697 m^2 g^{-1} and pore volume of 0.4 cc g^{-1} than that of P-doped microporous carbon (633 m^2 g^{-1}, 0.31 cm^3 g^{-1}). Thus the improved supercapacitive properties of P-doped microporous carbon can be largely attributed to the presence of P-content.[175] In addition, the P-dopant also donates a lone pair of electrons to the graphene lattice which attracts the protons of electrolyte and thus contributes to the Faradaic redox reactions.[169] The higher gravimetric and volumetric capacitance of P-doped nanocarbons in 1 M H_2SO_4

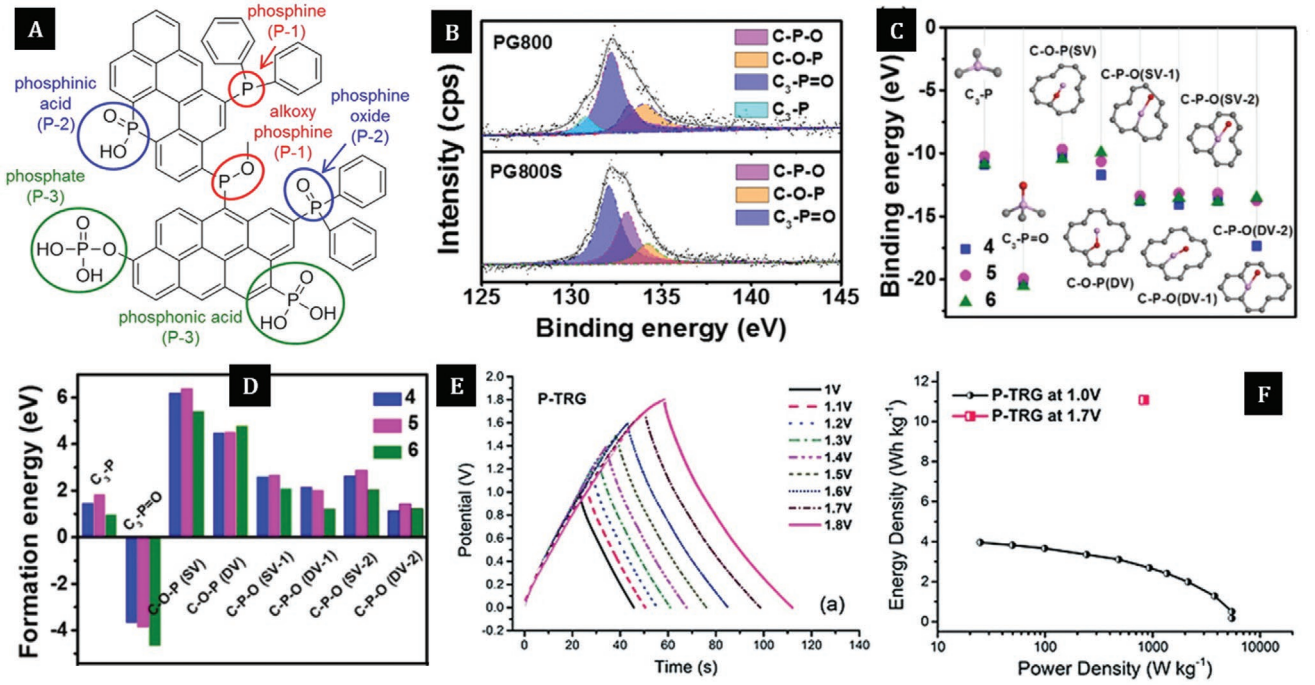

Figure 11. Possible P-bonding with carbon with associated binding energies and supercapacitor performance of P-doped nanocarbons. A) Possible P-configuration in carbon matrix. Reproduced with permission.[69] Copyright 2015, American Chemical Society. B) P 2p spectra of P-doped rGO. Reproduced with permission.[166] Copyright 2019, American Chemical Society. Theoretical modelling for C) binding energy and D) formation energy for the phosphorous and carbon binding (SV: single vacancy, DV: divacancy, 1 and 2 represent P atoms is connected to 1 and 2 C atoms, respectively, blue (4 × 4–3.1%), pink (5 × 5–2.0%), and green (6 × 6–1.6%), are graphene lattice size and corresponding phosphorous content in the model). Reproduced with permission.[166] Copyright 2019, American Chemical Society. Supercapacitive performance of P-doped carbon nanostructures in E–F) H_2SO_4. Reproduced with permission.[77] Copyright, 2015, Wiley-VCH.

than in 1 M Na_2SO_4 is attributed to the smaller size, higher mobility, molar ionic conductivity of H^+ ions and higher pseudocapacitive contributions.[181] The corresponding redox reactions involving P-functional groups in H_2SO_4 electrolyte are given below[102,169]

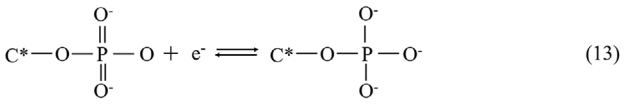
(13)

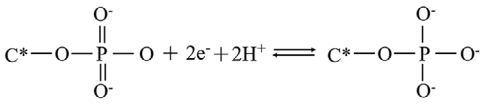
(14)

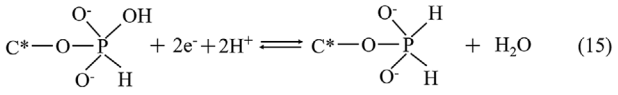
(15)

4.4.2. Quantum Capacitance

The quantum capacitance is also found to decrease with the increase in doping concentration. The estimated room temperature quantum capacitance of P-doped graphene has been predicted to reach a maximum of 346.1 μF cm^{-2} at 5.5% doping concentration using DFT calculations.[182] The DFT calculations have predicted that the adsorption of P-adatom on graphene surface is unstable above the doping concentration of 8%. Reliable experimental data to validate the theoretical predictions are thus warranted.

4.4.3. Effect of Phosphorus Atomic Configurations

Apart from P-content, the P-configurations C_3—P, C_3—P=O, C—O—P, and C—P—O (**Figure 11**A–D) may also play a significant role in the physicochemical changes of doped nanocarbons that can enhance the supercapacitor performances. It is natural to expect that each configuration plays a role different from the other, as observed in other heteroatoms doped nanocarbons discussed above.

Both P—C and P—O configurations have been demonstrated to enhance the capacitive performance. Moreover, the increased surface area, prevented agglomerations and passivated surface defect sites of graphene structure are observed after P-doping.[183,184] The amount of each atomic configuration and their relative ratio are found to depend on the underlying synthesis route. P-doped rGO hydrogel with requisite P-content and higher amount of P—O is achieved using phytic acid ($C_6H_{18}O_{24}P_6$) rather than KH_2PO_4 and H_3PO_4 as the source of phosphorous, ensures higher pseudocapacitance in H_2SO_4 electrolyte.[183] It has been reported that a higher amount of phosphorous bonded with oxygen rather than carbon shows a higher

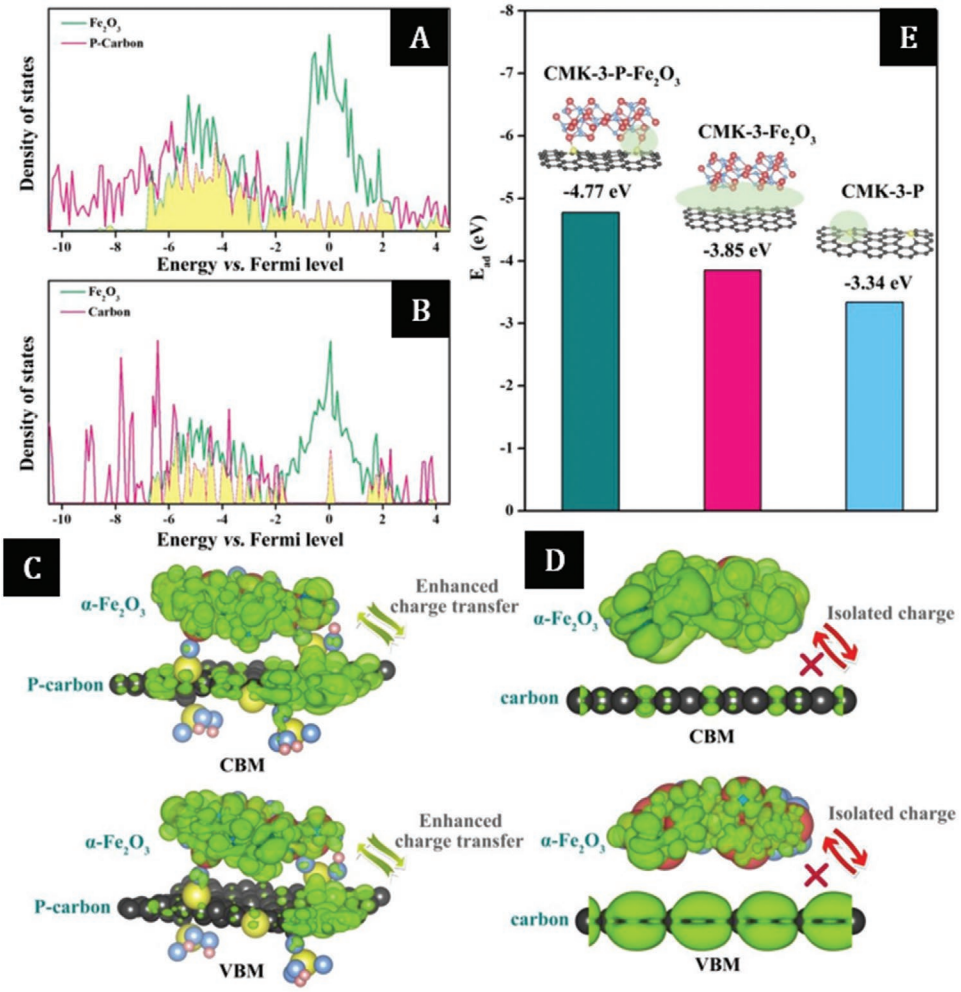

Figure 12. Electronic properties of electrode materials. a–b) Calculated density of states, c–d) charge density distribution, and e) adsorption energy for electrolyte on simulative models of CMK-3-P-Fe_2O_3, CMK-3-Fe_2O_3, and CMK-3-P (CMK: P-doped mesoporous carbon, CBM: conduction band minimum, VBM: valence band maximum). Reproduced with permission.[82] Copyright 2019, Elsevier.

pseudocapacitance.[183] The H_3PO_4 activated GO followed by passivation in an inert atmosphere results in a relatively higher amount of C_3—P=O and C—P—O bonding links, whereas the proportion of C_3—P and C—O—P bonds decreases in the final structure.[166] It is worth mentioning that the C_3—P=O and C—P—O improve the wettability of the carbon surface, increase the interlayer spacing and hence promote the electrolyte ionic diffusion into the electrode interior.[166]

4.4.4. P-Dopant as Protector

The advantageous features of P-doping into the nanocarbons include intentional structural defects, restricted electrophilic oxygen formation, suppressed unstable quinone and carboxyl group formation, protected carbon lattice defect sites, reduced self-discharge and lower leakage current since P-atom act as a bridging element in C_3—P=O and C—P—O atomic links.[166,181] Moreover, P-doping helps stabilize the surface functional groups of carbon structures. An introduction of P-dopant in the nanocarbons also has a significant effect on the concentration of nitrogen and oxygen functionalities in the carbon matrix. It has been reported that the adsorption energies of P-doped carbon have a strong affinity toward H_3O^+ (ΔE_{ads} = –1.02 for P-carbon fiber and –1.44 eV for 2P-carbon fiber).[185] This feature certainly strengthens the interaction between the metal oxide and carbon structures (**Figure 12**). As a result, an effective growth of heterostructures on the P-doped nanocarbons has been demonstrated where P-doped carbon serves as a support material to obtain high-performance supercapacitor electrodes.[82,185]

These results evidence that P-doping not only enhances the total capacitance but also extends the potential window and hence improves the energy density of the device. The specific capacitance and energy density of P-doped carbon electrodes still require substantial improvements. However, the impressive features of P-doped nanocarbons of lower leakage current, protecting nanocarbons from oxidation and stabilizing surface functional groups are promising to utilize in codoped nanocarbons, as discussed later in this review (Section 5).

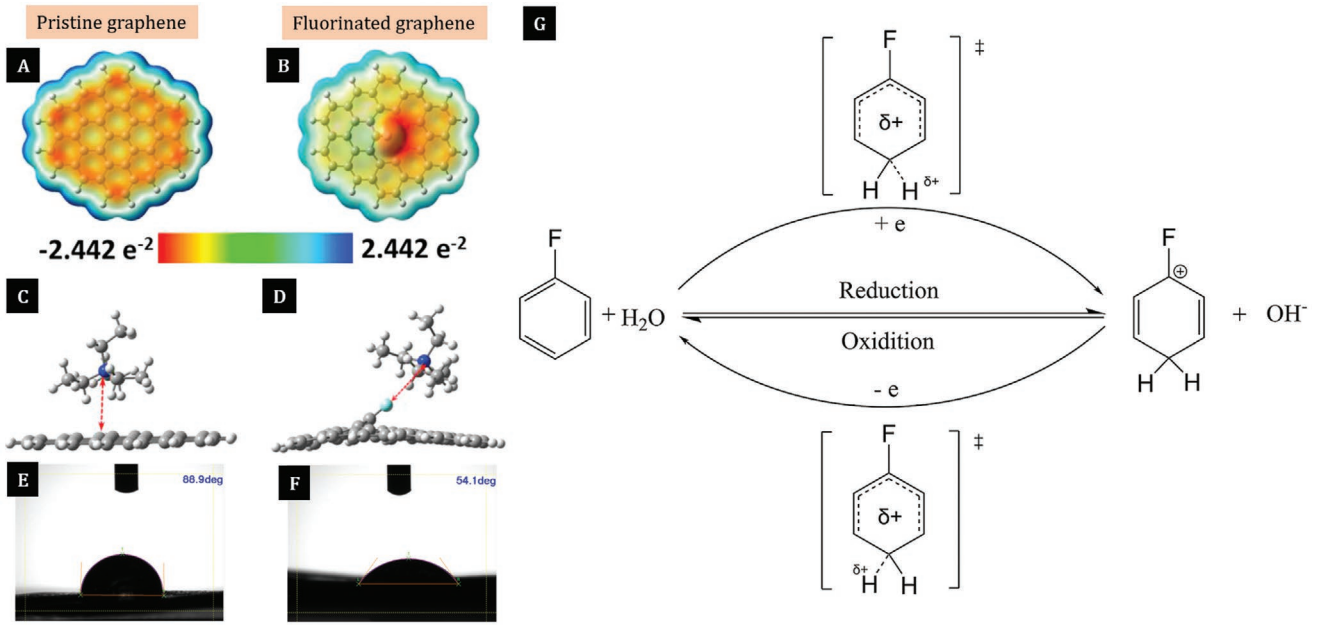

Figure 13. Structural changes and redox reactions by F-doping. Simulated electrostatic potential surface for A) pristine graphene and B) fluorine-doped graphene. The inset is electrostatic potential scale bar; the most negative value is red while the most positive value is blue. Optimized configuration of TEA^+ adsorbed on C) pristine graphene and D) fluorine-doped graphene. The contact angle of $TEABF_4$ on E) nanoporous carbon and F) F-doped nanoporous carbon. Reproduced with permission.[71] Copyright 2016, Elsevier. G) redox reaction scheme by F-functional group. Reproduced with permission.[192] Copyright 2016, Elsevier.

4.5. Fluorine

Fluorination is another effective strategy for improving the capacitive properties of carbon structures. Fluorine (F) doping is acidic in nature and serves as an electron-acceptor.[38] It increases the strain of the carbon matrix and repulsive interaction within the carbon lattice which leads to the amplified electroactive sites.[186] Fluorine doping may also transform sp^2 carbon to sp^3 carbon by bonding covalently. An introduction of F atoms increases the C—C bond length to ≈1.57 Å. Hence, F-atom protrudes out from the graphene plane and found to be more stable at edge compared to its interior counterpart.[187]

A stronger affinity between the organic electrolyte ion and F-containing surface has been observed (**Figure 13**A–D).[71] The calculated adsorption energy of F-doped carbon matrix with TEA^+ ions is –67.52 kJ mol^{-1} whereas it is –48.97 kJ mol^{-1} for the pristine material.[71] Hence, the F-rich mesoporous carbon in organic electrolyte exhibits a high energy density of 42.2 Wh kg^{-1} at 134.9 W kg^{-1}. The available data suggest that the improved electrochemical performance of F-rich mesoporous carbon compared to pristine is most likely due to the synergistic effect of pore distributions and surface chemistry. However, the extent of the synergy remains unclear and requires further studies. Besides F-doped nanocarbons in an organic electrolyte, an obvious increment in the gravimetric capacitance of 252.6 F g^{-1} at 0.5 A g^{-1} in 1 M H_2SO_4 versus Ag/AgCl from 209.6 F g^{-1} (for pristine carbon nanofiber) is observed after F-doping into the nanofiber.[186] Likewise, thermal reduction applied to the fluorographene improves the capacitive features while maintaining excellent structural stability in neutral electrolyte.[188] Generalizing the results from the recent reports,[71,186,189,190] we can conclude that the improved charge-storage kinetics can be attributed to the enhanced polarization from the high electronegativity of the C—F semi-ionic bonding, higher surface area, pore refinement, improved graphitic quality, and higher wettability. Oxyfluronitrated activated carbon exhibits higher gravimetric capacitance of 397 F g^{-1} at 5 mV s^{-1} in 1 M H_2SO_4 versus Ag/AgCl than the untreated ones due to the synergistic effect of the higher density of micropores, optimum mesopore volume and electrochemically active surface functionalities like C—F and quinone C=O.[191]

DFT calculations also suggest that the F-doping redistributes the charges of N atoms and reduces the energy gap between the valence and conduction bands.[38] The maximum quantum capacitance of F-doped graphene is estimated to be 209 μF cm^{-2}.[193] Moreover, fluorine is stable at edges of the lattice which has been observed to prevent corrosion over the long-term cycle life.[186] We emphasize however, that no pseudo-Faradaic reactions are involved in charge-storage of F-doped nanocarbons as reported.[71,189] Hence, it can be concluded that the F-doping into the nanocarbons has mostly improved the structural properties and enhanced the EDL capacitance. On the contrary, the observed redox peaks in the cyclic voltammogram of fluorinated rGO hydrogel is an indicator of the occurrence of the oxidation and reduction reactions which contribute to the pseudocapacitance (Figure 13G).[192] Further investigations are thus needed to explore the associated charge-storage mechanism induced by F-doping.

Another important function of fluorine is to protect carbon surface from oxidation during the growth of heterostructures. The F-doped carbon has been utilized as a backbone to grow heterostructures to obtain a high-performance supercapacitor electrode.[194]

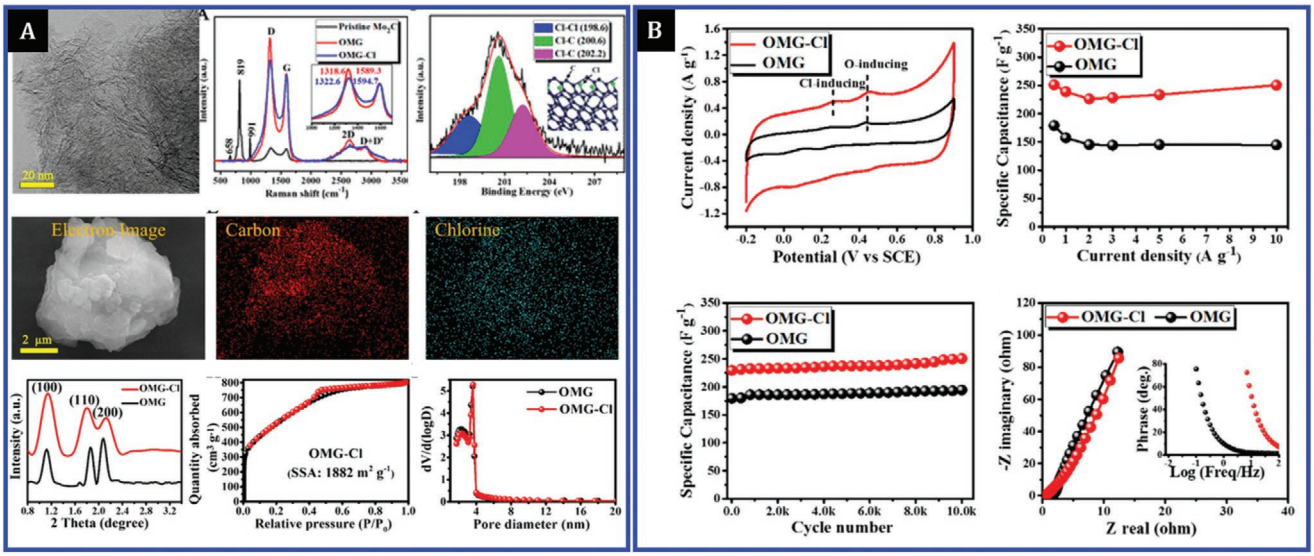

Figure 14. Structural and capacitive changes by Cl-doping. A) Micrograph, Raman spectra, XP spectra, elemental mapping, XRD, pore structure analysis. B) Supercapacitive properties of Cl-doped ordered mesoporous carbons with few-layer graphene with their pristine counterpart. Reproduced with permission.[168] Copyright 2016, American Chemical Society.

4.6. Chlorine

Apart from fluorination, chlorination process has also received significant attention to improve the supercapacitor performance of nanocarbons. Chlorination such as high-temperature chlorine treatment is a common practice to synthesize carbide-derived carbons (CDC) by etching metal part from the metal carbide.[195,196] These CDC are among the most popular carbon structures with tunable pore and surface areas for applications in supercapacitors.[197] Unfortunately, the gravimetric capacitance of CDC is limited to ≈150 F g^{-1}.[13] The chlorination temperature has been reported to define the final structure including the number and type of impurities.[198,199] However, the discussion on the impact of Cl-impurities on the supercapacitor performance of CDC is scarce. Nearly rectangular cyclic voltammogram of CDC over a range of –0.6 to 0.6 V in various aqueous electrolytes[197] manifests the absence of a large number of functional groups, thus diminishing the pseudocapacitive contribution. On the other hand, the poor rate performance and power characteristics of CDC in ionic liquids at high current density can be attributed to the presence of Cl-residues whereas no significant effects by Cl-residues on the supercapacitor performance have been observed in 1 M H_2SO_4.[198] Moreover, CDC with higher Cl-content and lower surface area have been reported to have a higher specific capacitance in 1 M H_2SO_4 (2E) than the nanocarbons with lower Cl-content.[198] Interestingly, the scenario appears to be quite opposite for the electrodes in $EMIBF_4$ ionic electrolyte. One can argue that the observed trends can be explained by the interaction between the solvent molecules and structural defects of the CDC, yet the specific mechanism remains unclear.

Chlorination improves the rate capability and hence the power density of ordered mesoporous CDC in ionic electrolyte as chlorination reduces the polarity of carbon surface and protects against reoxidation.[200] An improved specific capacitance, rate performance, lower charge-transfer resistance in Cl-doped rGO over pristine rGO are certainly indicative of better capacitive properties.[201] With the improvement in electrical conductivity, Cl-doping also assists to integrate the rGO film, decomposes the oxygen groups present on graphene and converts them to gases subsequently as well as serves as a reducing agent in Cl-rGO film. HCl assisted solvothermal method is an effective method to prepare the Cl-rGO samples.[202] Hierarchically porous CDC with Cl and N functionalities deliver the highest gravimetric capacitance of 277.7 F g^{-1} at 0.5 A g^{-1} in 6 M KOH (3E) which is higher than that of any reported CDC.[199] Hence the enhanced capacitance can be ascribed to the N-functionalities and corresponding changes. However, Cl-doping into the ordered mesoporous carbon with few-layer graphenes does not affect the pore structures, BET surface area, wettability, charge-distributions or XPS-derived O-content (**Figure 14**A).[168] Thus the improved capacitive performance of the electrode material can be attributed to the Cl-induced pseudo-Faradaic reactions. The pseudocapacitive contribution from the Cl-species, as evidenced from the charging peaks at ≈0.24 and 0.44 V in cyclic voltammogram (Figure 14B), is related to the improved specific capacitance of CDC.[168] Similar redox-peaks are also observed from the cyclic voltammogram of Cl-rGO in 1 M H_2SO_4[201] but we would like to point out that those peaks in this case are related to the O-functionalities. Although the enhancement in capacitive properties of rGO after Cl-doping does not show any clear correlation with process parameters,[201] the observed physical changes after Cl-doping includes short-range ordering, increased inter-layer spacing higher amount of wrinkles and relatively higher defects in the graphene sheets. Revealing the relevant correlations represents an obvious opportunity for research. Collectively, the above results clarify that there is a significant impact of Cl-doping on the charge-storage

performance of nanocarbons. More attention should be paid to the underlying mechanisms of Cl-doping and their relation to the charge storage performance.

Similar to N and P elements, controlled Cl-doping in graphene results in a significant enhancement in the quantum capacitance.[182] It has been seen that the charge transfer per atom to Cl-atom from graphene sheet is higher (0.6e) than for the N-functionalization (0.5e), and P-functionalization (0.3e). With the high electronegativity of 3.16, the Cl-functionalized graphene (Cl-FG) shows a comparatively high quantum capacitance of 553.7 μF cm^{-2} at 300 K than other functionalized graphenes (FG–P: 346.1162 μF cm^{-2}; FG–N: 256.4227 μF cm^{-2}) and pristine graphene (1.2947 μF cm^{-2}) according to DFT calculations considering 5.5% doping concentration for all cases.[182] The quantum capacitance of Cl-FG is found to increase to 1141.7 μF cm^{-2} up to 12% Cl-concentration. It is important to note that the quantum capacitance of Cl-doped nanocarbons is higher than for any other doped nanocarbons. The quantum capacitance reduces beyond 12% Cl-concentration since the localized states near Fermi energy are getting affected due to the interaction between the impurity centers and stronger Cl–Cl interaction leading to Cl_2 formation and hence desorption from the surface.[182] Moreover, C—Cl bond weakens at 366 °C and Cl evaporates at 600 °C completely.[203] Thus, C—Cl bond is not stable compared to C—F and C—C bonds. In addition, C—Cl bond length is larger than the length of C—F and C—H bonds. We note that a larger bond length can distort the graphene matrix.

Noteworthy, halogenated nanocarbons typically show a higher rate performance than other doped nanocarbons (Table 1). In spite of several promising features of halogenated nanocarbons, further research to improve the specific capacitance and to widen the potential window are needed to implement the Cl-doping, especially for the development of industry relevant processes.

4.7. Silicon Doping

Silicon is the workhorse of the semiconductor industry, where it is extensively used as a host matrix in which various dopants are added to modify its electronic band structure. In the area of supercapacitor devices, Si acts as a dopant in the carbon matrix leading to better supercapacitive properties. Indeed, Si-doping into the N/P-doped carbon nanofibers increases the capacitance by 30 F g^{-1}, enhances the rate capability, cycle stability, and accelerates the EDL formation.[170]

Si-doped nanocarbons are semiconducting in nature.[204] These structures have the lowest formation energy compared to the cases of P and S doping. However, Si-doping does not open the band gap in graphene.[205] Si-doping changes the chemical composition and physical parameters of the nanocarbons as shown in Table 1. The polar group Si—O—C/Si—O—Si enhances the wettability of doped nanocarbons.[206] It is noteworthy that Si-based precursor not only dope Si into carbon but also produces pores and increases the surface area, pore volume, and pore diameter in the doped nanocarbons.[206,207] These pores can accommodate a large number of electrolyte ions. Importantly, the presence of mesopores leads to higher adsorption rates. As a result, the electrolyte resistance and charge-transfer resistance reduce rapidly leading to better charge-transfer kinetics for the Si-doped carbon nanofiber in organic electrolyte.[206] Si-doping also introduces defects in GO, breaks basal planes and provides sites for the ion adsorption.[208] The distortion or defects in graphene structure is obvious due to the larger bond length of Si—C (1.75 Å) compared to C—C bond. A significant electrochemical performance enhancement observed in Si-doped carbon nanofibers can be attributed to electrical conductivity and functional groups in the matrix after Si-doping along with the increased surface area.[167] Since Si has a lower electronegativity than carbon which results in an increased electron density of adjacent carbon atoms and hence accelerate the Faradaic reactions.[169] The possible redox reaction due to Si-dopant in H_2SO_4 electrolyte is as follows[170]

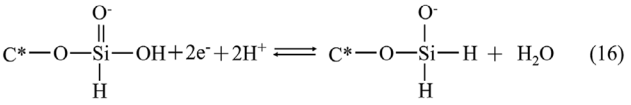

$$C^*—O—\underset{\underset{H}{|}}{\overset{\overset{O^-}{\|}}{Si}}—OH + 2e^- + 2H^+ \rightleftharpoons C^*—O—\underset{\underset{H}{|}}{\overset{\overset{O^-}{|}}{Si}}—H + H_2O \quad (16)$$

Based on the literature survey, it has been seen in most of the cases that Si atoms are simultaneously doped along with other dopants.[169,170] In spite of the reported improvements, it is important to single out the effect of Si-doping on supercapacitive features of carbon nanostructures, the issue which presently remains unresolved. However, one should be aware that Si-doping into nanocarbons may have negative effects such as i) higher atomic radius (111 pm) of Si than that of carbon can introduce severe stress in the as-synthesized doped nanocarbons, ii) high oxidation probability of Si can deteriorate full structure, and iii) poor mechanical characteristics while being used in flexible and wearable devices. These points represent an obvious opportunity for improvements where codoping examined in the following section may offer viable solutions.

4.8. Oxygen-Functionalization

It has been observed that synthesizing the nanocarbons without oxygen content is nearly impossible as the dangling carbon bonds are known to absorb the moisture rapidly. However, this minimal O-content is neither sufficient to make the carbon surface hydrophilic[209] nor is enough to provide a significant pseudocapacitive contribution. Therefore, it is of interest to increase the O/C ratio up to a certain level with the appropriate configuration such that the carbon surface can transform from hydrophobic to hydrophilic without degrading the desirable characteristics of carbon. It has also been seen that doped nanocarbons contain a significant amount of oxygen which usually increases with doping concentration in the carbon-matrix. The inevitable oxygen functional groups have a significant impact on the charge-storage properties of nanocarbons as discussed above. In addition, oxygen functionalization has received a great deal of attention to improve the carbon-based energy storage electrode properties. This is why we discuss the effect of oxygen functionalization here. Unfortunately, the terminology of "doping" has been used extensively instead of the more appropriate term of oxygen functionalization. Indeed, term "doping" is usually defined as an introduction of small amount of impurities into the host material to tailor its

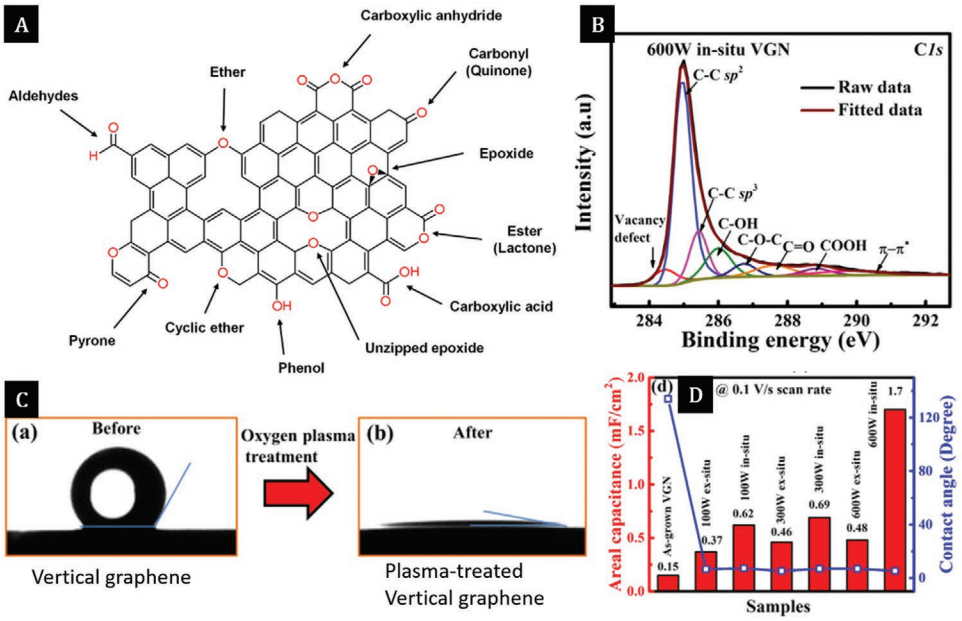

Figure 15. Possible O-configurations in carbon. A) O-configuration in graphene matrix. Reproduced with permission.[210] Copyright 2019, American Chemical Society. B) C1s spectra of plasma treated vertical graphene, C) water contact angle of vertical graphene before and after O-plasma treatment, and D) Plot of areal capacitance and water contact angle with respect to the plasma treated vertical graphenes. Reproduced with permission.[211] Copyright 2015, Elsevier.

properties. On the other hand, functionalization is achieved by the attachment of functional groups onto the host surface and it is a surface-related process which is different from conventional doping. Hence functionalization is an appropriate term in this context except for the case when *in-plane* cyclic ether groups are used rather than O-doping. We will follow the same terminology related to O-functionalization throughout this review.

The various possible configurations of oxygen links with carbon are shown in **Figure 15**A, but not all of these groups participate in the charge storage activity. With the hydrophilic features, the O-functional groups mainly contribute to the physicochemical changes of O-doped nanocarbons, as shown in the XP spectra except for physisorbed oxygen (Figure 15B).

4.8.1. Wettability and Porosity

Most popular ways to simultaneously make the surface hydrophilic and introduce controlled O-functionalities in nanocarbon matrix are chemical activation or plasma treatment.[10,212–214] It has been observed that KOH activation of the vertically graphenes assists in reducing its water contact angle by 30° along with pore formation, better graphitic quality and higher specific capacitance than that of the pristine material.[10] It is also possible to create mesoporous channels with micropores which significantly enhance the ion accessible surface area and ion diffusion onto the entire electrode surface.[215] The higher rate of wettability of pristine nanocarbons in KOH is ascribed to the higher specific capacitance compared to H_2SO_4 and Na_2SO_4.[49,216] Since KOH activation results in disordered pores with random distribution and drastic damages in the structure,[142,212] it may weaken the electrochemical performance, mechanical properties of carbon structures, and hence lead to properties undesirable in applications in flexible/wearable electronics. We emphasize that the activation reaction mechanism in KOH and NaOH is different: NaOH reacts with energetic sites of the carbon surface whereas KOH intercalates between the carbon layers.[217] Oxygen plasma functionalization can make the surface near or completely hydrophilic, a higher amount of defects and hence higher ion diffusion rate at the electrode–electrolyte interface, excellent charge-transfer, reduced contact resistance and internal resistance (Figure 15C,D).[10,163,211] It is also reported that the oxygen plasma activated biochar contains larger pore volumes with higher average pore size compared to that of chemically activated biochar. Not surprisingly, plasma-activated biochar exhibits around two times higher specific capacitance compared to that of chemically activated biochar although chemically activated biochar showed a higher BET surface area.[164] From these results we can conclude that the enhanced wettability of the surface suits more effective electrode–electrolyte interactions that stimulate the migration rate of electrolyte ions into the surface and reduces the mass transfer resistance which results in the better EDL formation across the interface, which is consistent with relevant literature.[163,211,218,219] The oxygen-containing functional groups serve as electrochemically active sites and do not contribute to the EDL formation. However, these groups enhance the total capacitance by providing pseudocapacitance via redox reactions. The relationship between the O-content and capacitance is (Equation (15))[220]

$$C\left(\mathrm{F\ g^{-1}}\right) = C_0\ \exp\left\{-5.32\times10^{-3}\, j\left(1+0.0158[\mathrm{O}]^2\right)\right\} \tag{17}$$

where C is the capacitance, C_0 is the coefficient, j is the low current density, and $[O]$ is the O-content.

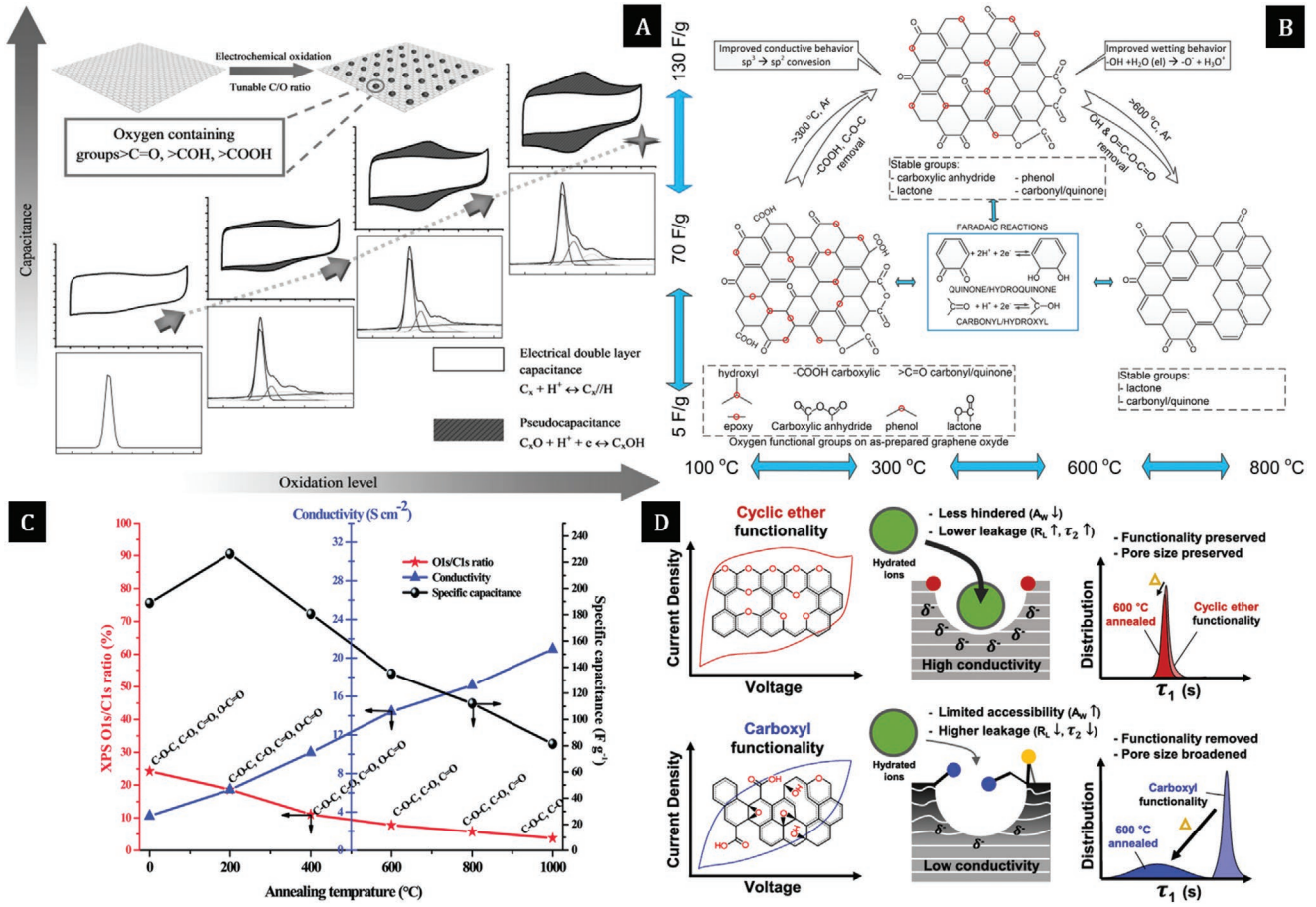

Figure 16. Supercapacitor performance of O-functionalized nanocarbons. A) Pseudocapacitive contribution with respect to the oxidation level of graphene frameworks with tunable C/O Ratios. Reproduced with permission.[224] Copyright 2013, Wiley-VCH. B) Schematic of thermally reduced graphene and its specific capacitance. Reproduced with permission.[222] Copyright 2017, Elsevier. C) Plot of physicochemical properties of graphene oxide versus annealing temperature. Reproduced with permission.[165] Copyright 2014, The Royal Society of Chemistry. D) Schematic of supercapacitive properties of carbon nanostructure with in-plane cyclic ether group and out-of-plane oxygen functional group. Reproduced with permission.[210] Copyright 2019, American Chemical Society.

4.8.2. Graphene Oxides

First-principles study shows that the quantum capacitance can be increased from 19.997 to 247.379 μF cm^{-2} by increasing the O/C ratio from 0.02 to 0.39%.[97] We stress that the charge-storage features of O-functionalized nanocarbons are usually enhanced compared to their pristine counterparts. These facts may lead to the idea that GO, intrinsically O-containing graphene, can have excellent supercapacitor performance. However, the very large amount of oxygen makes GO a poor conductor with poor graphitic quality. An O-concentration in carbon matrix beyond a certain limit has been observed to induce a self-discharge, increase the internal resistivity, decrease the micropores, mesopores, and BET surface area in the carbon-based electrochemical capacitor (**Figure 16**A–C).[221] Figure 16B–C is self-explanatory on the role of specific O-functional groups along with their structural changes.[165, 222] Rather than thermally-treated GO (314 F cm^{-3}) or chemically-reduced GO (134.2 F cm^{-3}), functional pillared graphene framework, prepared by low-temperature treatment of GO by O_3, with highly stable O-content and packing density shows better capacitive properties with ultrahigh volumetric capacitance of 400 F cm^{-3} at 2 mV s^{-1} in 6 M KOH versus Hg/HgO. In addition, electric field-induced continuous diffusion of polarized electrolyte ions into the dense network results in 104% cycle stability after 10 000 charge–discharge cycles at 200 mV s^{-1}.[223] Thus, selecting and controlling the amount of the functional groups in the carbon matrix is important to obtain high-performance supercapacitor electrodes. The critical discussion of the roles of each specific oxygen functional group in the charge storage properties of doped nanocarbons is therefore an urgent need of the hour.

4.8.3. Role of O-Functionalities

The possible configurations of oxygen bonding with carbon are shown in Figure 15A. Among the oxygen functional

group, the carboxyl, anhydride and lactone groups evolve CO_2 as confirmed by the temperature-programmed desorption study.[225] Meanwhile, CO evolves from hydroxyl, carbonyl and quinone groups. Out of them, CO-type oxygen group contributed positively to the pseudocapacitance of porous carbon which is validated by thorough investigations on a variety of activated carbons.[214] Most importantly, a linear correlation is established between the specific capacitance (capacitance in F g^{-1} divided by BET surface area) of porous carbons with the amount of CO-type surface functional groups.[214] One can estimate the pseudocapacitive contribution from each specific oxygen containing functional group.[49,226] The quinone groups can provide two times higher capacitance than the other groups in an acidic electrolyte medium since two electrons per one quinone group take part in one redox reaction (Equation (18)).[49] On the other hand, the carboxylic groups (COOH) on the carbon surface are thermally unstable, nonreversible with time and are hence nonpreferable compared to the phenol (C—OH) and quinone (C=O) groups. The unstable oxygen functional groups are eliminated from rGO by thermal treatment. As a result, rGO displays a higher cycle stability in KOH medium in a 3E system. These features can be attributed to the higher amount of unstable functional groups in GO reduced at 250 °C.[227] Therefore, carbon surface with the higher concentration of C—OH and C=O groups is highly desirable to make the carbon surface hydrophilic and to provide pseudocapacitance. In this context, in situ oxygen plasma functionalization treatment immediately after the growth of vertical graphene has been found to be more effective than the ex situ one. The presence of these hydroxyl and carbonyl type functional groups can be increased by increasing the plasma power.[228] Although oxygen plasma functionalization does not alter the geometry, the etching of sp^2-C, sp^3-C, and amorphous-C at a different rate is observed and results in the reduction of the vertical graphenes height.[228] On the contrary, edge-carboxylated graphene nanoplatelets have been shown as a promising supercapacitor electrode in 1 M H_2SO_4 electrolytes.[229] Moreover, the presence of COOH-groups on GO promotes the N-doping, pyrrolic-N, and pyridinic-N formation compared to the pristine GO.[230] We can thus conclude that particular oxygen configurations are preferential to obtain high-performance carbon-based energy electrodes,[165,222,224] despite some controversy among the available reports. Besides, oxygen functional groups immobilized on the micropores improve the pseudocapacitive contribution more effectively than the same groups tethered on the planar carbon surface.[231] Caution should be exercised when using *out-of-plane* oxygen functional groups as they have several flaws causing limited charge accessibility and retention.

Not surprisingly, *in-plane* cyclic ether group (C—O—C) in graphene matrix have been found to be beneficial for this purpose (Figure 16D). It has been shown that the thermal oxidation in air is preferential than the electrochemical oxidation of carbon fiber paper to obtain *in-plane* cyclic ether group in the graphene matrix.[210] Therefore, thermal oxidation of the doped nanocarbon is recommended to obtain the structure with stabilized oxygen functional groups and restored sp^2 hybridized graphitic network.

4.8.4. Effect of Electrolyte

Along with the oxygen concentration and specific configuration, the electrolyte medium has a significant role in defining the charge-storage properties of an electrode. The pseudocapacitive contribution from the oxygen functional group is found to be higher in the acidic medium compared to the basic medium.[232] In particular, 30% capacitance loss for the carbon cloth has been observed by changing pH from 0 (H_2SO_4) to 11 (NaOH). On the other hand, pyrone and other unknown species have been found to activate the charge-storage beyond pH 11 which results in the 20% higher specific capacitance of the electrode. Initial loss in capacitance while changing pH from 0 to 3 has been attributed to the low activity of quinone functionalities in redox reactions without sufficient H^+ within the pores of the carbon surface.[233] Surprisingly, no redox peaks appear in cyclic voltammogram when the electrode is tested in an alkaline medium.[233] This is why researchers should pay attention to pH of electrolyte based on the dominant and stabilized O-functionalities present in the structures to obtain the best charge storage performance from the optimum electrode–electrolyte combination.

Recent research suggests that the pseudocapacitive contribution of O-functional groups in alkaline medium can be attributed to the insertion and desertion of hydrated ions into and out of the pores.[218] In the study of rGO in different aqueous electrolyte, a flat roundish shape of redox peaks has been noticed in 6 M KOH whereas a prominent redox peak is obtained in 1 M H_2SO_4.[49] Moreover, rGO in KOH electrolyte exhibits higher gravimetric capacitance (220 F g^{-1} at 5 mV s^{-1} in 3E) and better stability of 92% after 1000 charge–discharge cycles compared to H_2SO_4 electrolyte (171 F g^{-1} with retention of 54%). On the contrary, the pseudocapacitance of carbon materials in KOH electrolyte reduces continuously for the larger number of cycles.[234] The underlying observation is that unstable carboxyl groups are neutralized and reduced during charge–discharge while the electrodes are subjected to KOH medium.[227] It has also been reported that the acidic sites (carboxyl, phenol) on nanocarbon surface play a dominant role and react with OH^- ions in alkaline medium (Equations (15) and (16)) while the basic sites are unfavorable for the redox reactions[49,227]

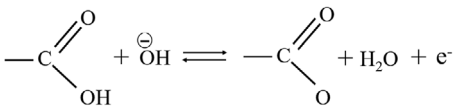

(18)

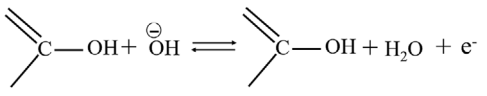

(19)

On the other hand, O-functionalized nanocarbons show better supercapacitive performance in H_2SO_4 medium due to the higher ionic mobility and better accessibility of the surface by smaller ions.[216] Meanwhile, the basic functional groups (carbonyl and quinone) present on the nanocarbons react with protons contributing pseudocapacitance in acidic aqueous electrolyte.[49] Eventually, the use of acidic electrolytes enhances the hydrogen evolution at the anode and also induces the oxygen functional groups in the carbon matrix.[159] The redox reactions

of carbonyl and quinone group in H_2SO_4 electrolyte are as follows

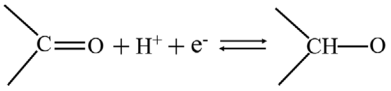

(20)

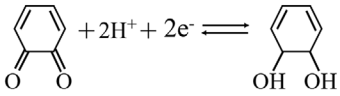

(21)

In summary, O-functionalization is one of the most established techniques to improve the interaction of carbon electrodes with the electrolyte. The choice of a suitable aqueous electrolyte based on the dominant functional group present on the carbon matrix is necessary since redox reactions are very different between the functional groups and electrolyte ions. In spite of the commonly acknowledged success, O-functionalized carbon structures have several shortcomings like distributed capacitance effect, higher potential drop, high leakage current, lower surface conductivity, hindered electrolyte ion migration to micropores, and electrolyte decomposition.[210,218,225,235,236] In addition, corrosive oxidation can severely damage the carbon basal planes, creates a high level of chemical and topological defects and eventually results in deteriorated supercapacitor performance.[229] As a result, poor rate performance and cycle life are frequently reported from the O-functionalized nanocarbon electrodes. This is why researchers sometimes intentionally remove oxygen functional groups from the carbon surface to obtain better performance as a supercapacitor electrode.[237]

4.9. Doped and Defected Nanocarbons

Moreover, the presence of defects in nanocarbons obviously enhances the total electrode capacitance.[238,239] The types of defects induced in the structure are defined by the specific materials and dopants. For example, small pores contribute more edge-site defects than *in-plane* defects.[240] It has been already seen that vertical graphenes with higher edge density and vacancy-like defects are better suited as supercapacitor electrodes compared to their planar counterpart.[238] Moreover, introduction of high-density defects in vertical graphene improves the wettability and hence charge-storage performances.[241]

In addition, quantum capacitance of the electrode materials can be tailored by introducing specific defects in the structure. In particular, the calculated maximum quantum capacitances of vacancy defected graphene and stone-wall defected graphene are found to be 120.72 and 44.38 μF cm^{-2}, respectively. The quantum capacitance can be enhanced further for the graphene with coexistence of both defects and dopants.[242] Si-doped vacancy defected graphene provides the higher maximum quantum capacitance of 169.76 μF cm^{-2} than other graphenes with defects created by other (B, N, P, and S) dopants.[242] On the other hand, S-doped stone-wall defected graphene (88.31 μF cm^{-2}) shows higher maximum capacitance than the other dopants (B, N, P, and Si) stone-wall defected graphenes.[242] It can thus be concluded that the density of states and hence the quantum capacitance of doped nanocarbons can be maximized by choosing the proper combination of dopants with the optimized concentrations and defects. It has also been seen from DFT computations that the vacancy formation and substitutional doping enhance the reactive sites at the basal planes of graphene which attracts OH functional groups.[243] This is why O-functional groups have been reported for most of the doped nanocarbons and typically increase with the dopant concentrations.

5. Codoping

Table 1 highlights the changes in physicochemical features and its consequences on the capacitive properties in different electrolyte medium with respect to the corresponding pristine counterpart. Meanwhile, one dopant can be superior over the other one in one set of physicochemical properties and the other way around in another set. For example, the wettability is found to be better for N-doped nanocarbons compared to B-doped ones.[41] From the theoretical study, it is found that the 0.5e charge transfer from Si to graphene and 0.4e charge transfer to N.[97] The quantum capacitance of N-doped graphene (256.420 μF cm^{-2}) is found to be higher theoretically than the B-doped graphene (60.847 μF cm^{-2}) and Si-doped graphene (174.825 μF cm^{-2}).[97] The N-doped nanocarbons show higher gravimetric and volumetric capacitance, P-doped nanocarbons are capable to operate in a wider potential window in aqueous electrolyte, O-functionalities on the nanocarbon surface promote the electrode–electrolyte interaction, halogen-doped nanocarbons are remarkable in terms of capacitance retention and structural improvements, and so on. The capacitance of doped nanocarbons is found to be depend on the electron affinity and electronegativity of dopants and carbons via the following relation

$$\text{descriptor, } \varnothing = \frac{\left(\text{electronegativity} \times \text{electron affinity}\right)_{\text{dopant}}}{\left(\text{electronegativity} \times \text{electron affinity}\right)_{\text{carbon}}} \quad (22)$$

It is predicted that the value of ∅ should be between 0.5 and 2 in order to obtain the higher capacitance and energy density (**Figure 17**A).[244] First principle calculations using DFT prove that the adsorption energy of B/N/P-doped rGO hydrogel with $EMIMBF_4$ and H_2SO_4 is higher compared to their mono-doped and pristine counterparts.[245] The higher gravimetric capacitance of 525 F g^{-1} at 1 A g^{-1}, good rate performance, and charge transfer kinetics are noticeable for the N/P/S-self-doped hierarchically porous carbon in H_2SO_4 versus Ag/AgCl than the activated carbons (BET surface area is 1484 m^2 g^{-1}).[246] These results pushed the recent research toward codoping into the carbon matrix to achieve the overall positive effects of individual dopants (Figure 17B–F and **Figure 18**).[103] As-engineered codoped nanocarbons have striking properties such as more active sites, hydrophilicity, increased surface area with balanced micro-meso-macropores, excellent structural stability, enhanced DOS(E_F), improved electronic conductivity, enhanced charge-transfer kinetics, better electrode–electrolyte interactions which enhance the total capacitance via quantum capacitance and pseudocapacitive contributions.[215,245–249]

The codoping into nanocarbons can be classified into two categories: i) dopants with the same charge carriers (n-types

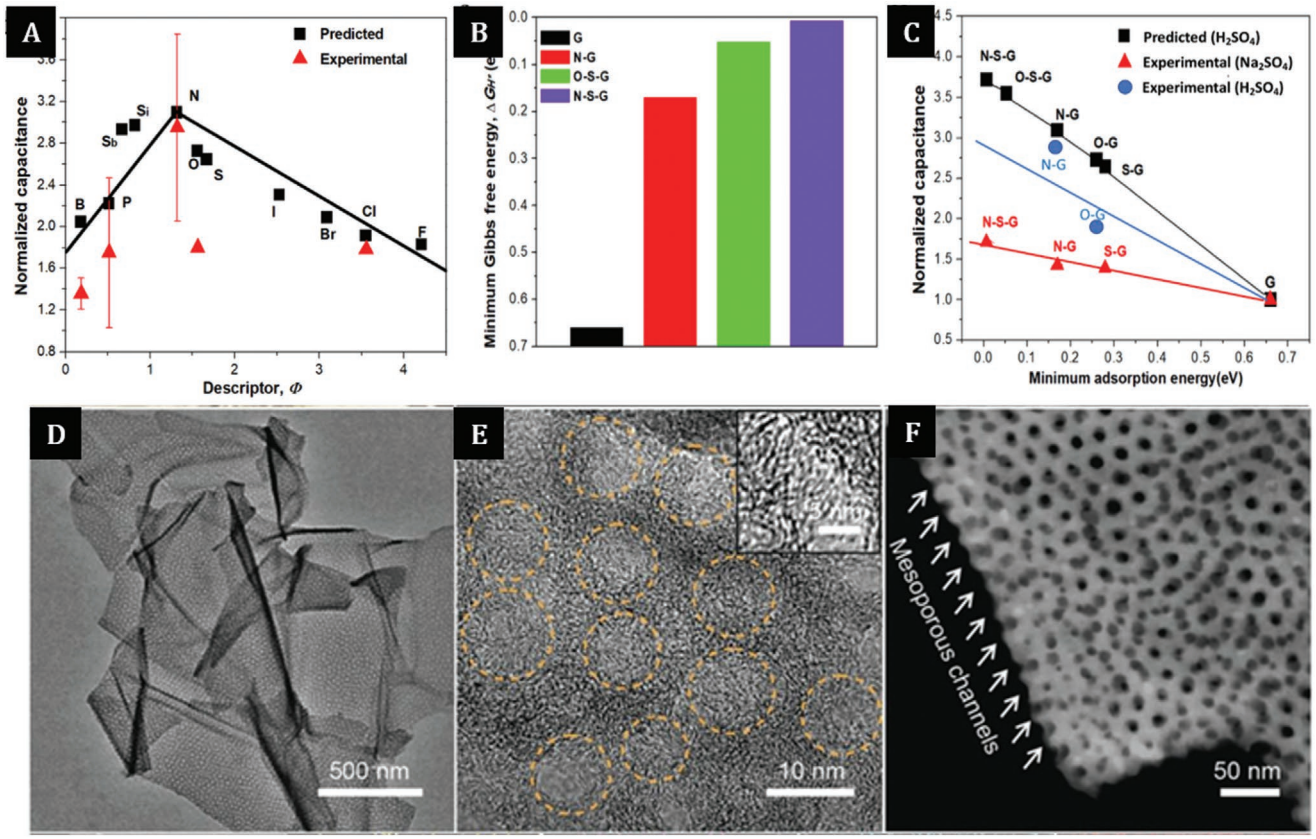

Figure 17. Codoped nanocarbons. A) Plot of normalized capacitance with respect to the descriptor; B) minimum Gibbs free energy of dopant(s); C) plot of normalized capacitance versus minimum adsorption energy of doped nanocarbons in various aqueous electrolytes. Reproduced with permission.[244] Copyright 2020, Elsevier. D–F) Electron micrograph hierarchical porous N/O/S-enriched carbon foam (KNOSC) showing mesoporous channels and well-distributed heteroatom dopants. Reproduced with permission.[215] Copyright 2019, Wiley-VCH.

or p-types) and ii) dopants with the opposite charge carriers (n-types and p-types). The following subsections cover the effects of codoping (binary, ternary, etc.) on the supercapacitor performance of nanocarbons.

5.1. Dopants with the Same Charge Carriers

5.1.1. N/S Codoping

The dopants with the same charge carriers are found to be promising in terms of physicochemical properties of nanocarbons since electronegative S and N atoms, for example, possess outer shell *p* orbitals and similar electronic structure. Coordinated effect via indirect bonding between N and S-dopants and N···H—S— bond or N—H···S bond formations enhance the doping level and improve pseudocapacitance of N/S codoped porous ultrathin carbon.[250]

As an example of superior nanocarbon-based supercapacitor electrode with both dopants, the N/S codoped graphene nanoribbons (GNR) exhibit higher gravimetric capacitance of 442 F g^{-1} at 0.5 A g^{-1} in 1 M Na_2SO_4 (3E) than the N-doped GNR (289 F g^{-1}), S-doped GNR (227 F g^{-1}) and pristine GNR (91 F g^{-1}).[80] Simultaneous N/S doping promotes the pore utilization in the carbon structures for better EDL formation by replacing O-functionalities from the carbon matrix.[251] An enhanced electrical conductivity and higher contact area with narrow pore size distributions are attributed to the efficient electron transport, high gravimetric and volumetric capacitance and energy density of rGO scrolls after N-incorporation and thiofunctionalization.[252] It is important to note that the rate capability of N/S codoped ordered mesoporous carbon can be improved by increasing the S-content and reducing the pyridine-N content.[139] In addition to the pseudocapacitance, the quantum capacitance of the codoped nanocarbons also relies on the relative ratio of dopants. In fact, the highest quantum capacitance is obtained for N/S codoped graphene with N to S ratio of 1:2 since the Fermi level is shifted toward the conduction band, whereas it is shifted toward the valence band when only nitrogen is doped.[253]

5.1.2. P/N Codoping

The P/N codoped carbon (PNDC) with the optimized physicochemical properties, prepared by microwave-assisted technique with different amount of ammonium polyphosphate, is observed to exhibit excellent electrochemical properties in the both acidic and basic aqueous electrolyte (Table 1).[102] PNDC with lower BET surface area, pore volume and

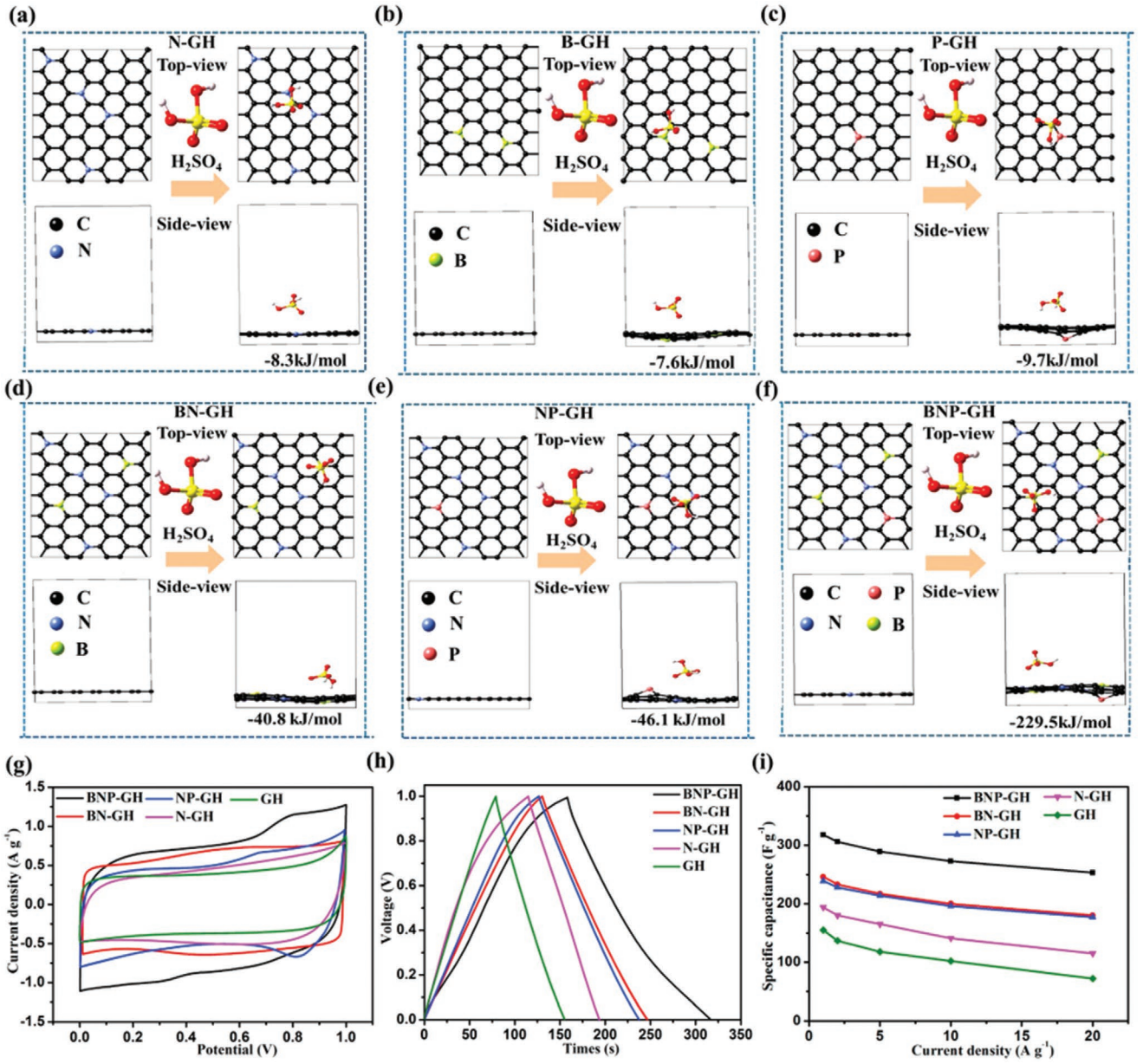

Figure 18. Adsorption energy and capacitive features of doped nanocarbons. Ab initio calculated structures and energies of H_2SO_4 adsorption on the doped holey rGO hydrogels (B, N, BN, NP, and BNP) and their supercapacitive performances. Reproduced with permission.[245] Copyright, 2018, Elsevier.

O-content shows higher gravimetric capacitance in 6 M KOH (270 F g^{-1} vs Hg/HgO) whereas, PNDC with higher BET surface area, pore volume and O-content outperform in 1 M H_2SO_4 (286 F g^{-1} vs Ag/AgCl). As the ammonium polyphosphate content is increased during the synthesis, the observable changes in the as-synthesized codoped carbons are i) increased the BET surface area and average pore volume and ii) increased O-content and decreased C-content while N- and P-contents remain unchanged. In addition, the simultaneous doping of nitrogen and phosphorous are found to promote the C=O and P=O double bonds and pyrrolic nitrogen sites which is seen to have a positive effect on capacitive properties. On the other hand, P/N codoping suppresses the COOH group in the carbon matrix, which otherwise has a negative effect on the capacitive properties of doped nanocarbons.[254]

5.2. Dopants with Opposite Charge Carriers

Dopants with the opposite charge carriers are also found to enhance the charge storage properties of nanocarbons. The doping concentration is found to be higher for the simultaneous doping of n-type and p-type carriers since electron-deficient holes nearby carbon atoms combine with electron-donating atoms.[255] In addition, the charge effectively redistributes to reduce the bandgap of the electrode material

in this context.[116] Codoping with the opposite charge carriers does not merely improve the specific capacitance, even though the lowest charge-transfer resistance and Warburg impedance have been seen for the B/N codoped rGO in 6 M KOH electrolyte, compared to the rGO electrode doped with two types of carriers separately.[255] Consequently, a higher volumetric capacitance of B/N-doped rGO films (488 F cm^{-3} at 10 mV s^{-1} in PVA–H_2SO_4) has been obtained than that of mono-doped (N-rGO: 425 F cm^{-3}) and pristine (245 F cm^{-3}) counterparts.[256] Quantitatively, the increased EDLC contributions are estimated to be 2.9% for B-doped porous carbon-tube bundles (PCTB) and 8.6% for B/N-doped PCTB (B/N-PCTB) whereas the increased pseudocapacitive contributions are 7.7%, 15.3%, and 17.5% for N-PCTB, B-PCTB, and B/N-PCTB, respectively, compared to the pristine counterparts in similar testing conditions.[257] This fact reveals that the codoping not only enhances the pseudocapacitance but also improves the EDL capacitance of codoped nanocarbons compared to the single-doped nanocarbons.

It is important to note for the case of B/N codoping that the B—N bond formation can take place along with B—C and B—O bonds and found to enhance the charge-storage properties.[258] Along with the synergistic effect of charge distribution, redox reactions due to B-C, pyridinic-N, and pyrrolic-N, improved wettability and structural integrity, the C–N–B link formation leads to the increased pseudocapacitance of codoped nanocarbons.[259] The content of B-N and N-6, BET surface area and pore volume are observed to increase with the dopant concentration in B/N codoped graphene-like carbon.[258] Simultaneous doping with the opposite charge carriers also produces surface defects on carbon surface which in turn increases the O-content due to the moisture and CO_2 adsorption.[106] As a result, supercapacitive properties of the electrode are enhanced with the gravimetric capacitance of 389 F g^{-1} at a scan rate of 5 mV s^{-1} in 6 M KOH electrolyte, 68.6% retention at 1 V s^{-1}, 93% electrochemical stability after 20 000 charge–discharge cycles and excellent charge-transfer kinetics (2E).[258]

5.3. Choice of Appropriate Dopant Combination

Among the codoping combinations, N/F/B-doped porous carbon shows higher gravimetric capacitance in both acidic and alkaline aqueous electrolytes compared to N/S/B-doped, single-doped and other codoped porous carbons.[171] With the higher gravimetric capacitance, good rate capability and excellent electrochemical stability, the N/F/B-doped porous carbon also ensures excellent electrolyte ion accessibility as evidenced from the impedance spectra. The better supercapacitor performance of N/F/B-doped porous carbon is attributed to the enhanced i) conductivity due to N and F-doping, ii) redox reactions due to B-configurations and O-functionalities, and iii) wettability due to N, F, and B–O related configurations. On the other hand, insufficient N-content yields lower gravimetric capacitance of N/S/B doped porous carbon.[171]

As in the previous cases, the appropriate choice of dopant combinations may help boost the quantum capacitance. For instance, the quantum capacitance for the N–S–P atomistic model is found to be higher due to five outer electrons of phosphorous in comparison to N–S–B and N–S–Al atomistic model since both boron and aluminium have fewer outer electrons than phosphorus.[253] The above investigations,[171,253] indicate that the simultaneous doping of N, S, and B elements into nanocarbons may not be the most effective way to obtain high-performance doped nanocarbon-based supercapacitor electrodes, and better understanding of the underlying processes is warranted.

5.4. Porosity and Surface Area

N/P/Si-doped carbon with the higher surface area and suitable dopant contents shows higher gravimetric capacitance in 6 M KOH electrolyte.[172] This implies that ions easily access the pores of N/P/Si-doped carbon in KOH. On the other hand, N/P/Si-doped carbon with the relatively lower surface area and higher dopant content exhibits higher gravimetric capacitance in H_2SO_4 electrolyte.[172] This fact reveals that the redox reactions and hence pseudocapacitive contributions from the functional groups are more prominent in acidic electrolytes such as H_2SO_4. On the other hand, Si/P codoped carbon with high surface area, meso–micro–macro pores and enriched dopants (Si, P, and O) exhibits higher gravimetric capacitance and good charge-storage kinetics both in H_2SO_4 and KOH electrolytes compared to other Si/P codoped carbons.[169] Thus one should chose the suitable electrolyte depending on the porosity and surface area of doped nanocarbons. We stress that high surface area, large pore volume, and well balanced micro-mesopores along with the dopants are critical to improve the electrode–electrolyte interactions and hence to achieve better performance in terms of gravimetric capacitance, quantum capacitance, pseudocapacitance, rate performance, and cycle stability.[97,260–264]

5.5. Codoping with O-Functionalities

Controlling the O-functionalization and associated surface features may improve the electrochemical performances. The symmetric device of KOH-activated hierarchical porous N/O/S-enriched carbon foam in 1 M Na_2SO_4 electrolyte leading to an improved energy density of 39.8 Wh kg^{-1} at a power density of 900 W kg^{-1}.[215] Due to the synergistic effect of multidopants, the high-density N/P-doped and O-functionalized porous carbon exhibits high volumetric capacitance of 925 F cm^{-3} in 0.5 M H_2SO_4 (434.7 F g^{-1} at 0.1 A g^{-1} vs Ag/AgCl) and 760 F cm^{-3} in 6 M KOH (356.9 at 1 A g^{-1} vs Hg/HgO, 629 F cm^{-3} and 295.2 F g^{-1} in 2E).[265] The enhanced performances of N/P-doped and O-functionalized activated carbon are attributed to the P—N and P—C bond formation.[266] It is important to note that the capacitance retention of N/P-doped and O-functionalized activated carbons is found to enhance with the decrease in pyrophosphate content and the improvement in the heterogeneity of the carbon surface.[266] Extending potential window up to 1.5 from 1 V in H_2SO_4 electrolyte results in better electrochemical stability, higher charge-storage capacity and 2.2 times higher energy density of P/N-doped and O-functionalized core-shell carbon spheres based supercapacitor device potential window in the same electrolyte.[267] The

N/P-doped and O-functionalized porous carbon also shows its ability to operate in the potential window up to 1.5 V in KOH electrolyte versus Hg/HgO which leads to a higher volumetric energy density and competitive performance compared with some Ni-metal hydride cells.[265]

5.6. Limitations

We would like to emphasize that codoping can also have a negative impact on the physicochemical properties and hence supercapacitor performances unless i) the right choice of dopants and their combination with appropriate stoichiometry is made and ii) the relative ratio of dopants and/or atomic bonding configurations are optimized. For example, S-doping into the N-doped porous carbon is seen to increase the water contact angle whereas B-doping into N/S-doped porous carbon is observed to lower the electrical conductivity and increase the charge-transfer resistance while the electrode material is subjected to the electrolyte medium.[171] N-doping into the edge-carboxylated graphene nanoplatelets increases the structural defects from 16.2% to 48.9% which severely affects the electroactive surface area and electrical conductivity.[229] As a result, gravimetric capacitance decreases from 365.72 to 175.05 F g^{-1} at 1 A g^{-1} after doping.[229] Moreover, the GO–OOH–N exhibits poor rate capability and stability than the GO-N in spite of their higher capacitance initially in 6 M KOH versus SCE.[230]

In the case of multidoping, the stronger interaction between the coadatoms or codopants sometimes lead to unstable adsorption of dopants on the graphene surface once the structure is doped beyond certain concentrations.[182] As a result, monodoped nanocarbons performed sometimes better than the codoped nanocarbons.[42] A similar observation has been reported for mono- and codoped hybrid nanocarbon materials.[75] Generalizing the analysis in this section, we stress that extra caution should be paid for codoped nanocarbons to proper selection of doping environment and suitable aqueous electrolyte to further explore them as a high-performance energy storage electrodes.

6. Influence of Nonaqueous Electrolytes

When enhancing the energy density is concerned, the organic or ionic electrolyte may also be the choice of electrolyte to enhance wettability, electrode/electrolyte interactions and potential window. Wettability of the electrode can be improved by using organic electrolyte further with S-content. The contact angle of S-rich carbon cryogel electrode in an organic electrolyte is improved from 42.6° (±1.4°) to 15.5° (±1.1°) with the increase of S-content from 0.5% to 2.5%.[162] Better wettability and efficient electrode–electrolyte interactions leads to the better accessibility of the pores by electrolyte ions which are preferable to enhance the energy and power density of device.

It is noteworthy to mention that the pseudocapacitive effect of doping does not show significant effects in organic or ionic electrolyte.[89,268] Hence, the total capacitance of doped nanocarbons in organic or ionic electrolyte is mostly found to be lower than that in aqueous electrolyte (**Figure 19**A–C).[67,112,153,263] Although EDL features have been seen, 3D porous carbon nanosheets with N-doping and O-functionalization deliver higher gravimetric capacitance of 421 F g^{-1} at 1 A g^{-1}, 80% capacitance retention at 50 A g^{-1} and faster electrolyte penetration than those of thermally treated GO in 3-E configuration.[269] Surprisingly, N-doped graphene shows higher gravimetric capacitance in 1 M $BMIMBF_4$/AN

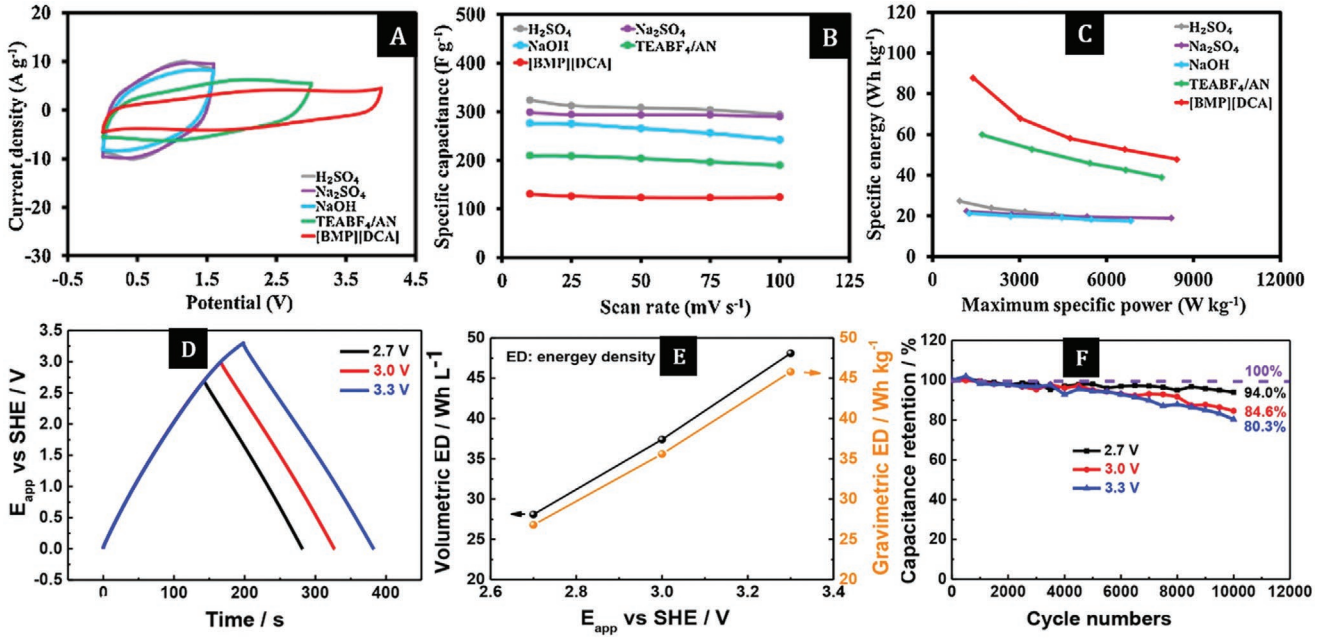

Figure 19. Influence of electrolytes. Supercapacitive properties of A–C) carboxylate-modified hollow carbon nanospheres with its supercapacitor performance in the various electrolytes. Reproduced with permission.[271] Copyright 2017, Elsevier; and D–F) P-doped nanocarbons in TEABF4/PC. Reproduced with permission.[177] Copyright 2019, Elsevier.

(631 F g^{-1} at 5 mV s^{-1} within 3 V potential window) than that in 1 M H_2SO_4 (348 F g^{-1} at 5 mV s^{-1} within 1 V) with respect to the corresponding reference electrode.[270] In the case of N-doped and O-functionalized nanocarbons, the change in adsorption energy of TEA^+ before and after NH_4^+ adsorption on 3D porous carbon nanosheets with N and O-doping (interlayer spacing of 0.419 nm) was negative, which reveals the stable adsorption of electrolyte ions and hence the enhanced capacity. Whereas, rGO with an interlayer spacing of 0.391 nm shows the positive change in adsorption energy which indicates an endothermic process and hence unstable TEA^+ adsorption.[269]

Regarding the extended potential window of the device, one should be extremely careful to identify the voltage threshold when the cycle stability is maintained. For example, although the potential window of P-doped carbon electrodes in organic electrolyte is extended up to 3.3 V, the cycle stability of the electrode in 3.3 V is not promising as the electrode performed within the 2.7 V window (Figure 19D–F).[177] The highest potential window of 4 V has been achieved with asymmetric EDLC device with vertical graphene and N-doped vertical graphene nanostructures in $TEABF_4$/PC electrolyte.[272] The redox reactions in an organic electrolyte ($TEABF_4$/PC) are proposed as follows[273]

$$-C-PH_2 : + (C_2H_5)_4N^+ \leftrightarrow -C-PH_2-(C_2H_5)_4N^+ \quad (23)$$

$$-C-PH : + (C_2H_5)_4N^+ \leftrightarrow -C-PH-(C_2H_5)_4N^+ \quad (24)$$

$$-C\equiv P : + (C_2H_5)_4N^+ \leftrightarrow -C\equiv P-(C_2H_5)_4N^+ \quad (25)$$

Doped nanocarbons are also tested in various ionic electrolytes namely, 1-ethyl-3-methyl imidazolium tetrafluoroborate ($EMIMBF_4$), 1-butyl-3-methylimidazolium phosphate ($BMIMPO_4$) and 1-butyl-4-methyl pyridinium tetrafluoroborate ($BMPyPBF_4$). We can see that the higher energy density of B-doped RGO in $EMIMBF_4$ compared to other ionic electrolytes can likely be attributed to the low viscosity, high ionic conductivity, and relatively lower cation size.[112] As-fabricated symmetric cell of carboxylate-modified hollow carbon nanospheres exhibits higher energy and power densities in an ionic electrolyte although the electrode showed higher capacitance in H_2SO_4 electrolyte (Figure 19A–C).[271] The stable operating potential window of 3.5 V is obtained using $EMIMBF_4$-ionogel for the N/S-doped and O-functionalized carbon-based symmetric device in order to drastically increase the energy density. The solid-state device also exhibited excellent flexibility under various bending angles and electrochemical stability over charge–discharge cycles.[72]

Not only the specific capacitance and voltage window seen to be enhanced in the higher potential window, the P-doped carbon electrode also shows the lowest leakage current (<1.2 μA) in $TEABF_4$ electrolyte.[174] The lower leakage current of 0.009 mA for P-doped rGO after 2.5 h of testing and higher voltage of 0.5146 V after experiencing 6.5 h of open-circuit conditions compared to undoped rGO (0.1 mA and 0.1615 V) are certainly a proof of the positive effect of P-doping.[166] A higher stabilizing effect and lowest leakage current have also been exhibited by N-doped activated carbon fiber in organic electrolyte compared to bare carbon nanofiber.[274] This effect can be attributed to the presence of positively charged pyrrole and/or pyridone N-groups.

The use of nonaqueous electrolytes has several shortcomings in terms of safety, toxicity, decomposition, moisture-sensitivity, cost, etc. In addition, for example, edge-functionalized oxygen groups showed poor electrochemical stability and capacitive performance of the carbon nanostructures in the organic medium due to pore blockage of material and separator by the evolved gas.[235] Another acknowledged flaw of oxygenated carbon composites in the organic electrolyte is irreversible redox reactions between the organic electrolyte and oxygen.[275] However, one should beware of the recurring problem of organic electrolyte decomposition for N-doped nanocarbons due to the amine group through the nucleophilic attack.

7. Key Features and Guidelines

The key features of the effects of dopants on the physicochemical properties of nanocarbons are presented in Figure 2 whereas the supercapacitor performance is summarized in Tables 1 and 2. The Ragone plot of doped nanocarbon based symmetric supercapacitor devices is shown in **Figure 20** and found to be on the par with the existing advanced energy storage materials.[276–278] We have excluded the data of energy density and power density calculated from 3E test in Figure 20 since they do not add to the discussion.

While tabulating the results of electrochemical performances of electrode materials (Tables 1 and 2), we have found many missing electrochemical parameters in the published articles. Readers are encouraged to follow the general guidelines for supercapacitor research, such as reporting normalized capacitance minimum at the scan rate of 10 mV s^{-1} or the current density of 2 A g^{-1}, providing information on Self-discharge or leakage current, from relevant references.[47,90,285–288] Below we formulate and refine the following general guidelines related to the supercapacitor research involving doping processes in electrode preparation.

1. *Doping content*: It has been seen that the normalized capacitance does not necessarily increase with the doping concentration. Since the codoping often has a synergistic effect, doping with more than one dopant tends to enhance the electrochemical performance, yet increases the overall doping concentration. We emphasize that the concentration of foreign atoms in the base matrix beyond a certain threshold should not be considered as doping. Moreover, capacitive features such as reversible capacitance, rate performance, capacity retention of doped nanocarbons may deteriorate beyond a certain doping level.[289] As defined, the content of dopant in the matrix should be minimum and within a certain limit (e.g., typically around 5 at. %).
2. *Balance between capacitive contributions*: Since the total capacitance is a combination of EDLC, pseudocapacitance and quantum capacitance, one should strike a balance between them to obtain the higher capacitance, rate performance, cycle stability, and improve other capacitive features.

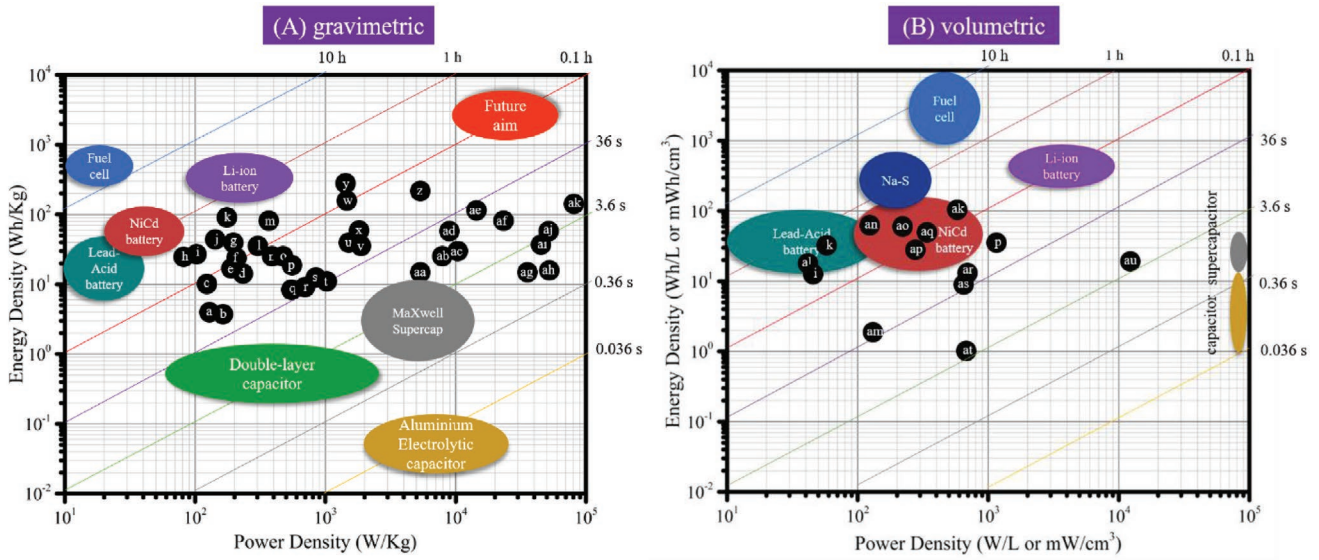

Figure 20. Ragone plot of doped nanocarbon-based supercapacitor device. A) Gravimetric and B) Volumetric Ragone plot of doped nanocarbon-based symmetric supercapacitor at a gravimetric/volumetric power density in comparison with existing energy storage devices. Each letter(s) with black circle represents the data of doped nanocarbons based supercapacitors. a) B-doped rGO,[120] b) B/N codoped porous carbon,[117] c) O-rich hierarchical porous carbon,[279] d) N-doped porous nanosheet carbon,[280] e) P-doped hierarchical porous carbon aerogel,[178] f) B/N codoped porous carbon nanowire,[118] g) N/O/P-doped porous carbon,[281] h) N/O codoped honeycomb porous carbon,[263] i) porous carbon layer/graphene hybrids containing N and O,[282] j) F-rich nanoporous carbon,[71] k) O/N/S-tridoped carbon,[72] l) N-doped multiscale porous carbon,[78] m) N/O-3D porous carbon nanosheets,[269] n:N/P/S self-doped porous carbon,[246] o) N/S-GNR,[80] p) N/P/O-doped porous carbon,[265] q) N-rGO,[89] r) S-doped mesoporous AC,[155] s) P-doped rGO,[77] t) S-doped carbon nano-onions,[150] u) P-doped porous carbon,[174] v) Passivated P-doped RGO,[166] w) N-doped rGO,[131] x) SN-rGO,[261] y) N-doped rGO aerogel coated on carboxyl-modified carbon fiber paper,[67] z) N/O-enriched nanoporous carbon,[283] aa) N/S-codoped graphene hydrogel,[143] ab) N-rich carbon nanorod arrays,[68] ac) N/S-rGO hydrogel,[250] ad) P-ErGO,[184] ae) carboxylate-modified hollow carbon nanospheres,[271] af) N/S-enriched porous carbon,[251] ag) hierarchical porous N/O/S-enriched carbon foam,[215] ah) Rich S-doped porous carbon,[152] ai) N-doped mesoporous carbon,[66] aj) S-doped porous carbon,[152] ak) BNP-holey graphene hydrogel,[245] al) N-doped microporous carbon microspheres,[268] am) hemispherical N-doped carbon spheres,[84] an) N-incorporated thiol-functionalized rGO scrolls,[252] ao) N-doped hierarchical porous carbon,[85] ap) functional pillared graphene frameworks,[223] aq) P-modified porous carbon aerogel microspheres,[177] ar) B/N-doped porous carbon-tube bundles,[257] as) fluorinated AC,[190] at) N-doped CNT,[144] au) ordered mesoporous few layer carbon-N[66] (some data are extracted and/or calculated data from the corresponding figure of cited reference and volumetric energy/power density of device is either calculated multiplying gravimetric counterpart with the packing density of materials or simply converting cm^3 unit to liter unit).

3. *Choice of aqueous electrolyte*: Choice of proper aqueous electrolyte is crucial since the doping configurations behave differently in acidic and basic media. Noteworthy, the pseudocapacitive contribution of heteroatom-enriched nanoporous carbon depends on the voltage range applied to aqueous electrolyte containing alkali cation charge carriers.[283] The potential window of the aqueous-based symmetric device in KOH, H_2SO_4, and Na_2SO_4 electrolytes is typically 1–1.4, 1–1.9, and 1.6–2.6 V, respectively (**Table 2**). Besides, almost rectangular cyclic voltammogram with the lower area under the curve is observed for doped nanocarbons in neutral electrolyte and hence better rate performance is obvious, whereas voltammogram with the higher area under the curve and distinct redox peaks testifies to the pronounced and higher pseudocapacitive effects in H_2SO_4 and KOH electrolytes along with the EDLC contribution.[118,216] Surprisingly, the higher gravimetric capacitance of doped nanocarbons is observed in Na_2SO_4 than in H_2SO_4.[150,159,163] Moreover, it has been seen in a few reports that the charge-storage performance of doped nanocarbons is explored either in an acidic or basic aqueous electrolyte with respect to the reference electrode while the device performance is demonstrated in a neutral electrolyte.[86,215,280,281] The use of pH-neutral electrolyte along with the doped nanocarbons allows operation within the relatively higher potential window (≥2 V) and this behavior is ascribed to the high overpotential for hydrogen evolution (0.6 V).[280,290] We emphasize that the charge-storage performance of doped nanocarbons in a neutral electrolyte is important to validate the pseudocapacitive contribution by the dopants. In addition, one needs to maintain the molar concentration of electrolytes where comparison on the performance of the electrode has been discussed, since molar concentration has a significant impact on the supercapacitive performance.[291]
4. *Asymmetric supercapacitor*: To enhance the potential window of device operation and hence the energy density, asymmetric supercapacitor fabrication is a promising solution. F-doping and N-doping of negative and positive electrodes, respectively, is predicted as a highly promising combination for the development of doped nanocarbon-based next-generation asymmetric aqueous supercapacitors.[193] N-doped and S-doped nanocarbons can be used as a negative electrode.[150,292] B-doped nanocarbons also could be effective for asymmetric supercapacitor whereas P-doped CNTs are better suited for symmetric supercapacitors.[173] Although

Table 2. Supercapacitor performances of heteroatom doped nanocarbons compared to their pristine counterpart in various electrolytes (HPC: hierarchical porous carbon; activated carbon: AC; NW: nanowires; CF: carbon fiber, 3E: 3-electrode, 2E: 2-electrode), and versus the reversible hydrogen electrode (RHE), saturated calomel electrode (SCE).

Ref.	Nanocarbons	Mass loading	Specific capacitance [F g^{-1}]	Potential window/voltage, electrolyte, reference electrode	Rate performance [%], current density/scan rate	Cap. retention [%], CD cycles, current density/scan rate	ESR or charge-transfer resistance [Ω]
[112]	rGO	3 mg cm^{-2}	170, 1 A g^{-1}	–0.9 to 0.1 V, 20% KOH, Hg/HgO	72.35, 10 A g^{-1}	–	1.2
	B-rGO by supercritical fluid		286, 1 A g^{-1}		69.93, 10 A g^{-1}	–	0.8
	B-rGO by hydrothermal		142, 1 A g^{-1}		77.46, 10 A g^{-1}	–	3
	B-rGO‖B-rGO (supercritical fluid)		152, 1 A g^{-1}	1 V, 20% KOH	81.7, 5 A g^{-1}	67%, 3k, 5 A g^{-1}	–
			106, 1 A g^{-1}	2.4 V, 1 M $NaClO_4$,	62.4, 5 A g^{-1}	84%, 3k, 5 A g^{-1}	–
			139, 0.1 A g^{-1}	3 V, $EMIMBF_4$	62.9, 1 A g^{-1}	92%, 1k, 1 A g^{-1}	–
			45, 1 A g^{-1}	3 V, $BMIMPO_4$	–	–	–
			56, 1 A g^{-1}	3 V, $BMPyPBF_4$	–	–	–
[114]	Thermally rGO	1 mg cm^{-2}	135, 10 mV s^{-1}	–0.9 to –0.1V, 6 M KOH, Hg/HgO	45, 200 mV s^{-1}	101, 3k, 50 mV s^{-1}	–
	B-doped TrGO		448, 10 mV s^{-1}		50, 200 mV s^{-1}	108, 3k, 50 mV s^{-1}	–
[81]	Virgin CF	–	0.17, 1 A g^{-1}	–1.4 to 1.0 V, 1 M Na_2SO_4, SCE	–	–	–
	Solvothermal RCF		0.375, 1 A g^{-1}		–	–	–
	Aerobic RCF		52, 1 A g^{-1}		29%, 8 A g^{-1}	90, 10k, 8 A g^{-1}	lowest
	ARCF‖ARCF		–	1 V, 6 M KOH	–	–	–
			–	1.9 V, 1 M H_2SO_4	–	–	–
			–	2.4 V, 1 M Na_2SO_4	–	93.6, 10k	–
[279]	O-rich HPC-500 activated at 500 °C	5 mg on 1 × 1 cm^2 Ni foam	217.3, 0.5 A g^{-1}	–1.0 to 0 V, 6 M KOH, Hg/HgO	55.7, 50 A g^{-1}	–	0.78
	O-rich HPC-600		426.9, 0.5 A g^{-1}		71, 50 A g^{-1}	–	0.8
	O-rich HPC-800		286.1, 0.5 A g^{-1}		86.3, 50 A g^{-1}	–	0.74
	O-HPC‖O-HPC		269, 0.5 A g^{-1}	1 V, 6 M KOH	63, 40 A g^{-1}	97, 10k, 5 A g^{-1}	–
	YP-50F‖YP-50F		113, 0.5 A g^{-1}		82, 40 A g^{-1}	–	
[66]	YP-50		175, 1 A g^{-1}	–0.2 to 0.8 V, 0.5 H_2SO_4 (pH 0)	–	81[a], 40k	–
	Ordered mesoporous carbon (OMC)		135, 1 A g^{-1}		–	–	–
	OM few-layer carbon (OMFLC)		325, 1 A g^{-1}		–	–	–
	8.2% N-OMFLC (S1)		715, 1 A g^{-1}		67.5[a], 40 A g^{-1}	81.2[a], 50k	–
			690, 1 A g^{-1}	–0.5 to 0.8 V, 2 M Li_2SO_4	–	79.3[a], 50k	–
			405, 1 A g^{-1}	–0.8 to 0.1 V, 1 M KOH	63.1[a], 30 A g^{-1}	–	–
	7.5% N-OMFLC (S2)		730, 1 A g^{-1}	–0.2 to 0.8 V, 0.5 H_2SO_4 (pH 0)	–	–	–
	11.9% N-OMFLC (S3)		655, 1 A g^{-1}		–	–	–
	SM (Mixed of S1, S2 and S3)		855, 1 A g^{-1}		71.9, 40 A g^{-1}	–	0.8
	SM‖SM	0.5 mg cm^{-2}	840 (69 F cm^{-3})[a], 1 A g^{-1}	1.2 V, 0.5 H_2SO_4 (pH 0)	–	82, 50k	
		10 mg cm^{-2}	737[a] (475 F cm^{-3})[a], 1 A g^{-1}		–	–	–
		0.5 mg cm^{-2}	742[a] (60 F cm^{-3})[a], 1 A g^{-1}	1.6 V, 2 M Li_2SO_4 (pH 1.8)	–	80, 50k	–
		10 mg cm^{-2}	648[a] (417 F cm^{-3})[a], 1 A g^{-1}		–	–	–

Table 2. Continued.

Ref.	Nanocarbons	Mass loading	Specific capacitance [F g^{-1}]	Potential window/voltage, electrolyte, reference electrode	Rate performance [%], current density/scan rate	Cap. retention [%], CD cycles, current density/scan rate	ESR or charge-transfer resistance [Ω]
[67]	N-rGO aerogel	≈0.5 mg cm^{-2} on carboxyl-modified CF paper	592.25[a], 1 A g^{-1}	1.5 V[a], NaOH	96[a], 4 A g^{-1}	–	–
			579.33[a], 1 A g^{-1}	1.6 V[a] H_2SO_4	86.3[a], 4 A g^{-1}	–	–
			463.05[a], 1 A g^{-1}	1.8 V[a], Na_2SO_4	79.1[a], 4 A g^{-1}	–	–
			303.73[a], 1 A g^{-1}	2.5 V[a], $TEABF_4$/AN	63.9[a], 4 A g^{-1}	–	–
			764.53[a], 1 A g^{-1}	4 V, [BMP][DCA]	88, 4 A g^{-1}	66.1, 3k	11.44
	N-rGO nanosheets		493.2[a], 1 A g^{-1}		97[a], 4 A g^{-1}	85.6, 3k	17.38
[68]	PANI nanorod array	1.5 mg cm^{-2}	408.36[a], 1 A g^{-1}	–0.2 to 0.7 V, 1 M H_2SO_4, SCE	–	49.2, 0.5k, 50 mV s^{-1}	–
	N-rich carbon nanorods (N-CNR)		776, 1 A g^{-1}		66, 20 A g^{-1}	94.43, 5k, 40 A g^{-1}	–
		4.5 mg cm^{-2}	560.38, 1.5 mA cm^{-2}		54.96, 30 mA cm^{-2}	–	–
	N-CNR‖N-CNR	1.5 mg cm^{-2}	116[a], 1 A g^{-1}	1.6 V, 1 M H_2SO_4	58[a], 20 A g^{-1}	85.76, 10k, 20 A g^{-1}	–
[146]	Porous carbon	4.5 mg	92, 0.5 A g^{-1}	–1.0 to 0 V, 6 M KOH, Hg/HgO	25, 10 A g^{-1}	–	0.62
	N-hollow carbon sphere (HPC) with closed pores		189.2, 0.5 A g^{-1}		74.3, 10 A g^{-1}	–	0.42
	N-HPC with semi-closed pores		255, 0.5 A g^{-1}		83.1, 10 A g^{-1}	–	0.42
	N-HPC with open pores (N-HPC-O)		436.5, 0.5 A g^{-1}		84.1, 10 A g^{-1}	95.2, 20k, 5 A g^{-1}	0.35
	N-HPC-O‖N-HPC-O		340, 0.5 A g^{-1}	1 V, 6 M KOH	75.2, 10 A g^{-1}	–	–
[131]	Coin cell: rGO‖rGO	10 ml paste on 5 × 15 cm^2 CF	464, 1 A g^{-1}	3 V, 0.2 M PPD + 1 M $TEABF_4$/ACN	–	77[a], 1k, 1 A g^{-1}	8.6
	Coin cell: N-doped rGO ‖ N-doped rGO		272, 1 A g^{-1}	3 V, 1 M $TEABF_4$/ACN	–	92, 1k, 1 A g^{-1}	–
			562, 1 A g^{-1}	3 V, 0.2 M PPD + 1 M $TEABF_4$/ACN	–	85, 1k, 1 A g^{-1}	3.74
	Pouch cell: N-doped rGO‖ N-doped rGO	Paste on 4 × 6 cm^2 CF	153, 1 A g^{-1}	3 V, 1 M $TEABF_4$/ACN	–	88.7, 1k, 1 A g^{-1}	–
			340, 1 A g^{-1}	3 V, 0.2 M PPD + 1 M $TEABF_4$/ACN		80.3, 1k, 1 A g^{-1}	–
[148]	3D porous carbon (PC)-rGO	2 mg cm^{-2}	610, 2 A g^{-1}	–1 to 0 V, 1 M H_2SO_4, Ag/AgCl	–	–	0.32
	3D PC-rGO/PANI		1198, 2 A g^{-1}		–	–	–
	N-PC(rGO-C_3N_4)		740, 2 A g^{-1}		–	–	–
	3D PC-rGO/PANI ‖ 3D PC-rGO/PANI		440, 2 A g^{-1}	1 V, 1 M H_2SO_4	80.45, 30 A g^{-1} g^{-1}	94, 10k, 5 A g^{-1} g^{-1}	0.65
			212, 2 A g^{-1} g^{-1}	1.8 V, 0.5 M Na_2SO_4	72, 20 A g^{-1} g^{-1}	–	–
	3D PC-rGO/PANI// N-PC(rGO-C_3N_4)		216, 2 A g^{-1} g^{-1}	1.8 V, 0.5 M Na_2SO_4	75, 20 A g^{-1} g^{-1}	91, 10k, 5 A g^{-1} g^{-1}	–
[124]	HPC-0	10 mg cm^{-2}	62.7[a], 0.5 A g^{-1}	–	19.8[a], 10 A g^{-1}	–	–
	N-enriched HPC-activated at 800 °C		641.6 (0.412 F m^{-2}), 1 A g^{-1}	–0.9 to 0 V, 6 M KOH, Hg/HgO	69, 40 A g^{-1}	–	–
	N-HPC‖ N-HPC		563.9, 1 A g^{-1}	0.9 V, 6 M KOH	61.7, 40 A g^{-1}	94.3, 5k, 5 A g^{-1}	–
			305, 2 A g^{-1}	1 V, 1 M Na_2SO_4	57, 11 A g^{-1}	95, 10k, 5 A g^{-1}	–
[150]	Carbon nano-onions (CNO)‖CNO	–	110.8[a], 1 A g^{-1}	1 V, 1 M Na_2SO_4	69[a], 7 A g^{-1}	–	–

Table 2. Continued.

Ref.	Nanocarbons	Mass loading	Specific capacitance [F g^{-1}]	Potential window/voltage, electrolyte, reference electrode	Rate performance [%], current density/scan rate	Cap. retention [%], CD cycles, current density/scan rate	ESR or charge-transfer resistance [Ω]
	S-CNO‖S-CNO		188.2, 1 A g^{-1}	1 V, 1 M H_2SO_4	72, 10 A g^{-1}	–	–
			305, 2 A g^{-1}	1 V, 1 M Na_2SO_4	57, 11 A g^{-1}	95, 10k, 5 A g^{-1}	–
[153]	rGO aerogel	2 mg	118.3, 5 mV s^{-1}	0–0.7 V, 1 M H_2SO_4 vs Ag/AgCl	73.5, 100 mV s^{-1}	73.2, 1.5k, 100 mV s^{-1}	–
	S- rGO aerogel		445.6, 5 mV s^{-1}		78.2, 100 mV s^{-1}	83.4, 1.5k, 100 mV s^{-1}	–
			85.9, 1 A g^{-1}	1.8 V, 1 M $LiClO_4$	49, 100 mV s^{-1}	–	–
			91.92	3.5 V, 1 M $BMIMPF_6$	36, 100 mV s^{-1}	–	–
[77]	Thermally (T) rGO	1–2 mg cm^{-2}	29, 0.05 A g^{-1}	1 V, 1 M H_2SO_4	22, 30 A g^{-1}	–	–
	P doped TRGO		115, 0.05 A g^{-1}		24, 30 A g^{-1}	–	–
	P-TrGO‖P-TrGO		29, 1 A g^{-1}	1.7 V, 1 M H_2SO_4	–	97, 5k, 5 A g^{-1}	–
[178]	HPC aerogel	2 mg cm^{-2}	175.2, 1 A g^{-1}	1 V, 6 M KOH vs standard Hg	55.9, 100 A g^{-1}	95, 10k, 4 A g^{-1}	0.4
	P-doped HPC aerogel		406.2, 5 mV s^{-1}; 208.9, 1 A g^{-1}		65.8, 500 mV s^{-1}; 66.8, 100 A g^{-1}	100, 10k, 4 A g^{-1}	0.39
		60 mg cm^{-2}	348.8		–	–	–
	P-HPC‖P-HPC	2 mg cm^{-2}	149.1, 1 A g^{-1}	1 V, 6 M KOH	83, 10 A g^{-1}	100, 10k, 2 A g^{-1}	
[184]	Exfoliated GO (EGO)	–	74.31, 5 mV s^{-1}	–0.9 to 0.9 V, 1 M H_2SO_4	20.1[a], 100 mV s^{-1}	94.4[a], 5k	0.91053
	REGO		148.63, 5 mV s^{-1}		23.1[a], 100 mV s^{-1}	93.4[a], 5k	1.6947
	P-EGO		245.08, 5 mV s^{-1}		56.8[a], 100 mV s^{-1}	97.2[a], 5k	0.86495
	P-REGO		367.62, 5 mV s^{-1}		45.7[a], 100 mV s^{-1}	97.6[a], 5k	0.80874
[189]	Undoped AC	–	375, 2 mV s^{-1}	0–1 V, 1 M H_2SO_4 Ag/AgCl	38, 50 mV s^{-1}	–	4.82
	F-doped AC		491, 2 mV s^{-1}		43, 50 mV s^{-1}	–	7.69
[201]	rGO	1.5 mg	101.1, 10 mV s^{-1}	–0.2 to 1.1 V, 1 M H_2SO_4 Ag/AgCl	80.3, 100 mV s^{-1}	–	6.2
	Cl-rGO		179.6, 10 mV s^{-1}		86.3, 100 mV s^{-1}	–	3.4
[202]	rGO film	1 mg cm^{-2}	140.5, 1 A g^{-1}	0–1 V, 6 M KOH, 2E	19.5, 100 A g^{-1}	94.3, 5k, 30 A g^{-1} g^{-1}	3.52
	Cl-rGO film		210 (266.7 F cm^{-3}), 1 A g^{-1}		71.2, 100 A g^{-1}	92.1, 5k, 30 A g^{-1}	0.90
	Flexible SSC	11 mg cm^{-2}	2.312 mF cm^{-2}, 1 mA cm^{-2}	1 V, PVA-KOH	78.7, 20 mA cm^{-2}	98, 500 bending cycles	–
[247]	rGO aerogels	1.5 mg cm^{-2}	240, 10 mV s^{-1}	0–0.8 V, 1 M H_2SO_4, Ag/AgCl	80, 500 mV s^{-1}	78.1, 10k, 1 A g^{-1}	–
	S-rGO aerogels		347, 10 mV s^{-1}		–	–	–
	P-rGO aerogels		313, 10 mV s^{-1}		–	–	–
	SP-rGO aerogels		438, 10 mV s^{-1}; 425, 1 A g^{-1}		87.2, 500 mV s^{-1}; 86, 20 A g^{-1}	93.4, 10k, 1 A g^{-1}	–
			198, 1 A g^{-1}	0.8 V, 1 M $LiClO_4$	62, 20 A g^{-1}	–	–
			208, 1 A g^{-1}	0.8 V, $BMIMPF_6$	54, 20 A g^{-1}	–	–
[284]	N/O codoped carbon nanospheres	–	627, 1 A g^{-1}	1.5 V, 3 M H_2SO_4	42.6, 6 A g^{-1}	224.9, 10k, 7 A g^{-1}	0.36
[263]	N/O codoped honeycomb carbon‖ N/O codoped honeycomb carbon	15 mg cm^{-2}	533, 0.5 A g^{-1}	1 V, 6 M KOH, $Hg/HgCl_2$	39.9[a], 20 A g^{-1}	–	0.98
			92, 0.1 A g^{-1}	1 V, 6 M KOH	48.9, 20 A g^{-1}	93.9, 20k, 2 A g^{-1}	0.89
			59, 0.1 A g^{-1}	1.8 V, Na_2SO_4	58, 20 A g^{-1}	90.7, 20k, 2 A g^{-1}	3.01
			48.4, 0.5 A g^{-1}	3.5 V, EMIMBF4	52.8[a], 10 A g^{-1}	91.5, 10k, 2 A g^{-1}	–
[250]	S-doped GO	2 mg cm^{-2}	282, 0.5 A g^{-1}	–1.2 to –0.2 V, 6 M KOH, SCE	64.7[a], 10 A g^{-1}	–	≈1.90[a]
	N-doped GO		371, 0.5 A g^{-1}		54.9[a], 10 A g^{-1}	–	≈1.85[a]
	NS-codoped GO		566, 0.5 A g^{-1}		39[a], 10 A g^{-1}	95, 2k, 3 A g^{-1}	≈0.77[a]
	NS-GO‖NS-GO		193, 100 mV s^{-1}	1 V, 6 M KOH	62.6, 1 V s^{-1}	93, 2k, 5 A g^{-1}	–

Table 2. Continued.

Ref.	Nanocarbons	Mass loading	Specific capacitance [F g^{-1}]	Potential window/voltage, electrolyte, reference electrode	Rate performance [%], current density/scan rate	Cap. retention [%], CD cycles, current density/scan rate	ESR or charge-transfer resistance [Ω]
[261]	SN-rGO	3.4 mg cm^{-2}	503, 1 A g^{-1}	0–0.9 V, 6 M KOH, Ag/AgCl	52, 5 A g^{-1}	89.4, 10k, 10 A g^{-1}	–
	SN-rGO‖ SN-rGO		509, 1 A g^{-1}	0.9 V, 6 M KOH	63.8, 5 A g^{-1}	–	–
[262]	N,S codoped HPC nanospheres	0.5 mg cm^{-2}	800, 1 A g^{-1}	0–1 V, 6 M KOH, RHE	–	94.8, 15k, 5 A g^{-1}	–
		3 mg cm^{-2}	500, 1 A g^{-1}		–	–	–
		0.5 mg cm^{-2}	710, 1 A g^{-1}	0–1 V, 1 M H_2SO_4, RHE	–	92.1, 15k, 5 A g^{-1}	–
[118]	BN codoped PC (BNDC) NW	0.35 mg cm^{-2}	504, 1 A g^{-1}	–0.2 to 0.8 V, 1 M H_2SO_4, SCE	67, 10 A g^{-1}	104.8, 5k, 10 A g^{-1}	–
			358.4, 1 A g^{-1}	–0.7 to 0.3 V, 1 M KOH, SCE	60.3, 10 A g^{-1}	96.8, 5k, 10 A g^{-1}	–
			265.2, 1 A g^{-1}	–0.2 to 0.8 V, 1 M Na_2SO_4, SCE	56, 10 A g^{-1}	98.5, 5k, 10 A g^{-1}	–
	BN-DC NW‖BN-DC NW		255.7, 1 A g^{-1}	1.6 V, PVA-H_2SO_4	62, 10 A g^{-1}	91, 5k, 5 A g^{-1}	–
[257]	B/N-doped porous carbon-tube bundles (PCTB)	10 mg cm^{-2}	277, 1 A g^{-1}	6 M KOH, Ag/AgCl	81.2, 20 A g^{-1}	–	–
		30 mg cm^{-2}	235, 1 A g^{-1}		78.7, 20 A g^{-1}	–	–
		40 mg cm^{-2}	216, 1 A g^{-1}		69.4, 20 A g^{-1}	96, 10k, 20 A g^{-1}	–
	AC		119[a], 1 A g^{-1}		61.1[a], 20 A g^{-1}	85.9[a], 10k, 20 A g^{-1}	–
	BN-PCTB‖ BN-PCTB	(40 + 40) mg cm^{-2}	33.9[a] (27 F cm^{-3}), 0.5 A g^{-1}	1.8 V, 1 M Na_2SO_4	64, 20 A g^{-1}	92, 10k, 20 A g^{-1}	–
[245]	GH	1 mg cm^{-2}	148[a], 1 A g^{-1}	3.5 V, 1 M $EMIMBF_4$/AN, symmetric cell	31[a], 100 A g^{-1}	74.3, 30k, 10 A g^{-1}	–
	Holey GH (HGH)		200[a], 1 A g^{-1}		42[a], 100 A g^{-1}	82.7, 30k, 10 A g^{-1}	–
	BNP-GH		305[a], 1 A g^{-1}		68[a], 100 A g^{-1}	89.6, 30k, 10 A g^{-1}	–
	BNP-HGH		350 (234 F cm^{-3}), 1 A g^{-1}		71.8, 100 A g^{-1}	90.5, 50k, 20 A g^{-1}	–
		10 mg cm^{-2}	316 (212 F cm^{-3}), 1 A g^{-1}		67.5	81.3, 50k, 20 A g^{-1}	
		1 mg cm^{-2}	362, 1 A g^{-1}	1 V, 1 M H_2SO_4/glass fiber membrane	71, 100 A g^{-1}	–	–
		1 mg cm^{-2}	345, 1 A g^{-1}	1 V, PVA-H_2SO_4	58, 100 A g^{-1}	91.6, 20k under 180 °C bending angle, 10 A g^{-1}	–
[72]	ONS-C‖ONS-C	10 mg cm^{-2}	324, 0.2 A g^{-1}	1.0 V, 6 M KOH	59, 20 A g^{-1}	90.8, 20k, 5 A g^{-1}	0.95
			256, 0.2 A g^{-1}	1.8 V, 1 M Na_2SO_4	53, 20 A g^{-1}	93.2, 20k, 5 A g^{-1}	0.93
			196, 0.5 A g^{-1}	3.5 V, $EMIMBF_4$ ionogel	56, 10 A g^{-1}	91.6, 10k, 1 A g^{-1}	16.8
[248]	Carbonized buckwheat flour	3 mg cm^{-2}	190 (149.7 F cm^{-3}), 1 A g^{-1}	–1 to 0 V, 0.5 M Na_2SO_4, Ag/AgCl	4[a], 20 A g^{-1}	–	–
	KOH-activated buckwheat flour		407 (320.7 F cm^{-3}), 1 A g^{-1}		9[a], 20 A g^{-1}	–	–
	3D honeycomb like PC foam (O, N, S, P)		767 (604.3 F cm^{-3}), 1 A g^{-1}		36, 20 A g^{-1}	92.6%, 10k, 10 A g^{-1}	–

[a]Extracted and/or calculated data from the corresponding figure of cited reference.

the impact of dopants is found to be pronounced mostly in aqueous electrolytes rather than in organic or ionic electrolytes, asymmetric devices of doped nanocarbons in organic and ionic electrolytes are capable to operate with the potential windows of 2.5–3 and 3–4 V, respectively.

5. *Pseudocapacitance and rate performance*: Since the pseudocapacitive contribution originates from the dopants alone, the rate capability of doped nanocarbon is found to be poor at higher current densities although it exhibits much higher gravimetric and volumetric capacitance at lower current

densities.[73] A poor rate performance has been seen when the electrode material provides higher pesudocapacitive contributions.[73] Hence, we envision a doped nanocarbon electrode with balanced EDLC and pseudocapacitance contributions to achieve a good rate capability while maintaining other supercapacitive features since the rate capability defines the power density of device.[282]

6. *Cycle life*: Cycle life is another important parameter of supercapacitors. Surprisingly, a drastic enhancement in capacitance of doped and/or functionalized nanocarbons with retention of more than 100% with charge–discharge cycles is observed.[49,284,293] It may happen due to the higher wettability, change in the O-functionalities in the structure and structural improvement during the cycles.[168] However, this drastic enhancement in capacitance retention certainly requires further direct evidences, particularly on the physicochemical properties changes of active materials after a certain number of charge–discharge cycles. In addition, one needs to ensure the better wettability of electrode by immersing it in a suitable electrolyte for at least for 12–24 h before carrying the electrochemical tests.[294]
7. *Electroactive surface area versus BET surface area*: The BET surface area of doped nanocarbon is in most cases different from the corresponding undoped materials. The variation of BET surface area has been found to depend on the doping concentration and dopant type. This implies that the electroactive sites and surface area are more relevant than the BET surface area of nanocarbons after doping, which is one of the factors for the improved supercapacitive properties.[54] In addition, the BET surface area often overestimates the actual surface area of the sample.[52,260,286] Hence, establishing the correlation between electroactive surface area with the supercapacitive performance could provide a more in-depth understanding.

   In order to estimate the electroactive surface area, one can find out the double layer capacitance C_{dl} (mF) from the capacitive charging–discharging current (i_C) versus the scan rate (v in V s^{-1}) plot ($C_{dl} = i_C / v$) and divide it by the general specific capacitance 40 µF cm^{-2} in 1 M NaOH or 35 µF cm^{-2} in 1 M H_2SO_4 electrolytes. In this test, the cyclic voltammogram should be recorded in the non-Faradaic region which is typically a 0.1 V potential window over the open circuit potential assuming the measuring current is due to the double-layer charging.[295] The estimated value is generally an approximate electroactive surface area since several assumptions are taken into considerations.

   The electrochemically active surface area of the electrode materials can also be measured from the cyclic voltammogram study in 5-mM potassium ferricyanide solutions with 0.1 M KCl solution in a 0.1 M phosphate buffer and using the following Randles–Sevcik equation[296,297]

$$i_p = 26800 n^{3/2} D^{1/2} C v^{1/2} A \quad (26)$$

   where i_p, n, D, C, v, A are anodic peak current, number of electrons (in this case, $n = 1$) involved in the Faradaic activity associated with the peak, diffusion coefficient (7.2×10^{-6} cm^2 s^{-1}), concentration (5×10^{-6} mol cm^{-3}) of ferricyanide ion, scan rate and electroactive surface area of electrode (cm^2), respectively.
8. *Clear and concise title* with proper naming of structure is indispensable for quality publication. Some articles termed the electrodes as carbon nanostructures (or single-doped carbon nanostructures) in the title but close inspection of the results reveals that the carbon structures contain heteroatoms (or more than one excluding inevitable oxygen). Therefore, it is recommended to name the materials properly and title precisely for better reference and use by other researchers.
9. *Proper X-axis notation* for the cyclic voltammogram and charge–discharge profile in 2E versus 3E tests. It is necessary to mention the reference electrode along with the potential in the *X*-axis of both cyclic voltammogram and charge–discharge profile for 3E test whereas labelling the axis as potential alone without reference electrode in 2E test.

8. Challenges and Outlook

Among all dopants for nanocarbon based supercapacitor electrodes, boron, and nitrogen have received a higher priority due to their similar atomic radius with carbon. Although sulfur and phosphorus doping into carbon have been reported, the studies on other dopants are very limited. The major concerns of using sulfur and phosphorous are safety, stability, and toxicity. For example, the phosphorous functional group is very unstable even at room temperature. However, each heteroatom doping into carbon nanostructures has its own merits and demerits, which has been discussed above in this review.

Overarchingly, introduction of dopants into nanocarbons leads to simultaneous changes in several associated properties like wettability, structural stability, surface chemistry, morphology, and some others. Therefore, dopant associated changes have to be taken into consideration while discussing the improvement in any kind of properties of nanocarbons after doping.[240] Pinpointing a specific factor to be responsible for the enhanced supercapacitor performance of electrode materials is often inconclusive. Unfortunately, this kind of correlations and insights is missing in many reports. Rather, several (often conflicting) trends in showing superiority of performances of supercapacitor device in terms of normalized capacitance, energy density, and power density, etc., compared to other existing literature sources, prevails. Surprisingly, a very large number of the available comparison tables (or Ragone plots) of supercapacitor performances of electrode (or device) do not even present any results which are superior to their own results. Hence, insightful discussions on supercapacitor performance of an electrode influenced by physicochemical changes in the materials structure will be greatly appreciated by the community and generate more consistent new knowledge. Where possible, commercial devices should be used as benchmarks for comparison purposes. This convention is commonly used in electrocatalysis field, which is not as clearly seen among the supercapacitor-related literatures.

In spite of large promises as a capable energy storage device, the present state-of-the art of doped carbon-based supercapacitor is still far away from the commercial utilization as a stand-alone device.[1] The bottleneck challenges here that need much-devoted attention are

1. *Enhancement in specific capacitance*: Considering the specific capacitance, the values for heteroatom-doped carbons, 2D materials and pseudocapacitive materials are almost in the same range (Figure 1).[21] The observed gravimetric capacitance of doped nanocarbons typically varies from 100 to 855 F g^{-1} based on the existing reports. In some cases, the pseudocapacitive materials shows higher capacitance than that obtained for heteroatom doped carbon structures.[13]
2. *Higher potential window without sacrificing specific capacitance*: Although some heteroatom doped carbon-based materials could be able to be operated in the extended potential window, for example, up to 1.7 V, in 1 M H_2SO_4 electrolyte, the specific capacitance of the device is not impressive (29 F g^{-1} at 1 A g^{-1} only).[77]
3. *Structure with optimized functional groups*: Acidic functional groups are detrimental for the capacitive properties. Indeed, the capacitance drop is proportional to the density of acidic groups.[130] Since the acidic functional groups reduce the local pH and hence stimulate hydrogen generation at negative electrode. To neutralize the local charge equilibrium, the adsorbed ions are released from the double layer. Similar phenomena occur at a positive electrode due to the presence of basic groups which results in CO and CO_2 generation. This fact causes self-discharge and leakage current in the device.[159]
4. *Understanding the role of dopant and its configuration*: The effects of a particular group versus its configuration on supercapacitor performances should be clarified. For example, the role of COOH group, pyridine-N, or pyrrolic-N, charge storage mechanism of phosphorous or silicon doping, and several other factors are not completely understood yet.
5. *Rate performance and cyclability*: These two parameters are the key factors where high volumetric energy density is required for the practical usage. The rate performance is a key factors where high volumetric energy density is required for the practical usage. The poor rate performance and cyclability for the heteroatom doped carbon structures are due to the "electrolyte starvation effect", where free electrolyte ions are adsorbed on the distributed double-layer surface which in turn results in inaccessible surfaces and reduces the conductivity of accompanying free electrolyte ions.[298,299] In addition, the bond length and bond angles in the carbon matrix change upon doping which can also affect the rate capability of doped carbon.
6. *Ageing effect*: Various chemical groups (OH, COOH, CONH and F) formed on the electrode surface from water traces and the electrolyte which is responsible for ageing of porous carbon nanostructures, particularly in nonaqueous electrolytes.[300,301] The ageing in the organic electrolyte is much higher in the positive electrode as well as faster at a higher temperature and a wider potential window.[301]

The impressive recent advances in materials science and nanotechnology are expected to help tackle the above-mentioned challenges. The key aspects to mitigate the challenges is in designing doped-carbon structures via an economical synthesis process with minimum steps with the doped nanocarbons meeting the following requirements.

1. *Well-balanced meso-micro-macropores structure with high electrochemically active areas*: Macropores can serve as ion reservoir, mesopores for an efficient ion diffusion into the entire surface and micropores for ion accumulator-cum-charge storage enhancer.[279]
2. *Dual wetting surface*: Surface with dual wetting nature where the inner graphitic layers can be utilized effectively for charge-transport while the functionalized outer part can be efficient for charge storage. Hierarchically porous carbons with an interlinked hydrophilic and hydrophobic surface,[302] vertical graphene,[238] or open-ended multilayer CNT[303] could be the potential candidates for this aspect as an example.
3. *The right choice of dopant*: It is well known that the oxygen or boron doping diminishes the electrical properties of carbon.[210] Functional groups are sometimes detrimental in terms of leakage current and self-discharge of device. Therefore, one should select proper dopants or combination of dopants with an appropriate stoichiometry to design doped nanocarbons keeping their behavior in a chosen electrolyte in mind without losing the advantageous features of nanocarbons.
4. *Optimization between dopant features and properties of doped carbon*: The content of heteroatom doping, their bonding and physical properties like pore distribution, surface area, structural qualities are intimately interlinked. During the synthesis process, it is difficult to control a single parameter while keeping another unchanged and thus the selection of suitable precursors is crucial to develop a novel design strategy. The scenario becomes more complex when the carbon structures are doped with more than one dopant. It is imperative to balance the physical changes in the structure due to the codoping, ratio of multidopant content, and amount of preferable configurations which have a positive contribution for capacitive performances.

9. Concluding Remarks

Considering benefits and bottleneck challenges, *there is plenty of room* for new strategies to be developed in carbon-based supercapacitor research. We foresee the exciting progress and further in-depth understanding of the heteroatom doped nanocarbons with the enriched physicochemical properties. Additionally, we do believe that the knowledge provided here will be helpful for the research of doped nanocarbons not only for supercapacitor alone but also toward battery, metal-ion capacitor, fuel cell, sensor, catalysis, and many more applications.

Acknowledgements

S.G. and S.B. acknowledge financial support from Heilongjiang Huasheng Graphite Co., People's Republic of China, S.M.J. acknowledges financial support from National Research Foundation of Korea (NRF, 2018R1A4A1024691) and K.O. thanks the Australian Research Council and QUT Centre for Materials Science for partial support. S.G. acknowledges T. R. Devidas from Hebrew University of Jerusalem, Israel, S. Chakraborty, and S. Parida from Indira Gandhi Centre for Atomic Research, India for careful reading of the manuscript and James Bird, Michael Graves, and Gustavo Tontini from the University of Manchester

for useful discussions. The authors are very thankful to all researchers who have contributed to the relevant research areas and do apologize for not including every relevant publication because of the obvious limitations in their knowledge, time, and available space. The authors also highly appreciate and grateful to anonymous reviewers for their valuable and constructive suggestions.

Conflict of Interest

The authors declare no conflict of interest.

Keywords

doping, energy storage, nanocarbons, plasma, supercapacitors

Received: April 9, 2020
Revised: June 18, 2020
Published online: July 9, 2020

[1] C. Schütter, S. Pohlmann, A. Balducci, *Adv. Energy Mater.* **2019**, *9*, 1900334.
[2] P. Simon, Y. Gogotsi, B. Dunn, *Science* **2014**, *343*, 1210.
[3] D. P. Dubal, Y. P. Wu, R. Holze, *ChemTexts* **2016**, *2*, 13.
[4] F. Béguin, V. Presser, A. Balducci, E. Frackowiak, *Adv. Mater.* **2014**, *26*, 2219.
[5] Y. Kumar, S. Rawal, B. Joshi, S. A. Hashmi, *J. Solid State Electrochem.* **2019**, *23*, 667.
[6] R. Ramachandran, F. Wang, *Supercapacitors—Theoretical and Practical Solutions*, InTech, London **2018**.
[7] B. Pal, S. Yang, S. Ramesh, V. Thangadurai, R. Jose, *Nanoscale Adv.* **2019**, *1*, 3807.
[8] P. Simon, Y. Gogotsi, *Nat. Mater.* **2008**, *7*, 845.
[9] F. Bonaccorso, L. Colombo, G. Yu, M. Stoller, V. Tozzini, A. C. Ferrari, R. S. Ruoff, V. Pellegrini, *Science* **2015**, *347*, 1246501.
[10] S. Ghosh, G. Sahoo, S. R. Polaki, N. G. Krishna, M. Kamruddin, T. Mathews, *J. Appl. Phys.* **2017**, *122*, 214902.
[11] Poonam, K. Sharma, A. Arora, S. K. Tripathi, *J. Energy Storage* **2019**, *21*, 801.
[12] M. Inagaki, H. Konno, O. Tanaike, *J. Power Sources* **2010**, *195*, 7880.
[13] A. Muzaffar, M. B. Ahamed, K. Deshmukh, J. Thirumalai, *Renew. Sustain. Energy Rev.* **2019**, *101*, 123.
[14] R. Basu, S. Ghosh, S. Bera, A. Das, S. Dhara, *Sci. Rep.* **2019**, *9*, 4621.
[15] D. Majumdar, T. Maiyalagan, Z. Jiang, *ChemElectroChem* **2019**, *6*, 4343.
[16] J. Cherusseri, N. Choudhary, K. Sambath Kumar, Y. Jung, J. Thomas, *Nanoscale Horiz.* **2019**, *4*, 840.
[17] W. Yang, J. Yang, J. J. Byun, F. P. Moissinac, J. Xu, S. J. Haigh, M. Domingos, M. A. Bissett, R. A. W. Dryfe, S. Barg, *Adv. Mater.* **2019**, *31*, 1902725.
[18] Y. Zeng, M. Yu, Y. Meng, P. Fang, X. Lu, Y. Tong, *Adv. Energy Mater.* **2016**, *6*, 1601053.
[19] S. Ghosh, S. R. Polaki, G. Sahoo, E.-M. Jin, M. Kamruddin, J. S. Cho, S. M. Jeong, *J. Ind. Eng. Chem.* **2019**, *72*, 107.
[20] K. D. Fong, T. Wang, S. K. Smoukov, *Sustainable Energy Fuels* **2017**, *1*, 1857.
[21] K. S. Kumar, N. Choudhary, Y. Jung, J. Thomas, *ACS Energy Lett.* **2018**, *3*, 482.
[22] M. Huang, F. Li, F. Dong, Y. X. Zhang, L. L. Zhang, *J. Mater. Chem. A* **2015**, *3*, 21380.
[23] V. D. Nithya, N. S. Arul, *J. Power Sources* **2016**, *327*, 297.
[24] S. Ghosh, S. M. Jeong, S. R. Polaki, *Korean J. Chem. Eng.* **2018**, *35*, 1389.
[25] Z. Bo, C. Li, H. Yang, K. Ostrikov, J. Yan, K. Cen, *Nano-Micro Lett.* **2018**, *10*, 33.
[26] J. R. Miller, R. A. Outlaw, B. C. Holloway, *Science* **2010**, *329*, 1637.
[27] Y. Zhang, Q. Zou, H. S. Hsu, S. Raina, Y. Xu, J. B. Kang, J. Chen, S. Deng, N. Xu, W. P. Kang, *ACS Appl. Mater. Interfaces* **2016**, *8*, 7363.
[28] S. Ghosh, T. Mathews, S. R. Polaki, S. M. Jeong, in *Nanostructured Materials for Energy Related Applications* (Eds: S. Rajendran, M. Naushad, S. Balakumar), Springer, Cham **2019**, pp. 163–187.
[29] J. J. Yoo, K. Balakrishnan, J. Huang, V. Meunier, B. G. Sumpter, A. Srivastava, M. Conway, A. L. Mohana Reddy, J. Yu, R. Vajtai, P. M. Ajayan, *Nano Lett.* **2011**, *11*, 1423.
[30] J. Lin, H. Jia, Y. Cai, S. Chen, H. Liang, X. Wang, F. Zhang, J. Qi, J. Cao, J. Feng, W. Fei, *J. Mater. Chem. A* **2018**, *6*, 908.
[31] B. E. Conway, *J. Electrochem. Soc.* **1991**, *138*, 1539.
[32] L. Weinstein, R. Dash, *Mater. Today* **2013**, *16*, 356.
[33] A. K. Farquhar, M. Supur, S. R. Smith, C. Dyck, R. L. McCreery, *Adv. Energy Mater.* **2018**, *8*, 1802439.
[34] D. E. Lobo, P. C. Banerjee, C. D. Easton, M. Majumder, *Adv. Energy Mater.* **2015**, *5*, 1500665.
[35] N. Jha, P. Ramesh, E. Bekyarova, M. E. Itkis, R. C. Haddon, *Adv. Energy Mater.* **2012**, *2*, 438.
[36] J. Xu, N. Yuan, J. M. Razal, Y. Zheng, X. Zhou, J. Ding, K. Cho, S. Ge, R. Zhang, Y. Gogotsi, R. H. Baughman, *Energy Storage Mater.* **2019**, *22*, 323.
[37] Y. Liu, Y. Shen, L. Sun, J. Li, C. Liu, W. Ren, F. Li, L. Gao, J. Chen, F. Liu, Y. Sun, N. Tang, H.-M. Cheng, Y. Du, *Nat. Commun.* **2016**, *7*, 10921.
[38] J. Zhou, J. Lian, L. Hou, J. Zhang, H. Gou, M. Xia, Y. Zhao, T. A. Strobel, L. Tao, F. Gao, *Nat. Commun.* **2015**, *6*, 8503.
[39] C. Q. Sun, *Nanoscale* **2010**, *2*, 1930.
[40] Y. Meng, D. Voiry, A. Goswami, X. Zou, X. Huang, M. Chhowalla, Z. Liu, T. Asefa, *J. Am. Chem. Soc.* **2014**, *136*, 13554.
[41] T. Kwon, H. Nishihara, H. Itoi, Q.-H. Yang, T. Kyotani, *Langmuir* **2009**, *25*, 11961.
[42] Z. J. Han, C. Huang, S. S. Meysami, D. Piche, D. H. Seo, S. Pineda, A. T. Murdock, P. S. Bruce, P. S. Grant, N. Grobert, *Carbon* **2018**, *126*, 305.
[43] N. A. Kumar, J.-B. Baek, *Nanotechnology* **2015**, *26*, 492001.
[44] M. Gupta, P. K. Singh, B. Bhattacharya, Y. M. Shulga, N. Y. Shulga, Y. Kumar, *Appl. Phys. A* **2019**, *125*, 122.
[45] J. P. Paraknowitsch, A. Thomas, *Energy Environ. Sci.* **2013**, *6*, 2839.
[46] M. Antonietti, M. Oschatz, *Adv. Mater.* **2018**, *30*, 1706836.
[47] H. Li, C. Qi, Y. Tao, H. Liu, D. Wang, F. Li, Q. Yang, H. Cheng, *Adv. Energy Mater.* **2019**, *9*, 1900079.
[48] M. F. El-Kady, V. Strong, S. Dubin, R. B. Kaner, *Science* **2012**, *335*, 1326.
[49] Y. J. Oh, J. J. Yoo, Y. Il Kim, J. K. Yoon, H. N. Yoon, J.-H. Kim, S. Bin Park, *Electrochim. Acta* **2014**, *116*, 118.
[50] X. Yu, S. Yun, J. S. Yeon, P. Bhattacharya, L. Wang, S. W. Lee, X. Hu, H. S. Park, *Adv. Energy Mater.* **2018**, *8*, 1702930.
[51] M. Harilal, S. G. Krishnan, A. Yar, I. I. Misnon, M. V. Reddy, M. M. Yusoff, J. Ojur Dennis, R. Jose, *J. Phys. Chem. C* **2017**, *121*, 21171.
[52] O. Barbieri, M. Hahn, A. Herzog, R. Kötz, *Carbon* **2005**, *43*, 1303.
[53] D. Hulicova-Jurcakova, M. Kodama, S. Shiraishi, H. Hatori, Z. H. Zhu, G. Q. Lu, *Adv. Funct. Mater.* **2009**, *19*, 1800.
[54] T. V. Pham, J. Kim, J. Y. Jung, J. H. Kim, H. Cho, T. H. Seo, H. Lee, N. D. Kim, M. J. Kim, *Adv. Funct. Mater.* **2019**, *29*, 1905511.
[55] R. Narayanan, H. Yamada, M. Karakaya, R. Podila, A. M. Rao, P. R. Bandaru, *Nano Lett.* **2015**, *15*, 3067.
[56] H. Yamada, P. R. Bandaru, *Appl. Phys. Lett.* **2013**, *102*, 173113.

[57] C. Zhan, Y. Zhang, P. T. Cummings, D. Jiang, *Phys. Chem. Chem. Phys.* **2016**, *18*, 4668.
[58] T. T. Duignan, X. S. Zhao, *J. Phys. Chem. C* **2019**, *123*, 4085.
[59] J. M. Hurst, L. Li, H. Liu, *Carbon* **2018**, *134*, 464.
[60] G. Xiong, C. Meng, R. G. Reifenberger, P. P. Irazoqui, T. S. Fisher, *Adv. Energy Mater.* **2014**, *4*, 1300515.
[61] S. D. Perera, B. Patel, N. Nijem, K. Roodenko, O. Seitz, J. P. Ferraris, Y. J. Chabal, K. J. Balkus, *Adv. Energy Mater.* **2011**, *1*, 936.
[62] H. Kim, M.-Y. Cho, M.-H. Kim, K.-Y. Park, H. Gwon, Y. Lee, K. C. Roh, K. Kang, *Adv. Energy Mater.* **2013**, *3*, 1500.
[63] D. H. Seo, Z. J. Han, S. Kumar, K. K. Ostrikov, *Adv. Energy Mater.* **2013**, *3*, 1316.
[64] R. B. Rakhi, W. Chen, D. Cha, H. N. Alshareef, *Adv. Energy Mater.* **2012**, *2*, 381.
[65] P. R. Deshmukh, S. N. Pusawale, R. N. Bulakhe, C. D. Lokhande, *Bull. Mater. Sci.* **2013**, *36*, 1171.
[66] T. Lin, I.-W. Chen, F. Liu, C. Yang, H. Bi, F. Xu, F. Huang, *Science* **2015**, *350*, 1508.
[67] P. Iamprasertkun, A. Krittayavathananon, M. Sawangphruk, *Carbon* **2016**, *102*, 455.
[68] D. Yang, Y. Song, Y.-J. Ye, M. Zhang, X. Sun, X.-X. Liu, *J. Mater. Chem. A* **2019**, *7*, 12086.
[69] G. Hasegawa, T. Deguchi, K. Kanamori, Y. Kobayashi, H. Kageyama, T. Abe, K. Nakanishi, *Chem. Mater.* **2015**, *27*, 4703.
[70] S. Shiraishi, M. Kibe, T. Yokoyama, H. Kurihara, N. Patel, A. Oya, Y. Kaburagi, Y. Hishiyama, *Appl. Phys. A* **2006**, *82*, 585.
[71] H. Zhou, Y. Peng, H. Bin Wu, F. Sun, H. Yu, F. Liu, Q. Xu, Y. Lu, *Nano Energy* **2016**, *21*, 80.
[72] Z. Song, H. Duan, L. Li, D. Zhu, T. Cao, Y. Lv, W. Xiong, Z. Wang, M. Liu, L. Gan, *Chem. Eng. J.* **2019**, *372*, 1216.
[73] H. Zhang, M. Lu, H. Wang, Y. Lyu, D. Li, S. Sun, J. Shi, W. Liu, *Sustainable Energy Fuels* **2018**, *2*, 2314.
[74] A. S. Rajpurohit, N. S. Punde, C. R. Rawool, A. K. Srivastava, *Chem. Eng. J.* **2019**, *371*, 679.
[75] R. Santhosh, S. R. S. Raman, S. M. Krishna, S. sai Ravuri, V. Sandhya, S. Ghosh, N. K. Sahu, S. Punniyakoti, M. Karthik, P. Kollu, S. K. Jeong, A. N. Grace, *Electrochim. Acta* **2018**, *276*, 284.
[76] R. K. Das, B. Liu, J. R. Reynolds, A. G. Rinzler, *Nano Lett.* **2009**, *9*, 677.
[77] Y. Wen, B. Wang, C. Huang, L. Wang, D. Hulicova-Jurcakova, *Chem. - Eur. J.* **2015**, *21*, 80.
[78] X. Liu, R. Mi, L. Yuan, F. Yang, Z. Fu, C. Wang, Y. Tang, *Front. Chem.* **2018**, *6*, 475.
[79] J. Wang, Z. He, X. Tan, T. Wang, L. Liu, X. He, X. D. Liu, L. Zhang, K. Du, *Carbon* **2020**, *160*, 71.
[80] K. Gopalsamy, J. Balamurugan, T. D. Thanh, N. H. Kim, J. H. Lee, *Chem. Eng. J.* **2017**, *312*, 180.
[81] Y. Zhou, Z. Zhu, C. Zhao, K. Zhang, B. Wang, C. Zhao, G. Chen, *ACS Sustainable Chem. Eng.* **2019**, *7*, 5095.
[82] F. Lai, J. Feng, T. Heil, G.-C. Wang, P. Adler, M. Antonietti, M. Oschatz, *Energy Storage Mater.* **2019**, *20*, 188.
[83] R. Jain, R. Mehrotra, S. Mishra, *J. Mater. Sci. Mater. Electron.* **2019**, *30*, 2316.
[84] M. Majumder, R. B. Choudhary, A. K. Thakur, *Carbon* **2019**, *142*, 650.
[85] X. Dong, H. Jin, R. Wang, J. Zhang, X. Feng, C. Yan, S. Chen, S. Wang, J. Wang, J. Lu, *Adv. Energy Mater.* **2018**, *8*, 1702695.
[86] P. Yu, Z. Zhang, L. Zheng, F. Teng, L. Hu, X. Fang, *Adv. Energy Mater.* **2016**, *6*, 1601111.
[87] G. Yuan, X. Zhao, Y. Liang, L. Peng, H. Dong, Y. Xiao, C. Hu, H. Hu, Y. Liu, M. Zheng, *J. Colloid Interface Sci.* **2019**, *536*, 628.
[88] S. N. Kanakaraj, Y.-Y. Hsieh, P. K. Adusei, B. Homan, Y. Fang, G. Zhang, S. Mishra, S. Gbordzoe, V. Shanov, *Carbon* **2019**, *149*, 407.
[89] Y.-H. Lee, K.-H. Chang, C.-C. Hu, *J. Power Sources* **2013**, *227*, 300.
[90] J. Xie, P. Yang, Y. Wang, T. Qi, Y. Lei, C. M. Li, *J. Power Sources* **2018**, *401*, 213.
[91] A. Bianco, H.-M. Cheng, T. Enoki, Y. Gogotsi, R. H. Hurt, N. Koratkar, T. Kyotani, M. Monthioux, C. R. Park, J. M. D. Tascon, J. Zhang, *Carbon* **2013**, *65*, 1.
[92] Z. Zapata-Benabithe, F. Carrasco-Marín, C. Moreno-Castilla, *Mater. Chem. Phys.* **2013**, *138*, 870.
[93] B. J. Mapleback, T. J. Simons, Y. Shekibi, K. Ghorbani, A. N. Rider, *Electrochim. Acta* **2020**, *331*, 135233.
[94] B. Ankamwar, P. Das, U. K. Sur, *Indian J. Phys.* **2016**, *90*, 391.
[95] P. M. Anjana, M. R. Bindhu, R. B. Rakhi, *Mater. Sci. Energy Technol.* **2019**, *2*, 389.
[96] G. Sahoo, S. R. Polaki, P. Anees, S. Ghosh, S. Dhara, M. Kamruddin, *Phys. Chem. Chem. Phys.* **2019**, *21*, 25196.
[97] T. Sruthi, K. Tarafder, *Bull. Mater. Sci.* **2019**, *42*, 257.
[98] R. Yadav, C. K. Dixit, *J. Sci. Adv. Mater. Devices* **2017**, *2*, 141.
[99] M. Inagaki, M. Toyoda, Y. Soneda, T. Morishita, *Carbon* **2018**, *132*, 104.
[100] L. Ma, J. Liu, S. Lv, Q. Zhou, X. Shen, S. Mo, H. Tong, *J. Mater. Chem. A* **2019**, *7*, 7591.
[101] W. Kiciński, M. Szala, M. Bystrzejewski, *Carbon* **2014**, *68*, 1.
[102] S. K. Ramasahayam, A. L. Clark, Z. Hicks, T. Viswanathan, *Electrochim. Acta* **2015**, *168*, 414.
[103] L. Wang, Z. Sofer, M. Pumera, *ACS Nano* **2020**, *14*, 21.
[104] W. Si, J. Zhou, S. Zhang, S. Li, W. Xing, S. Zhuo, *Electrochim. Acta* **2013**, *107*, 397.
[105] F. Lai, Y.-E. Miao, L. Zuo, H. Lu, Y. Huang, T. Liu, *Small* **2016**, *12*, 3235.
[106] Z. Ling, Z. Wang, M. Zhang, C. Yu, G. Wang, Y. Dong, S. Liu, Y. Wang, J. Qiu, *Adv. Funct. Mater.* **2016**, *26*, 111.
[107] D.-W. Wang, F. Li, Z.-G. Chen, G. Q. Lu, H.-M. Cheng, *Chem. Mater.* **2008**, *20*, 7195.
[108] M. Sahoo, K. P. Sreena, B. P. Vinayan, S. Ramaprabhu, *Mater. Res. Bull.* **2015**, *61*, 383.
[109] M. Enterría, M. F. R. Pereira, J. I. Martins, J. L. Figueiredo, *Carbon* **2015**, *95*, 72.
[110] R. Nankya, J. Lee, D. O. Opar, H. Jung, *Appl. Surf. Sci.* **2019**, *489*, 552.
[111] N. Shcherban, S. Filonenko, P. Yaremov, V. Dyadyun, I. Bezverkhyy, V. Ilyin, *J. Mater. Sci.* **2017**, *52*, 1523.
[112] S. S. Balaji, M. Karnan, P. Anandhaganesh, S. M. Tauquir, M. Sathish, *Appl. Surf. Sci.* **2019**, *491*, 560.
[113] Z. Peng, R. Ye, J. A. Mann, D. Zakhidov, Y. Li, P. R. Smalley, J. Lin, J. M. Tour, *ACS Nano* **2015**, *9*, 5868.
[114] D.-Y. Yeom, W. Jeon, N. D. K. Tu, S. Y. Yeo, S.-S. Lee, B. J. Sung, H. Chang, J. A. Lim, H. Kim, *Sci. Rep.* **2015**, *5*, 9817.
[115] S. Li, Z. Wang, H. Jiang, L. Zhang, J. Ren, M. Zheng, L. Dong, L. Sun, *Chem. Commun.* **2016**, *52*, 10988.
[116] B. Dahal, T. Mukhiya, G. P. Ojha, A. Muthurasu, S.-H. Chae, T. Kim, D. Kang, H. Y. Kim, *Electrochim. Acta* **2019**, *301*, 209.
[117] H. Guo, Q. Gao, *J. Power Sources* **2009**, *186*, 551.
[118] Z. Zhao, Y. Xie, *J. Power Sources* **2018**, *400*, 264.
[119] C. Kim, D.-Y. Kang, J. H. Moon, *Nano Energy* **2018**, *53*, 182.
[120] L. Niu, Z. Li, W. Hong, J. Sun, Z. Wang, L. Ma, J. Wang, S. Yang, *Electrochim. Acta* **2013**, *108*, 666.
[121] T. Kondo, T. Kato, K. Miyashita, T. Aikawa, T. Tojo, M. Yuasa, *J. Electrochem. Soc.* **2019**, *166*, A1425.
[122] X. Yang, D. Wu, X. Chen, R. Fu, *J. Phys. Chem. C* **2010**, *114*, 8581.
[123] B. K. Singh, A. Shaikh, R. O. Dusane, S. Parida, *Nano-Struct. Nano-Objects* **2019**, *17*, 239.
[124] L. Wan, J. Wang, L. Xie, Y. Sun, K. Li, *ACS Appl. Mater. Interfaces* **2014**, *6*, 15583.
[125] K. Xiao, L. X. Ding, G. Liu, H. Chen, S. Wang, H. Wang, *Adv. Mater.* **2016**, *28*, 5997.
[126] E. Frackowiak, G. Lota, J. Machnikowski, C. Vix-Guterl, F. Béguin, *Electrochim. Acta* **2006**, *51*, 2209.

[127] D. Hulicova, J. Yamashita, Y. Soneda, H. Hatori, M. Kodama, *Chem. Mater.* **2005**, *17*, 1241.
[128] R. Yuksel, O. Buyukcakir, P. K. Panda, S. H. Lee, Y. Jiang, D. Singh, S. Hansen, R. Adelung, Y. K. Mishra, R. Ahuja, R. S. Ruoff, *Adv. Funct. Mater.* **2020**, *30*, 1909725.
[129] G. Lota, K. Lota, E. Frackowiak, *Electrochem. Commun.* **2007**, *9*, 1828.
[130] M. Seredych, D. Hulicova-Jurcakova, G. Q. Lu, T. J. Bandosz, *Carbon* **2008**, *46*, 1475.
[131] C. Poochai, C. Sriprachuabwong, N. Srisamrarn, Y. Chuminjak, T. Lomas, A. Wisitsoraat, A. Tuantranont, *Appl. Surf. Sci.* **2019**, *489*, 989.
[132] F. M. Hassan, V. Chabot, J. Li, B. K. Kim, L. Ricardez-Sandoval, A. Yu, *J. Mater. Chem. A* **2013**, *1*, 2904.
[133] H. M. Jeong, J. W. Lee, W. H. Shin, Y. J. Choi, H. J. Shin, J. K. Kang, J. W. Choi, *Nano Lett.* **2011**, *11*, 2472.
[134] D. Hulicova-Jurcakova, M. Seredych, G. Q. Lu, T. J. Bandosz, *Adv. Funct. Mater.* **2009**, *19*, 438.
[135] D.-W. Wang, F. Li, L.-C. Yin, X. Lu, Z.-G. Chen, I. R. Gentle, G. Q. M. Lu, H.-M. Cheng, *Chem. - Eur. J.* **2012**, *18*, 5345.
[136] N. P. Wickramaratne, J. Xu, M. Wang, L. Zhu, L. Dai, M. Jaroniec, *Chem. Mater.* **2014**, *26*, 2820.
[137] O. Ornelas, J. M. Sieben, R. Ruiz-Rosas, E. Morallón, D. Cazorla-Amorós, J. Geng, N. Soin, E. Siores, B. F. G. Johnson, *Chem. Commun.* **2014**, *50*, 11343.
[138] C.-M. Chen, Q. Zhang, X.-C. Zhao, B. Zhang, Q.-Q. Kong, M.-G. Yang, Q.-H. Yang, M.-Z. Wang, Y.-G. Yang, R. Schlögl, D. S. Su, *J. Mater. Chem.* **2012**, *22*, 14076.
[139] D. Zhang, Y. Hao, L. Zheng, Y. Ma, H. Feng, H. Luo, *J. Mater. Chem. A* **2013**, *1*, 7584.
[140] W. Zhang, C. Xu, C. Ma, G. Li, Y. Wang, K. Zhang, F. Li, C. Liu, H.-M. Cheng, Y. Du, N. Tang, W. Ren, *Adv. Mater.* **2017**, *29*, 1701677.
[141] C. Moreno-Castilla, M. B. Dawidziuk, F. Carrasco-Marín, E. Morallón, *Carbon* **2012**, *50*, 3324.
[142] C. Ma, X. Chen, D. Long, J. Wang, W. Qiao, L. Ling, *Carbon* **2017**, *118*, 699.
[143] N. Q. Tran, B. K. Kang, M. H. Woo, D. H. Yoon, *ChemSusChem* **2016**, *9*, 2261.
[144] M. Karakaya, J. Zhu, A. J. Raghavendra, R. Podila, S. G. Parler, J. P. Kaplan, A. M. Rao, *Appl. Phys. Lett.* **2014**, *105*, 263103.
[145] L. Niu, C. Shen, L. Yan, J. Zhang, Y. Lin, Y. Gong, C. Li, C. Q. Sun, S. Xu, *J. Colloid Interface Sci.* **2019**, *547*, 92.
[146] J. Du, L. Liu, Y. Yu, Z. Hu, Y. Zhang, B. Liu, A. Chen, *ChemSusChem* **2019**, *12*, 303.
[147] M. Ghaemmaghami, R. Mohammadi, *Sustainable Energy Fuels* **2019**, *3*, 2176.
[148] S. R. Mangisetti, K. M, S. Ramaprabhu, *Electrochim. Acta* **2019**, *305*, 264.
[149] X. Zhao, Q. Zhang, C.-M. Chen, B. Zhang, S. Reiche, A. Wang, T. Zhang, R. Schlögl, D. Sheng Su, *Nano Energy* **2012**, *1*, 624.
[150] D. Mohapatra, G. Dhakal, M. S. Sayed, B. Subramanya, J.-J. Shim, S. Parida, *ACS Appl. Mater. Interfaces* **2019**, *11*, 8040.
[151] M. Seredych, K. Singh, T. J. Bandosz, *Electroanalysis* **2014**, *26*, 109.
[152] E. Hao, W. Liu, S. Liu, Y. Zhang, H. Wang, S. Chen, F. Cheng, S. Zhao, H. Yang, *J. Mater. Chem. A* **2017**, *5*, 2204.
[153] X. Yu, S. K. Park, S.-H. Yeon, H. S. Park, *J. Power Sources* **2015**, *278*, 484.
[154] W. Lei, J. Guo, Z. Wu, C. Xuan, W. Xiao, D. Wang, *Sci. Bull.* **2017**, *62*, 1011.
[155] F. R. Maria Sundar Raj, N. V. Jaya, G. Boopathi, D. Kalpana, A. Pandurangan, *Mater. Chem. Phys.* **2020**, *240*, 122151.
[156] W. Liu, Y. Tang, Z. Sun, S. Gao, J. Ma, L. Liu, *Carbon* **2017**, *115*, 754.
[157] W. Chen, J. Shi, T. Zhu, Q. Wang, J. Qiao, J. Zhang, *Electrochim. Acta* **2015**, *177*, 327.
[158] S. Yaglikci, Y. Gokce, E. Yagmur, Z. Aktas, *Environ. Technol.* **2020**, *41*, 36.
[159] W. Gu, M. Sevilla, A. Magasinski, A. B. Fuertes, G. Yushin, *Energy Environ. Sci.* **2013**, *6*, 2465.
[160] X. Zhang, R. Zhang, *Appl. Surf. Sci.* **2019**, *479*, 1039.
[161] Y. Huang, S. L. Candelaria, Y. Li, Z. Li, J. Tian, L. Zhang, G. Cao, *J. Power Sources* **2014**, *252*, 90.
[162] Y. Zhou, S. L. Candelaria, Q. Liu, Y. Huang, E. Uchaker, G. CaO, *J. Mater. Chem. A* **2014**, *2*, 8472.
[163] P. Dulyaseree, V. Yordsri, W. Wongwiriyapan, *Jpn. J. Appl. Phys.* **2016**, *55*, 02BD05.
[164] R. K. Gupta, M. Dubey, P. Kharel, Z. Gu, Q. H. Fan, *J. Power Sources* **2015**, *274*, 1300.
[165] S. H. Tamboli, B. S. Kim, G. Choi, H. Lee, D. Lee, U. M. Patil, J. Lim, S. B. Kulkarni, S. Chan Jun, H. H. Cho, *J. Mater. Chem. A* **2014**, *2*, 5077.
[166] Z. Bi, L. Huo, Q. Kong, F. Li, J. Chen, A. Ahmad, X. Wei, L. Xie, C.-M. Chen, *ACS Appl. Mater. Interfaces* **2019**, *11*, 11421.
[167] S. Y. Kim, K. Yang, B.-H. Kim, *Electrochim. Acta* **2014**, *137*, 781.
[168] Z. Kou, B. Guo, Y. Zhao, S. Huang, T. Meng, J. Zhang, W. Li, I. S. Amiinu, Z. Pu, M. Wang, M. Jiang, X. Liu, Y. Tang, S. Mu, *ACS Appl. Mater. Interfaces* **2017**, *9*, 3702.
[169] S. K. Ramasahayam, U. B. Nasini, A. U. Shaikh, T. Viswanathan, *J. Power Sources* **2015**, *275*, 835.
[170] Y. Yang, X. Hou, C. Ding, J.-L. Lan, Y. Yu, X. Yang, *Inorg. Chem. Front.* **2017**, *4*, 2024.
[171] D. K. Kim, S. Bong, X. Jin, K. Seong, M. Hwang, N. D. Kim, N.-H. You, Y. Piao, *ACS Appl. Mater. Interfaces* **2019**, *11*, 1996.
[172] S. K. Ramasahayam, Z. Hicks, T. Viswanathan, *ACS Sustainable Chem. Eng.* **2015**, *3*, 2194.
[173] S. M. Mousavi-Khoshdel, P. Jahanbakhsh-bonab, E. Targholi, *Phys. Lett. A* **2016**, *380*, 3378.
[174] W. Ma, L. Xie, L. Dai, G. Sun, J. Chen, F. Su, Y. Cao, H. Lei, Q. Kong, C.-M. Chen, *Electrochim. Acta* **2018**, *266*, 420.
[175] D. Hulicova-Jurcakova, A. M. Puziy, O. I. Poddubnaya, F. Suárez-García, J. M. D. Tascón, G. Q. Lu, *J. Am. Chem. Soc.* **2009**, *131*, 5026.
[176] C. Zhou, T. Gao, Y. Wang, Q. Liu, Z. Huang, X. Liu, M. Qing, D. Xiao, *Small* **2019**, *15*, 1803469.
[177] F. Li, A. Ahmad, L. Xie, G. Sun, Q. Kong, F. Su, Y. Ma, Y. Chao, X. Guo, X. Wei, C.-M. Chen, *Electrochim. Acta* **2019**, *318*, 151.
[178] J. Guo, D. Wu, T. Wang, Y. Ma, *Appl. Surf. Sci.* **2019**, *475*, 56.
[179] J. Patiño, N. López-Salas, M. C. Gutiérrez, D. Carriazo, M. L. Ferrer, F. del Monte, *J. Mater. Chem. A* **2016**, *4*, 1251.
[180] V. Bayram, M. Ghidiu, J. J. Byun, S. D. Rawson, P. Yang, S. A. Mcdonald, M. Lindley, S. Fairclough, S. J. Haigh, P. J. Withers, M. W. Barsoum, I. A. Kinloch, S. Barg, *ACS Appl. Energy Mater.* **2020**, *3*, 411.
[181] B. Nirosha, R. Selvakumar, J. Jeyanthi, S. Vairam, *New J. Chem.* **2020**, *44*, 181.
[182] T. Sruthi, T. Kartick, *J. Phys.: Condens. Matter* **2019**, *31*, 475502.
[183] X. Fan, H. Xu, S. Zuo, Z. Liang, S. Yang, Y. Chen, *Electrochim. Acta* **2020**, *330*, 135207.
[184] P. Karthika, N. Rajalakshmi, K. S. Dhathathreyan, *J. Nanosci. Nanotechnol.* **2013**, *13*, 1746.
[185] D. P. Dubal, S. Abdel-Azeim, N. R. Chodankar, Y.-K. Han, *iScience* **2019**, *16*, 50.
[186] W. Na, J. Jun, J. W. Park, G. Lee, J. Jang, *J. Mater. Chem. A* **2017**, *5*, 17379.
[187] R. Saito, M. Yagi, T. Kimura, G. Dresselhaus, M. S. Dresselhaus, *J. Phys. Chem. Solids* **1999**, *60*, 715.
[188] M. Petr, P. Jakubec, V. Ranc, V. Šedajová, R. Langer, M. Medveď, P. Błoński, J. Kašlík, V. Kupka, M. Otyepka, R. Zbořil, *Nanoscale* **2019**, *11*, 21364.

[189] M.-J. Jung, E. Jeong, S. Kim, S. I. Lee, J.-S. Yoo, Y.-S. Lee, *J. Fluorine Chem.* **2011**, *132*, 1127.
[190] M.-H. Kim, J.-H. Yang, Y.-M. Kang, S.-M. Park, J. T. Han, K.-B. Kim, K. C. Roh, *Colloids Surf., A* **2014**, *443*, 535.
[191] M.-J. Jung, E. Jeong, J. W. Lim, S. I. Lee, Y.-S. Lee, *Colloids Surf., A* **2011**, *389*, 274.
[192] H. An, Y. Li, P. Long, Y. Gao, C. Qin, C. Cao, Y. Feng, W. Feng, *J. Power Sources* **2016**, *312*, 146.
[193] D. A. C. da Silva, A. J. Paulista Neto, A. M. Pascon, E. E. Fileti, L. R. C. Fonseca, H. G. Zanin, *Phys. Chem. Chem. Phys.* **2020**, *22*, 3906.
[194] M. Karuppannan, Y. Kim, Y.-E. Sung, O. J. Kwon, *J. Mater. Chem. A* **2018**, *6*, 7522.
[195] L. Borchardt, D. Leistenschneider, J. Haase, M. Dvoyashkin, *Adv. Energy Mater.* **2018**, *8*, 1800892.
[196] S. Gupta, A. Yadav, S. Singh, N. Verma, *Ind. Eng. Chem. Res.* **2017**, *56*, 1233.
[197] M. Oschatz, S. Boukhalfa, W. Nickel, J. P. Hofmann, C. Fischer, G. Yushin, S. Kaskel, *Carbon* **2017**, *113*, 283.
[198] M. Rose, Y. Korenblit, E. Kockrick, L. Borchardt, M. Oschatz, S. Kaskel, G. Yushin, *Small* **2011**, *7*, 1108.
[199] H. Su, H. Huang, H. Zhang, X. Chu, B. Zhang, B. Gu, X. Zheng, S. Wu, W. He, C. Yan, J. Chen, W. Yang, *ACS Appl. Energy Mater.* **2018**, *1*, 3544.
[200] K. Pinkert, M. Oschatz, L. Borchardt, M. Klose, M. Zier, W. Nickel, L. Giebeler, S. Oswald, S. Kaskel, J. Eckert, *ACS Appl. Mater. Interfaces* **2014**, *6*, 2922.
[201] K. Kakaei, M. Hamidi, S. Husseindoost, *J. Colloid Interface Sci.* **2016**, *479*, 121.
[202] H. Jiang, X. Ye, Y. Zhu, Z. Yue, L. Wang, J. Xie, Z. Wan, C. Jia, *ACS Sustainable Chem. Eng.* **2019**, *7*, 18844.
[203] J. Zheng, H.-T. Liu, B. Wu, C.-A. Di, Y.-L. Guo, T. Wu, G. Yu, Y.-Q. Liu, D.-B. Zhu, *Sci. Rep.* **2012**, *2*, 662.
[204] S. Maiti, P. Banerjee, S. Purakayastha, B. Ghosh, *Mater. Chem. Phys.* **2008**, *109*, 169.
[205] P. A. Denis, *Chem. Phys. Lett.* **2010**, *492*, 251.
[206] B. H. Kim, K. S. Yang, *J. Electroanal. Chem.* **2014**, *714–715*, 92.
[207] B. H. Kim, K. S. Yang, H. G. Woo, *Electrochem. Commun.* **2011**, *13*, 1042.
[208] Z. Wang, Y. Chen, P. Li, J. He, W. Zhang, Z. Guo, Y. Li, M. Dong, *RSC Adv.* **2016**, *6*, 15080.
[209] S. Ghosh, S. R. Polaki, P. K. Ajikumar, N. G. Krishna, M. Kamruddin, *Indian J. Phys.* **2018**, *92*, 337.
[210] J. Lee, M. A. Abbas, J. H. Bang, *ACS Appl. Mater. Interfaces* **2019**, *11*, 19056.
[211] G. Sahoo, S. R. Polaki, S. Ghosh, N. G. Krishna, M. Kamruddin, K. K. Ostrikov, *Energy Storage Mater.* **2018**, *14*, 297.
[212] A. G. Kannan, A. Samuthirapandian, D.-W. Kim, *J. Power Sources* **2017**, *337*, 65.
[213] C.-C. Lai, M.-Y. Chung, C.-T. Lo, *Text. Res. J.* **2017**, *87*, 2337.
[214] M. J. Bleda-Martínez, J. A. Maciá-Agulló, D. Lozano-Castelló, E. Morallón, D. Cazorla-Amorós, A. Linares-Solano, *Carbon* **2005**, *43*, 2677.
[215] H. Peng, B. Yao, X. Wei, T. Liu, T. Kou, P. Xiao, Y. Zhang, Y. Li, *Adv. Energy Mater.* **2019**, *9*, 1803665.
[216] S. Ghosh, T. Mathews, B. Gupta, A. Das, N. Gopala Krishna, M. Kamruddin, *Nano-Struct. Nano-Objects* **2017**, *10*, 42.
[217] S. Ahmed, M. Rafat, A. Ahmed, *Adv. Nat. Sci. Nanosci. Nanotechnol.* **2018**, *9*, 035008.
[218] Y. He, Y. Zhang, X. Li, Z. Lv, X. Wang, Z. Liu, X. Huang, *Electrochim. Acta* **2018**, *282*, 618.
[219] D. Weingarth, M. Zeiger, N. Jäckel, M. Aslan, G. Feng, V. Presser, *Adv. Energy Mater.* **2014**, *4*, 1400316.
[220] T. A. Centeno, F. Stoeckli, *J. Power Sources* **2006**, *154*, 314.
[221] K. Okajima, K. Ohta, M. Sudoh, *Electrochim. Acta* **2005**, *50*, 2227.
[222] Z. Jovanovic, D. Bajuk-Bogdanović, S. Jovanović, Ž. Mravik, J. Kovač, I. Holclajtner-Antunović, M. Vujković, *Electrochim. Acta* **2017**, *258*, 1228.
[223] L. Jiang, L. Sheng, C. Long, T. Wei, Z. Fan, *Adv. Energy Mater.* **2015**, *5*, 1500771.
[224] F. Liu, D. Xue, *Chem. - Eur. J.* **2013**, *19*, 10716.
[225] C.-T. Hsieh, H. Teng, *Carbon* **2002**, *40*, 667.
[226] Y. Chen, Z. Zhang, Z. Huang, H. Zhang, *Int. J. Hydrogen Energy* **2017**, *42*, 7186.
[227] C.-M. Chen, Q. Zhang, M.-G. Yang, C.-H. Huang, Y.-G. Yang, M.-Z. Wang, *Carbon* **2012**, *50*, 3572.
[228] G. Sahoo, S. R. Polaki, S. Ghosh, N. G. Krishna, M. Kamruddin, *J. Power Sources* **2018**, *401*, 37.
[229] N. C. Deb Nath, I.-Y. Jeon, M. J. Ju, S. A. Ansari, J.-B. Baek, J.-J. Lee, *Carbon* **2019**, *142*, 89.
[230] B. Xie, Y. Chen, M. Yu, X. Shen, H. Lei, T. Xie, Y. Zhang, Y. Wu, *Nanoscale Res. Lett.* **2015**, *10*, 332.
[231] H. Wang, R. Fan, J. Miao, J. Deng, Y. Wang, *ACS Sustainable Chem. Eng.* **2019**, *7*, 11407.
[232] V. Ruiz, C. Blanco, E. Raymundo-Piñero, V. Khomenko, F. Béguin, R. Santamaría, *Electrochim. Acta* **2007**, *52*, 4969.
[233] H. A. Andreas, B. E. Conway, *Electrochim. Acta* **2006**, *51*, 6510.
[234] E. Frackowiak, F. Béguin, *Carbon* **2001**, *39*, 937.
[235] C.-H. Yang, Q. D. Nguyen, T.-H. Chen, A. S. Helal, J. Li, J.-K. Chang, *ACS Sustainable Chem. Eng.* **2018**, *6*, 1208.
[236] I. S. Ike, I. Sigalas, S. Iyuke, *Phys. Chem. Chem. Phys.* **2016**, *18*, 661.
[237] Y. T. Ju, M.-Y. Cho, M.-H. Kim, J.-W. Lee, S.-M. Park, B. H. Choi, K. C. Roh, *J. Ceram. Process. Res.* **2012**, *13*, S159.
[238] S. Ghosh, S. R. Polaki, M. Kamruddin, S. M. Jeong, K. (Ken) Ostrikov, *J. Phys. D: Appl. Phys.* **2018**, *51*, 145303.
[239] J. Zhu, A. S. Childress, M. Karakaya, S. Dandeliya, A. Srivastava, Y. Lin, A. M. Rao, R. Podila, *Adv. Mater.* **2016**, *28*, 7185.
[240] D. Hursán, A. A. Samu, L. Janovák, K. Artyushkova, T. Asset, P. Atanassov, C. Janáky, *Joule* **2019**, *3*, 1719.
[241] J. L. Qi, X. Wang, J. H. Lin, F. Zhang, J. C. Feng, W.-D. Fei, *Nanoscale* **2015**, *7*, 3675.
[242] Q. Zhou, W. Ju, Y. Liu, J. Li, Q. Zhang, *Appl. Surf. Sci.* **2020**, *510*, 145448.
[243] A. S. Dobrota, I. A. Pašti, S. V. Mentus, N. V. Skorodumova, *Phys. Chem. Chem. Phys.* **2017**, *19*, 8530.
[244] Y. Gao, J. Zhang, X. Luo, Y. Wan, Z. Zhao, X. Han, Z. Xia, *Nano Energy* **2020**, *72*, 104666.
[245] Z. Pan, H. Zhi, Y. Qiu, J. Yang, L. Xing, Q. Zhang, X. Ding, X. Wang, G. Xu, H. Yuan, M. Chen, W. Li, Y. Yao, N. Motta, M. Liu, Y. Zhang, *Nano Energy* **2018**, *46*, 266.
[246] G. Zhao, Y. Li, G. Zhu, J. Shi, T. Lu, L. Pan, *ACS Sustainable Chem. Eng.* **2019**, *7*, 12052.
[247] X. Yu, Y. Kang, H. S. Park, *Carbon* **2016**, *101*, 49.
[248] J. Huang, J. Wu, F. Dai, C. M. Li, *Chem. Commun.* **2019**, *55*, 9168.
[249] Y. Li, G. Wang, T. Wei, Z. Fan, P. Yan, *Nano Energy* **2016**, *19*, 165.
[250] T. Wang, L.-X. Wang, D.-L. Wu, W. Xia, D.-Z. Jia, *Sci. Rep.* **2015**, *5*, 9591.
[251] R. Thangavel, A. G. Kannan, R. Ponraj, V. Thangavel, D.-W. Kim, Y.-S. Lee, *J. Mater. Chem. A* **2018**, *6*, 17751.
[252] J. Rani, R. Thangavel, S.-I. Oh, Y. Lee, J.-H. Jang, *Nanomaterials* **2019**, *9*, 148.
[253] L. Xu, L. Chen, L. Li, X. Li, *J. Mater. Sci.* **2019**, *54*, 8995.
[254] C. Wang, Y. Zhou, L. Sun, P. Wan, X. Zhang, J. Qiu, *J. Power Sources* **2013**, *239*, 81.
[255] T. Zhu, S. Li, B. Ren, L. Zhang, L. Dong, L. Tan, *J. Mater. Sci.* **2019**, *54*, 9632.
[256] Z.-S. Wu, K. Parvez, A. Winter, H. Vieker, X. Liu, S. Han, A. Turchanin, X. Feng, K. Müllen, *Adv. Mater.* **2014**, *26*, 4552.
[257] J. Zhao, Y. Li, G. Wang, T. Wei, Z. Liu, K. Cheng, K. Ye, K. Zhu, D. Cao, Z. Fan, *J. Mater. Chem. A* **2017**, *5*, 23085.

[258] Z. Chen, L. Hou, Y. Cao, Y. Tang, Y. Li, *Appl. Surf. Sci.* **2018**, *435*, 937.
[259] H. Chen, Y. Xiong, T. Yu, P. Zhu, X. Yan, Z. Wang, S. Guan, *Carbon* **2017**, *113*, 266.
[260] R. Chulliyote, H. Hareendrakrishnakumar, M. G. Joseph, *Electrochim. Acta* **2020**, 135698.
[261] P. H. Wadekar, R. V. Khose, D. A. Pethsangave, S. Some, *ChemSusChem* **2019**, *12*, 3326.
[262] X. Zhang, Y. Wang, Y. Du, M. Qing, F. Yu, Z. Q. Tian, P. K. Shen, *Electrochim. Acta* **2019**, *318*, 272.
[263] Z. Song, L. Li, D. Zhu, L. Miao, H. Duan, Z. Wang, W. Xiong, Y. Lv, M. Liu, L. Gan, *J. Mater. Chem. A* **2019**, *7*, 816.
[264] F. R. M. S. Raj, G. Boopathi, N. V. Jaya, D. Kalpana, A. Pandurangan, *Diamond Relat. Mater.* **2019**, 107687.
[265] H. Jin, X. Feng, J. Li, M. Li, Y. Xia, Y. Yuan, C. Yang, B. Dai, Z. Lin, J. Wang, J. Lu, S. Wang, *Angew. Chem., Int. Ed.* **2019**, *58*, 2397.
[266] D. Hulicova-Jurcakova, M. Seredych, G. Q. Lu, N. K. A. C. Kodiweera, P. E. Stallworth, S. Greenbaum, T. J. Bandosz, *Carbon* **2009**, *47*, 1576.
[267] C. Huang, A. M. Puziy, O. I. Poddubnaya, D. Hulicova-Jurcakova, M. Sobiesiak, B. Gawdzik, *Electrochim. Acta* **2018**, *270*, 339.
[268] G. A. Ferrero, A. B. Fuertes, M. Sevilla, *Electrochim. Acta* **2015**, *168*, 320.
[269] X. Liu, C. Lai, Z. Xiao, S. Zou, K. Liu, Y. Yin, T. Liang, Z. Wu, *ACS Appl. Energy Mater.* **2019**, *2*, 3185.
[270] V. Sahu, S. Grover, B. Tulachan, M. Sharma, G. Srivastava, M. Roy, M. Saxena, N. Sethy, K. Bhargava, D. Philip, H. Kim, G. Singh, S. K. Singh, M. Das, R. K. Sharma, *Electrochim. Acta* **2015**, *160*, 244.
[271] N. Phattharasupakun, J. Wutthiprom, P. Suktha, P. Iamprasertkun, N. Chanlek, C. Shepherd, E. Hadzifejzovic, M. G. Moloney, J. S. Foord, M. Sawangphruk, *Electrochim. Acta* **2017**, *238*, 64.
[272] Y.-W. Chi, C.-C. Hu, H.-H. Shen, K.-P. Huang, *Nano Lett.* **2016**, *16*, 5719.
[273] Y. Zhou, R. Ma, S. L. Candelaria, J. Wang, Q. Liu, E. Uchaker, P. Li, Y. Chen, G. Cao, *J. Power Sources* **2016**, *314*, 39.
[274] D. Salinas-Torres, S. Shiraishi, E. Morallón, D. Cazorla-Amorós, *Carbon* **2015**, *82*, 205.
[275] S. L. Candelaria, B. B. Garcia, D. Liu, G. Cao, *J. Mater. Chem.* **2012**, *22*, 9884.
[276] Maxwell Technologies Enabling Energy's Future, https://www.maxwell.com/products/ultracapacitors (accessed: October 2019).
[277] Electropaedia Battery and Energy Technology, https://www.mpoweruk.com/performance.htm (accessed: October 2019).
[278] J. Ryu, D. Hong, H.-W. Lee, S. Park, *Nano Res.* **2017**, *10*, 3970.
[279] D. Zhang, C. He, Y. Wang, J. Zhao, J. Wang, K. Li, *J. Colloid Interface Sci.* **2019**, *540*, 439.
[280] K. Sun, J. Li, H. Peng, E. Feng, G. Ma, Z. Lei, *Ionics* **2017**, *23*, 985.
[281] Y. Deng, Y. Ji, H. Wu, F. Chen, *Chem. Commun.* **2019**, *55*, 1486.
[282] J. Yan, Q. Wang, C. Lin, T. Wei, Z. Fan, *Adv. Energy Mater.* **2014**, *4*, 1400500.
[283] J. K. Han, M. E. Lee, H. J. Choi, H.-J. Jin, Y. S. Yun, *Electrochim. Acta* **2019**, *302*, 71.
[284] Z. Ye, F. Wang, C. Jia, K. Mu, M. Yu, Y. Lv, Z. Shao, *Chem. Eng. J.* **2017**, *330*, 1166.
[285] A. Balducci, D. Belanger, T. Brousse, J. W. Long, W. Sugimoto, *J. Electrochem. Soc.* **2017**, *164*, A1487.
[286] G. Tontini, M. Greaves, S. Ghosh, V. Bayram, S. Barg, *J. Phys. Mater.* **2020**, *3*, 022001.
[287] M. D. Stoller, R. S. Ruoff, *Energy Environ. Sci.* **2010**, *3*, 1294.
[288] Z. Sanliang, P. Ning, *Adv. Energy Mater.* **2015**, *5*, 1401401.
[289] B. Li, F. Dai, Q. Xiao, L. Yang, J. Shen, C. Zhang, M. Cai, *Energy Environ. Sci.* **2016**, *9*, 102.
[290] L. Demarconnay, E. Raymundo-Piñero, F. Béguin, *Electrochem. Commun.* **2010**, *12*, 1275.
[291] E. Redondo, E. Goikolea, R. Mysyk, *Electrochim. Acta* **2016**, *221*, 177.
[292] D. P. Dubal, N. R. Chodankar, Z. Caban-Huertas, F. Wolfart, M. Vidotti, R. Holze, C. D. Lokhande, P. Gomez-Romero, *J. Power Sources* **2016**, *308*, 158.
[293] S. A. Evlashin, Y. M. Maksimov, P. V Dyakonov, A. A. Pilevsky, K. I. Maslakov, Y. A. Mankelevich, E. N. Voronina, S. V Vavilov, A. A. Pavlov, E. V Zenova, I. S. Akhatov, N. V Suetin, *Sci. Rep.* **2019**, *9*, 6716.
[294] G. Sahoo, S. Ghosh, S. R. Polaki, T. Mathews, M. Kamruddin, *Nanotechnology* **2017**, *28*, 415702.
[295] C. C. L. McCrory, S. Jung, J. C. Peters, T. F. Jaramillo, *J. Am. Chem. Soc.* **2013**, *135*, 16977.
[296] S. Kogikoski, C. P. Sousa, M. S. Liberato, T. Andrade-Filho, T. Prieto, F. F. Ferreira, A. R. Rocha, S. Guha, W. A. Alves, *Phys. Chem. Chem. Phys.* **2016**, *18*, 3223.
[297] A. Mir, G. N. Abhilesh, R. M. Tamgadge, A. Shukla, *J. Solid State Electrochem.* **2019**, *23*, 2281.
[298] S. He, C. Zhang, C. Du, C. Cheng, W. Chen, *J. Power Sources* **2019**, *434*, 226701.
[299] E. Lust, A. Jänes, M. Arulepp, *J. Electroanal. Chem.* **2004**, *562*, 33.
[300] Y. Liu, B. Réty, C. Matei Ghimbeu, B. Soucaze-Guillous, P.-L. Taberna, P. Simon, *J. Power Sources* **2019**, *434*, 226734.
[301] M. Zhu, C. J. Weber, Y. Yang, M. Konuma, U. Starke, K. Kern, A. M. Bittner, *Carbon* **2008**, *46*, 1829.
[302] G.-P. Hao, Q. Zhang, M. Sin, F. Hippauf, L. Borchardt, E. Brunner, S. Kaskel, *Chem. Mater.* **2016**, *28*, 8715.
[303] A. R. John, P. Arumugam, *J. Power Sources* **2015**, *277*, 387.

Subrata Ghosh is a Postdoctoral Research Associate in the University of Manchester, UK. Prior to the current position, he was Brain Korea 21 Postdoc Fellow in Chungbuk National University, Republic of Korea and Research associate in Indira Gandhi Centre for Atomic Research, India. He received Ph.D. from Homi Bhabha National Institute, India in 2016. His research involves designing smart nanostructures, understanding the growth mechanism, and exploring them for next-generation energy applications.

Suelen Barg is a Lecturer in the Department of Materials and Royce Institute at the University of Manchester. She leads a research group on nanostructured 3D assemblies (Nano-3D) focusing on the design of advanced nanostructured materials with focus on 2D Materials and additive manufacturing. Her research is developed in collaboration with governmental and industrial funding and aims to tackle global challenges in renewable energy, biomedical, and aerospace applications.

Kostya (Ken) Ostrikov is a Professor with Queensland University of Technology, Australia, a Founding Leader of the CSIRO–QUT Joint Sustainable Processes and Devices Laboratory, and Academician of the Academy of Europe and the European Academy of Sciences. His research focused on nanoscale control of energy and matter contributes to the solution of the grand challenge of directing energy and matter at nanoscales, to develop renewable energy and energy-efficient technologies for a sustainable future.